Development and Clinical Application of a Multiplexed Assay for Proximal Tubular Secretion

Maya Louise Hatten-Beck

A thesis

submitted in partial fulfillment of the

requirements for the degree of

Master of Science

University of Washington

2026

Committee:

Andrew Hoofnagle

William Phipps

Mariya Sweetwyne

Program Authorized to Offer Degree:

Laboratory Medicine and Pathology

University of Washington

Abstract

Development and Clinical Application of a Multiplexed Assay for Proximal Tubular Secretion

Maya Louise Hatten-Beck

Chair of the Supervisory Committee:
Andrew Hoofnagle
Department of Laboratory Medicine and Pathology

Proximal tubular secretion contributes to the elimination of metabolites, uremic toxins, and many medications, yet existing clinical tools rely on glomerular filtration markers with no common way to evaluate secretory capacity. A multiplexed targeted liquid chromatography-tandem mass spectrometry (LC-MS/MS) assay was developed and validated for 21 tubular secretory solutes (TSS) in plasma and urine, for measurement of solute clearance as an estimate of tubular secretory capacity. In a cohort of healthy adults and patients with chronic kidney disease (CKD) (n = 48), several solutes, including N2,N2-dimethylguanosine (DMG), correlated strongly with the clearance of furosemide and famciclovir, supporting their potential as secretory biomarkers. In a critically ill cohort (n = 246), baseline TSS clearances were associated with incident acute kidney injury (AKI) and major adverse kidney events at 30 days (MAKE30), and baseline inverse plasma DMG declined progressively across AKI stages. These findings support tubular secretory function as a clinically meaningful dimension of kidney physiology and identify DMG as a promising early biomarker of secretory impairment in critically ill patients.

Acknowledgements

There are so many people I would like to thank for supporting me through my master's project. First, thank you to my committee members Drs. Phipps, Sweetwyne, and Hoofnagle for taking the time to provide helpful, thoughtful feedback. Thank you to Dr. Kestenbaum for your mentorship. Thank you to Dr. Polyak for being so supportive and thank you to everyone else in the program, who have been nothing but encouraging and kind. Angelina, Amy, Alexis, and Sunny, it has been so great getting to be in this program with you (I'm so excited I finally caught up).

Thank you to everyone in the Hoofnagle Lab. I have learned so much since joining the lab, and I most certainly could not have done anything at all without you. Jess, thank you for your wisdom and patience while I struggled through being hazed by Claude (our Sciex 6500+). And Andy, thank you for having me in the lab, and for all of your mentorship and guidance.

Finally, thank you to my family and friends who have stuck around through this time. Frieda, mom, and dad, you are wonderful. Ava and Callie, thank you for being kind and fair givers of feedback. Kat, thank you for being in this with me. And thank you to everyone in my life who has listened to me yap about kidneys the past few years. They really are pretty cool.

AI Disclosure

Artificial intelligence tools were used in the preparation of this thesis for assistance with R code development and editorial suggestions. All research ideas, experimental design, data collection, data analysis, and interpretations are the original work of myself and others, and were not generated by AI.

TABLE OF CONTENTS

LIST OF FIGURES

LIST OF TABLES

LIST OF ABBREVIATIONS

AA	Acetic acid
ACN	Acetonitrile
AKI	Acute kidney injury
AmOH	Ammonium hydroxide
APACHE II	Acute Physiology and Chronic Health Evaluation II
CE	Collision energy
CKD	Chronic kidney disease
CXP	Collision cell exit potential
%CV	Percent coefficient of variation
DMG	N2,N2-dimethylguanosine
DMSO	Dimethyl sulfoxide
DP	Declustering potential
eGFR	Estimated glomerular filtration rate
EP	Entrance potential
FA	Formic acid
FDR	False discovery rate
FT	Freeze/thaw
GFR	Glomerular filtration rate
HILIC	Hydrophilic interaction liquid chromatography
HLB	Hydrophilic-lipophilic balance
IPA	2-isopropanol
IQR	Interquartile range
IS	Internal standard
LC-MS/MS	Liquid chromatography-tandem mass spectrometry
MAKE	Major adverse kidney events
MAKE30	Major adverse kidney events within 30 days
MCX	Mixed cation exchange
MeOH	Methanol
MRM	Multiple reaction monitoring
NPAR	Normalized peak area ratio
OR	Odds ratio
PAR	Peak area ratio
PROCLAIM	Proximal Tubular Clearance of Renal Medication
QC	Quality control
ROKIT	Role of Kidney Tubular Secretion in Critical Illness
RT	Room temperature
SOFA	Sequential Organ Failure Assessment
SPC	Single point calibrator
SPE	Solid phase extraction
TSS	Tubular secretory solute

1. CHAPTER 1 – INTRODUCTION

The kidneys are vital organs that maintain overall body homeostasis through multiple mechanisms.[1] These include balancing fluids, regulating electrolytes and minerals, and removing waste, including drugs and toxins. The kidneys also contribute to endocrine function, including the production of renin to regulate blood pressure, erythropoietin to support erythropoiesis and oxygen-carrying capacity, and vitamin D activation to maintain calcium homeostasis.[2,3] They are also capable of performing gluconeogenesis to support metabolism.[2] As paired retroperitoneal organs supplied by the renal arteries, they receive approximately 20% of resting cardiac output, corresponding to roughly 1.2 liters of blood per minute.[4] When the kidneys are damaged or diseased, these functions can become impaired.[5–7] Chronic kidney disease (CKD) affects an estimated 10–12% of the global population, and acute kidney injury (AKI) affects approximately 13.3 million people annually, substantially contributing to global morbidity and mortality.[8,9] CKD and AKI are important and growing public health issues, underscoring the clinical importance of measuring kidney function.

The kidney has a distinct internal anatomy that supports its many functions (**Figure 1.1A**).[10] The renal artery enters the kidney through the hilum, a recessed area on the concave border, while the renal vein and ureters exit through the same structure. The renal hilum extends into the renal sinus, a central cavity containing the renal pelvis, calyces, nerves, and fat. The renal parenchyma houses nephrons, the functional units of the kidney. Each kidney contains about 1 million nephrons, each consisting of a glomerulus and a tubule (**Figure 1.1B**).[11] Plasma is filtered across the glomerular filtration barrier, from the fenestrated capillaries of the glomerulus into Bowman's capsule, and the resulting filtrate then passes through the proximal tubule, loop of Henle, distal tubule, and collecting duct.

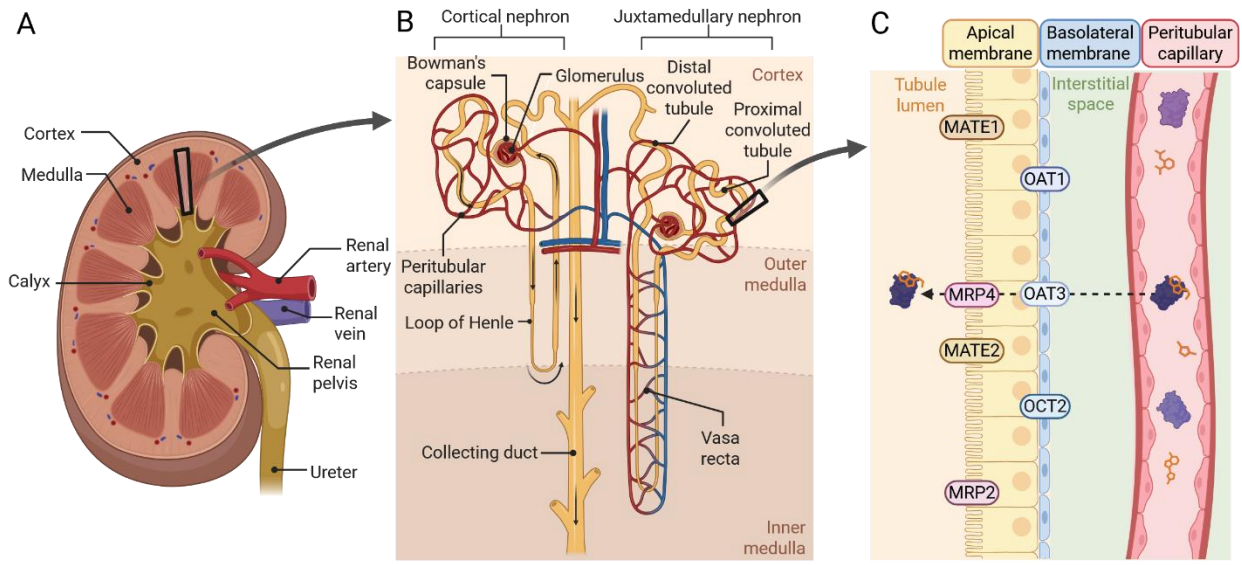

Figure 1.1. Kidney anatomy and proximal tubular secretion. Anatomy of the kidney, including the cortex, medulla, calyx, renal pelvis, ureter, and major vasculature (A). Nephron anatomy showing cortical and juxtamedullary nephron types, including the glomerulus, Bowman's capsule, proximal convoluted tubule, distal convoluted tubule, loop of Henle, collecting duct, peritubular capillaries, and vasa recta (B). Arrows indicate the direction of tubular fluid flow. Mechanism of proximal tubular secretion at the epithelial cell level, adapted from Wang and Kestenbaum (C).[12] Created with BioRender.com.

The renal parenchyma is organized into two distinct regions.[10] The nephron loops, vasa recta (vessels running parallel to the loop of Henle), and collecting ducts are densely arranged into cone-shaped structures called renal pyramids, which together form the renal medulla. The renal cortex is the parenchymal tissue surrounding the medulla. Nephrons are classified as either superficial cortical (residing in the cortex) or juxtamedullary (residing at the corticomedullary junction).[13] Juxtamedullary nephrons comprise approximately 15% of all nephrons and possess larger glomeruli and longer loops of Henle, enabling them to establish the osmotic gradient necessary for urinary concentration. Collecting ducts converge at the renal papilla at the apex of each medullary pyramid, where urine is funneled through the calyces into the renal pelvis and drained via the ureters into the bladder.[10] The nephron performs two key processes relevant to eliminating substances from the blood: glomerular filtration and tubular secretion. While

filtration is routinely assessed in clinical practice, tubular secretion remains unassessed by current clinical tools, despite its importance in drug and toxin elimination.

1.1. Glomerular filtration

The nephron is the site of filtration, secretion, and reabsorption.[11] Filtration occurs at the interface of the glomerulus and Bowman's capsule, where plasma passes through the semipermeable capillaries of the glomerular tuft across the filtration barrier and into the nephron (**Figure 1.1B**). The filtration barrier consists of three layers: glomerular endothelial cells, the glomerular basement membrane, and podocytes (specialized visceral epithelial cells). The basement membrane is a sheet-like matrix composed of type IV collagen, glycoproteins, and proteoglycans, situated between the glomerular capillary endothelium and the podocytes. Podocytes are characterized by cytoplasmic extensions called foot processes, which wrap around the glomerular capillaries.[14] These foot processes interdigitate to form filtration slits, which represent the principal site of glomerular filtration. The slit diaphragm is an extracellular structure that bridges these filtration slits, functioning like a sieve that allows water and small molecules to pass while restricting large plasma proteins such as albumin. Together, these structures establish the selective permeability of the filtration barrier, restricting passage based on solute size, shape, and charge.[13]

The glomerular filtration rate (GFR) is the volume of plasma filtered by the glomerulus per unit time. It is calculated as:

$$GFR = K_f \times \text{net filtration pressure},$$

where K_f is the filtration coefficient, a product of the surface area of the filtering membrane and its hydraulic conductivity, and net filtration pressure is the difference between the hydrostatic

and oncotic pressures acting across the glomerular capillary wall.[12] Hydrostatic pressure is influenced by vascular resistance that comes from the relative constriction of the efferent arteriole compared to the afferent arteriole.[11] It is also regulated by mesangial cells, specialized smooth muscle-like cells that provide structural support to the glomerulus and regulate capillary surface area through their contractile properties. Oncotic pressure is determined by the concentration of plasma proteins in the glomerular capillaries. In healthy adults, GFR is approximately 100 mL/min/1.73 m², normalized to the average adult body surface area, though this value varies with age and sex.[15] Small, non-protein-bound compounds are freely filtered at the glomerulus, whereas protein-bound substances bypass filtration and are eliminated via tubular secretion.[16]

1.2. Tubular secretion

In addition to filtration, the kidneys rely on tubular secretion to eliminate a wide range of solutes, including metabolites, medications, and uremic toxins that can adversely affect neurological and cardiovascular function.[16–18] After approximately 20% of renal plasma flow is filtered at the glomerulus, the remaining 80% enters the peritubular capillaries, a network of capillaries that surround the proximal tubule.[12] This unfiltered plasma serves as the source of solutes for tubular secretion, which takes place primarily in the proximal tubule, the first nephron segment distal to Bowman's capsule.[11] The proximal tubule is subdivided into the proximal convoluted tubule (PCT) and the proximal straight tubule (PST), which correspond to the S1 (PCT), S2 (PCT/PST), and S3 (PST) segments, respectively. The PCT is composed of polarized epithelial cells with two distinct membrane domains: an apical membrane (the brush border) facing the tubular lumen, and a basolateral membrane facing the interstitial fluid adjacent to the peritubular capillaries (**Figure 1.1C**).[19] The S1 segment resides in the renal cortex and has cells with a more amplified

brush border than the S2 and S3 segments, which extend into the outer medulla and transition into the loop of Henle.[11] The cells throughout the proximal tubule are rich in mitochondria that generate the ATP required for active transport. The S2 and S3 segments contain a higher density of smooth endoplasmic reticulum and peroxisomes, likely reflecting their role in metabolizing secreted substances.[20]

The proximal tubule supports extensive secretion of drugs, toxins, metabolites, and waste products, as well as reabsorption of glucose, sodium, bicarbonate, and other essential solutes.[16] Solutes are secreted either passively, down an electrochemical gradient, or actively, against an electrochemical gradient.[16] Both mechanisms depend on a group of transporters that play a central role in the absorption, distribution, metabolism, and elimination (ADME) of drugs.[21] These transporters belong to two superfamilies: the ATP-binding cassette (ABC) superfamily and the solute carrier (SLC) superfamily, the latter of which includes the organic anion transporter (OAT) and organic cation transporter (OCT) subfamilies.[22] Five OAT isoforms have been identified in humans (hOAT1–hOAT5); of these, OAT1 (SLC22A6) and OAT3 (SLC22A8) are the predominant basolateral transporters in the kidney.[16,22] The principal OCT isoform in the kidney is OCT2 (SLC22A2). Once across the basolateral membrane, solutes are exported into the tubular lumen by several apical transporters. These include the SLC-type multidrug and toxin extrusion (MATE) proteins MATE1 (SLC47A1) and MATE2 (SLC47A2), and the ABC-type multidrug resistance proteins (MRP) MRP2 (ABCC2) and MRP4 (ABCC4). All of these transporters have broad substrate specificity, allowing them to transport a wide range of solutes from the peritubular fluid across the tubular epithelium into the lumen.[20] As a result, most substrates are secreted by more than one renal transporter.[22] Together, these transport

systems enable the kidney to achieve near-complete clearance of drugs and solutes in a single pass.[12]

The structural and functional demands on the proximal tubule make it particularly susceptible to injury.[20,23] Its high density of ATPases creates a substantial oxidative energy requirement, making the proximal tubule especially vulnerable to ATP depletion under hypoxic conditions and, consequently, to ischemic acute kidney injury (AKI). Following AKI, regardless of cause (ischemia, nephrotoxins, or other insults), proximal tubule cells exhibit hallmarks of cellular stress, including loss of polarity and brush border disruption.[20] Downregulation of OAT1 and OAT3 has also been observed in rat models of AKI, resulting in the accumulation of uremic toxins in circulation.[22,24] The buildup of these toxins may also contribute to the progression of chronic kidney disease (CKD).[22]

Proximal tubule injury plays a central role in CKD.[23] Diabetes is the leading cause of CKD in adults, and the proximal tubule may be one of the earliest sites of pathological change, including cellular hypertrophy resulting from impaired downregulation of glucose transport during hyperglycemia. OAT transporter expression and activity are similarly reduced in diabetic and other forms of CKD.[25] Proximal tubule injury has been shown to drive the AKI-to-CKD transition, leading to interstitial inflammation, fibrosis, and nephron loss. Repeated AKI episodes produce cumulative and irreversible damage, establishing repeated AKI as an independent driver of CKD progression.[23] Given the rising global prevalence of CKD and incidence of AKI, reliable clinical methods for assessing kidney function are increasingly important.[9,26]

1.3. Clinical assessment of kidney function

Several methods are used to assess kidney function in clinical practice and research.[7] GFR is the most widely measured parameter of kidney function, and creatinine is the most commonly used endogenous marker for its estimation. Creatinine is a waste product of muscle catabolism, generated at a relatively constant rate proportional to an individual's muscle mass; however, creatinine levels are also influenced by other factors, including age and sex.[27] GFR can be estimated by combining a serum creatinine measurement with a timed urine collection to calculate creatinine clearance (ClCr) using the following equation:

$$\text{Clearance}_X = (U_x \times V) / P_x,$$

Equation 1

where X is the solute of interest (creatinine), Ux is the urinary concentration of X, Px is the plasma concentration of X, and V is the volume of urine over the timed collection period (mL/min). Because creatinine is also subject to proximal tubular secretion, creatinine clearance systematically overestimates true GFR. Blood urea nitrogen (BUN) represents an alternative filtration marker, urea being a nitrogenous waste product formed in the liver and excreted by the kidneys. However, tubular reabsorption of filtered urea can reach 40–50%, causing BUN-based estimates to underestimate true GFR. Averaging creatinine and urea clearances can partially correct for these opposing biases, as the effects of tubular secretion and reabsorption on each marker tend to cancel each other out. Cystatin C is a freely filtered endogenous protein increasingly used as a GFR marker, often in combination with serum creatinine.[27] Urinary markers are also measured, including the urine albumin-to-creatinine ratio (uACR) to detect

albuminuria and the urinary protein-to-creatinine ratio (uPCR) to detect proteinuria (more commonly measured in certain patients, like children and pregnant women).[8,28]

Given the logistical burden of timed plasma and urine collections, prediction equations are widely used to estimate GFR (eGFR). The original equation was the Cockcroft-Gault equation[29]:

$$\text{Estimated ClCr (mL/min)} = \frac{(140-\text{age})\times\text{weight (kg)}}{72\times\text{serum creatinine (mg/dL)}} \times (0.85 \text{ if female}).$$

Subsequent iterations of this equation incorporated adjustments for body surface area and race; however, the race coefficient has since been removed following recognition that its inclusion lacked biological justification.[30,31] The current recommended equation is the CKD Epidemiology Collaboration 2021 (CKD-EPI 2021) equation[30]:

$$\text{eGFR}\left(\frac{\text{mL/min}}{1.73\ \text{m}^2}\right) = 142 \times \min\left(\frac{S_{cr}}{\kappa}, 1\right)^{\alpha} \times \max\left(\frac{S_{cr}}{\kappa}, 1\right)^{-1.200} \times 0.9938^{\text{Age}} \times 1.012\ [\text{if female}],$$

where 1.73 m² represents the average adult body surface area, κ is 0.7 (female) or 0.9 (male), α is −0.241 (female) or −0.302 (male), S_{cr} is standardized serum creatinine in mg/dL, and age is in years. CKD-EPI 2021 is the preferred equation for CKD diagnosis, staging, and population screening because of its superior accuracy; however, the Cockcroft-Gault equation remains in use among clinical pharmacologists and geriatricians for the purposes of drug dosing.[32]

Each of these endogenous markers carries important limitations. Although creatinine is predominantly filtered at the glomerulus, up to 15% is eliminated via proximal tubular secretion, causing creatinine clearance to overestimate true GFR.[7] Serum creatinine is further confounded by inter-individual differences in muscle mass, dietary intake, and physical activity. Critically, up to 50% of nephrons must lose function before serum creatinine rises detectably, making it an insensitive marker of early kidney injury.[23] The CKD-EPI 2021 equation, being derived from

population-level data, does not adequately account for patients with atypical muscle mass, unusually large or small body size, or rapidly changing kidney function.[32] In the latter case, eGFR may lag behind true GFR by up to three days, as the equation assumes creatinine is produced and excreted at steady state.[33] The Cockcroft-Gault equation is not recommended for accurate GFR estimation and is frequently uncalibrated to standardized creatinine assays.[32] BUN is particularly non-specific, with concentrations substantially influenced by extrarenal factors including dietary protein intake, gastrointestinal bleeding, corticosteroid use, hepatic disease, and hydration status.[34] Serum cystatin C is susceptible to confounding by inflammation, corticosteroid use, thyroid dysfunction, and adiposity, and is more costly and less widely available than serum creatinine.[27]

Because there is no ideal endogenous GFR marker, exogenous filtration markers are used to obtain measured GFR (mGFR).[7,35] Inulin is the classical reference standard: it is not produced endogenously, is freely and avidly filtered, and is neither secreted nor reabsorbed. Following intravenous infusion, its clearance is determined from serial plasma and urine collections over several hours. Iohexol is an alternative exogenous marker used for the same purpose.[36] While mGFR provides the most accurate assessment of filtration, it is expensive, labor-intensive, and impractical for routine clinical use, often requiring patients to remain at a clinical site for several hours while samples are collected.[37]

Both AKI and CKD are diagnosed and staged according to the Kidney Disease: Improving Global Outcomes (KDIGO) guidelines, which were developed to standardize clinical classification of these conditions.[8,38] AKI is defined by any of the following criteria: a rise in serum creatinine of ≥0.3 mg/dL within 48 hours, a rise in serum creatinine to ≥1.5 times baseline within 7 days, or a urine output of <0.5 mL/kg/h for six or more hours.[38] AKI is further stratified

into Stages 1 through 3 according to the severity of these changes, with the guidelines also encompassing risk stratification, evaluation, and management recommendations. CKD is defined as persistent abnormalities in kidney structure or function lasting more than three months.[8,39] Staging employs the cause-GFR-albuminuria (CGA) classification system, in which GFR is stratified into six categories from G1 (≥90 mL/min/1.73 m²) to G5 (<15 mL/min/1.73 m²), and albuminuria into three categories: A1 (<30 mg/g), A2 (30–300 mg/g), and A3 (>300 mg/g). These parameters are integrated into a risk heat map that communicates overall prognosis and guides clinical decision-making, recognizing that GFR alone is insufficient to characterize disease severity. Notably, both the AKI and CKD KDIGO frameworks rely exclusively on measures of glomerular filtration, with no provision for assessing tubular function. Tubular secretion is a mechanistically distinct process that plays a critical role in drug elimination and uremic toxin clearance, yet it remains entirely unassessed by existing clinical tools.

1.4. Measuring tubular secretion

Tubular secretion cannot be directly observed, so a proxy method must be used to quantify proximal tubular secretory function. One physiologically relevant approach is measuring renal clearance of secretion biomarkers, calculated from paired plasma or serum and timed urine samples using **Equation 1**.[40] This represents the volume of plasma cleared of a secretory solute per unit time, providing a measure of tubular secretory capacity. Measuring the plasma concentration alone of a secretory solute biomarker would be more practically accessible, similar to measuring creatinine to estimate GFR, but this would be a less direct measure. A composite score aggregating clearances across multiple secretory solutes may help reduce solute-specific biological variability and provide a more stable overall estimate of secretory function.

Liquid chromatography-tandem mass spectrometry (LC-MS/MS) is an ideal platform for measuring these solutes because it can simultaneously quantify many chemically diverse endogenous solutes in plasma, serum, and urine with specificity and sensitivity.[40] LC-MS/MS separates compounds chromatographically and identifies them by their mass-to-charge ratio and characteristic fragmentation pattern. Several additional quality assurance parameters are included to ensure accurate and reproducible measurements. Stable isotope-labeled internal standards are added to correct for variability in extraction recovery and ionization efficiency across samples and runs. Matrix-matched quality control (QC) materials and a single-point calibrator (SPC) are included to monitor consistency and assign analyte concentrations. Together, these components allow for the measurement of multiple tubular secretory solutes (TSS) simultaneously in plasma, serum, and urine to estimate tubular secretion.

1.5. The tubular secretory solute assay

A method was previously developed to assess tubular secretion by quantifying the clearance of TSS using LC-MS/MS.[40] This initial assay measured four solutes known to be predominantly secreted by the proximal tubule: cinnamoylglycine, hippurate, indoxyl sulfate, and p-cresol sulfate.[41] Clearance was calculated from timed urine and spot serum samples using **Equation 1**.[40] The assay was evaluated in a prospective cohort of 298 patients with CKD. Moderate associations were observed between TSS clearance and eGFR (derived from the average of creatinine and urea clearances); however, substantial inter-individual variability of the relationship between tubular secretion and glomerular filtration markers suggested functional heterogeneity between these two nephron processes.

The TSS assay was subsequently expanded to 16 candidate secretory solutes. These solutes were selected based on one or more of the following criteria: known affinity for basolateral proximal

tubule transporters, which mediate the uptake of solutes for secretion; elevated circulating concentrations in OAT knockout mouse models, indicating reliance on OAT-mediated secretion for elimination; a high degree of plasma protein binding, which limits glomerular filtration; and/or renal clearance values exceeding those of creatinine or GFR, indicating a secretory contribution beyond filtration.[42] The expanded assay was first applied to a cohort of patients with autosomal dominant polycystic kidney disease (ADPKD), in whom TSS clearance was impaired independent of GFR, regardless of whether kidney function was preserved or CKD was present. The assay was next applied to an outpatient CKD cohort with diverse etiology, where TSS clearance was found to be varied, independent of GFR.[43] In a larger prospective cohort of 3,416 CKD participants, reduced clearance of several TSS was associated with a significantly increased risk of CKD progression even when controlling for glomerular filtration.[44] Further analyses in this cohort examined associations between TSS clearance and cardiovascular disease, for which no statistically significant associations were identified, and cognitive impairment, for which TSS clearance showed some association with cognitive decline.[45,46]

A refined version of the assay, retaining the best-performing solutes from the panel, was applied to a cohort of 54 participants with and without CKD to examine whether TSS clearance could predict the renal elimination of furosemide and penciclovir, two drugs highly dependent on active tubular secretion.[47] Notably, mGFR demonstrated comparable predictive accuracy to TSS clearance for both drugs, and the addition of secretory clearance measures provided only marginal improvement, suggesting that GFR and tubular secretory function are closely correlated in stable outpatients. The TSS assay was also applied to a cohort of 170 ICU patients and 70 healthy controls.[48] A composite secretory score was independently associated with a 25% lower risk of major adverse kidney events (MAKE) at 28 days per standard deviation increase,

suggesting that tubular secretory clearance offers prognostic information beyond conventional kidney function markers in critically ill patients.

Collectively, these studies demonstrated that TSS clearance may provide information about proximal tubule secretory function complementary to glomerular filtration across a range of clinical contexts. However, no individual solute proved ideal for this purpose, due to practical limitations including variable contributions from glomerular filtration, intraindividual fluctuations in circulating concentrations, and the requirement for timed urine collections to calculate renal clearance.[49]

1.6. Rationale and aims

The existing TSS assay provided important insights into proximal tubular secretion across multiple patient cohorts; however, no individual solute was sufficient as a standalone marker. Given that proximal tubular secretion is the predominant route of elimination for many medications and nephrotoxins, a dedicated and practical measure of secretory function could have direct utility in drug dosing, toxicity assessment, and disease monitoring. Development of an expanded TSS assay was therefore undertaken.

Candidate solutes for the expanded panel were identified through an untargeted metabolomics study conducted as an adjunct to the pharmacokinetic study of furosemide and penciclovir described above.[47,49] Plasma samples were collected at multiple time points following study drug administration, alongside a concurrent 10-hour urine collection, and analyzed by hydrophilic interaction liquid chromatography coupled with quadrupole time-of-flight mass spectrometry (HILIC-QTOF-MS). Unlike targeted assays, untargeted metabolomics detects all ionizable features in a sample without prior selection of analytes, with compound identities assigned post-

acquisition through database matching of mass spectrometric data. Of the 528 metabolites identified, 56 were significantly associated with furosemide clearance. A composite ranking score (HoofScore 3000), incorporating furosemide clearance association, plasma protein binding, and correlations with mGFR and eGFR, was used to prioritize solutes, identifying 15 candidates for inclusion in the updated assay. These were combined with nine solutes retained from the previous panel based on prior performance, producing a final panel of 24 solutes (solutes 1–15 newly identified; solutes 16–24 retained from previous TSS assays) (**Table 1.1**). Of the 24 candidate solutes, 21 were successfully validated for quantification in both matrices. For clinical analyses, a subset of 16 solutes with the strongest evidence for tubular secretion and acceptable analytical performance was carried forward.

This project aimed to characterize proximal tubular secretory function in healthy individuals, patients with CKD, and critically ill patients by measuring the clearance of a TSS panel. To achieve this, a multiplexed LC-MS/MS assay was developed to simultaneously quantify these solutes in paired plasma and timed urine samples. This assay was then applied to a cohort of critically ill adults in the intensive care unit (ICU) to evaluate solute clearances and to assess individual solutes for their potential utility as plasma-only biomarkers of proximal tubular secretory function.

Table 1.1. Secretory solute panel biological characteristics. Each solute identified for inclusion in the TSS assay is listed with its corresponding HoofScore 3000 rank and biological origin.

Rank	Compound	Origin	Notes
1	4-Hydroxyphenylacetic acid[50]	Phenylalanine/tyrosine metabolism; gut microbiota	Aromatic small-molecule metabolite; marker of gut microbial activity
2	N2,N2-Dimethylguanosine[51]	tRNA turnover	tRNA-derived nucleoside; linked to cellular stress and aging
3	5-Fluoro-1-methyl-1H-1,3-benzodiazole	Unknown	Synthetic compound; biological role unclear
4	Pimelic acid[52]	Biotin (Vitamin B7) precursor; adipic acid pathway	Dicarboxylic acid; limited endogenous role known
5	3-Methylcrotonylglycine[53]	Leucine catabolism	3-Methylcrotonyl-CoA carboxylase metabolite
6	3-Methoxy-4-hydroxyphenylglycol sulfate[54]	Norepinephrine metabolism	Predominant norepinephrine metabolite
7	2-[(4-Aminobenzoyl)-amino]acetic acid[55]	Medication	Aminobenzoic acid derivative; used to measure renal plasma flow
8	6'-Sialyl-N-acetyllactosamine[56]	Glycan metabolism; human milk	Involved in cellular recognition, immune modulation, and brain development
9	2-Hydroxyphenylacetic acid[57]	Phenylalanine/tyrosine metabolism; gut microbiota	Aromatic small-molecule metabolite; marker of gut microbial activity
10	1,4-Cyclohexanedicarboxylic acid[58]	Synthetic/dietary	Limited biological context known
11	5-Hydroxytryptophan[59]	Tryptophan metabolism	Serotonin biosynthesis intermediate; used therapeutically
12	4-Acetamidobutyric acid[60]	GABA metabolism	N-acyl-GABA derivative; role as a metabolite
13	L-Homocitrulline[61]	Ornithine metabolism	Non-proteinogenic amino acid; biomarker of protein carbamylation in CKD
14	Gentisic acid[62]	Aspirin metabolism; endogenous synthesis	Endogenously produced siderophore
15	5-Hydroxy-3-indoleacetic acid[63]	Serotonin metabolism	Primary urinary serotonin metabolite
16	Kynurenic acid[64]	Tryptophan metabolism	Linked to immune function and inflammation; possible uremic toxin
17	4-Pyridoxic acid[65]	Vitamin B6 metabolism	Major urinary vitamin B6 metabolite; clinical marker of vitamin B6 status
18	N-Isovalerylglycine[66]	Leucine catabolism	Acylglycine conjugate; elevated in isovaleric acidemia
19	Indoxyl sulfate[67]	Dietary tryptophan; gut microbiota	Protein-bound uremic toxin; associated with cardiovascular and renal toxicity
20	P-cresol sulfate[68]	Gut microbiota; tyrosine metabolism	Protein-bound uremic toxin; intestinally-derived
21	Xanthosine[69]	Purine metabolism	Purine nucleoside; product of nucleobase deamination
22	Tiglylglycine[70]	Isoleucine catabolism	Urinary metabolite
23	N-Cinnamoylglycine[71]	Dietary cinnamic acid; gut microbiota	Acylglycine conjugate; urinary biomarker of colonization resistance
24	Hippuric acid[72]	Benzoic acid conjugation; gut microbiota	Urinary metabolite; marker of gut microbial phenylalanine metabolism

2. CHAPTER 2 – ASSAY DEVELOPMENT

To enable the quantification of renal secretion analytes in clinical samples, a targeted LC-MS/MS assay was developed. Chromatographic conditions, sample preparation workflows, and analytical parameters were systematically optimized to achieve adequate sensitivity, selectivity, and chromatographic performance across a panel of 24 analytes in plasma, serum, and urine.

2.1. Chemical and sample acquisition

Ammonium hydroxide solution was purchased from Sigma. LC-MS grade water, acetonitrile, methanol, 2-propanol, acetic acid, and formic acid were purchased from Fisher Scientific. Deidentified serum, plasma, and urine samples were collected from discarded clinical specimens.

2.2. Sample tuning on the mass spectrometer

A stock mixture of each analyte was directly infused into a triple-quadrupole tandem mass spectrometer (Shimadzu LC-40, Sciex 6500+). Stock solution details are provided in **Table A.1.** Each analyte was individually tuned to determine optimal instrument parameters and precursor-to-product ion transitions. These parameters were then used to develop a targeted method for the simultaneous quantification of 24 analytes (**Table A.2–Table A.4**).

2.3. Column selection

Several stationary phases were evaluated to optimize analyte retention and selectivity. Initial experiments were conducted using a hydrophilic interaction liquid chromatography (HILIC) column (Atlantis Premier BEH Z-HILIC with VanGuard FIT, 1.7 µm, 2.1 x 150 mm; Waters PN: 186009983), a phenyl-hexyl column (ACQUITY Premier CSH Phenyl-Hexyl with VanGuard FIT, 1.7 µm, 2.1 x 150 mm; Waters PN: 186009479), and an amide column (ACQUITY Premier BEH Amide with VanGuard FIT, 1.7 µm, 2.1 x 150 mm; Waters PN:

186009509). A stock mixture of all 24 analytes was injected at a volume of 40 µL during initial development (**Table A.1**).

Additional experiments were performed using shorter column formats to evaluate potential improvements in analysis time and chromatographic performance. These included a C18 column (ACQUITY UPLC HSS T3, 1.8 µm, 2.1 × 50 mm; Waters PN: 189003538), a shorter HILIC column (Atlantis Premier BEH Z-HILIC column, 1.7 µm, 2.1 × 50 mm; Waters PN: 186009978), and a shorter phenyl-hexyl column (ACQUITY Premier CSH Phenyl-Hexyl column, 1.7 µm, 2.1 × 50 mm; Waters PN: 186009474). A summary of the column types evaluated is provided in **Table A.5**.

Chromatographic method development was conducted through iterative optimization of mobile phase composition, buffer systems, gradient profiles, and column chemistry. Initial conditions were selected based on commonly reported parameters for polar analytes analyzed by reversed-phase and hydrophilic interaction chromatography. The chromatographic program was systematically modified to improve analyte retention, chromatographic resolution, and peak symmetry.

2.3.1. HILIC column

The HILIC column was evaluated under normal-phase chromatographic conditions. A stock mixture containing the 24 analytes was injected at a volume of 40 µL, and chromatographic performance was evaluated based on analyte retention, separation, and peak shape.

The liquid chromatography conditions tested are summarized in **Table A.6**. Of the conditions evaluated, *Condition 11* (MPA: 0.1% formic acid in 95% acetonitrile/3% methanol/2% water; MPB: 100mM ammonium formate in 5% acetonitrile/95% water; maximum gradient: MPB

60%) provided the most favorable chromatographic performance and was selected for continued method development. Evaluation of a shorter column length (50mm) did not improve chromatographic performance compared with the longer column (150 mm).

2.3.2. Phenyl-hexyl column

The phenyl-hexyl column was evaluated under both reversed-phase and normal-phase chromatographic conditions. A stock mixture containing the 24 analytes was injected at a volume of 40 µL.

The liquid chromatography conditions evaluated are summarized in **Table A.7.** Among the reversed-phase conditions tested, *Condition 2* (MPA: 0.1% formic acid in 95% water/5% acetonitrile; MPB: 0.1% formic acid in 95% acetonitrile/5% water; maximum gradient: MPB 98%) provided the most favorable chromatographic performance and was therefore selected for further development. A shorter column format was also evaluated (50 mm); however, it did not provide improvements in retention, separation, or peak shape relative to the 150 mm column. After continuing with the column and chromatographic conditions from *Condition 2* for method development, it was ultimately retired in favor of the HILIC column.

2.3.3. Amide and C18 columns

The amide column was evaluated under normal-phase chromatographic conditions using the 24-analyte stock mixture with a 40 µL injection volume. None of the tested conditions using the amide stationary phase provided improved chromatographic performance compared with the phenyl-hexyl or HILIC columns. Therefore, further development using the amide column was not pursued. The evaluated conditions are summarized in **Table A.8A.**

The C18 column was evaluated under reversed-phase conditions. Chromatographic performance was inferior to that observed with the other stationary phases, particularly with respect to analyte retention and separation. As a result, the C18 column was not pursued further. The tested condition is summarized in **Table A.8B**.

2.4. SPE Development

Once an LC-MS/MS method was developed using pure standards, method development proceeded to in-matrix optimization for plasma and urine. The initial sample preparation approach was based on a previously published method for this project.[42] From this starting point, additional optimization was performed to improve sensitivity, chromatographic performance, and separation from matrix interferents.

2.4.1. Plasma and serum

The previously reported method consisted of organic precipitation, size filtration, filtration through a phospholipid removal plate, followed by evaporation and reconstitution. For the present study, the organic precipitation step was optimized by varying the organic solvent, solvent pH, and dilution ratio.

Eight organic precipitation conditions were evaluated by varying solvent type (ACN or MeOH), formic acid concentration (0 or 1.1%), and plasma-to-organic solvent ratio (1:3 or 1:4). The tested conditions are summarized in **Table A.9**.

Methanol-based precipitations did not perform well. *Conditions 6 and 8* (**Table A.9**) failed to pass through the filtration plate (Acroprep Advance 045µm filter plate; Pall PN: 8148), while *Conditions 5 and 7* yielded poor chromatographic performance. Among the acetonitrile-based

conditions, *Condition 2* (acetonitrile precipitation; 1:3 plasma to organic ratio; 1.1% formic acid) was selected due to its superior sensitivity and chromatographic performance.

Filtration through a phospholipid removal plate was optimized by comparing the Phree Phospholipid Removal Plate (30 mg; Phenomenex PN: 8E-S133-TGB) to the Ostro Protein Precipitation and Phospholipid Removal Plate (25 mg; Waters PN: 186005518). Samples processed through the conditions described in **Table A.9** were passed through each phospholipid removal plate type and evaluated by sample recovery, chromatography, and variability. The Phree plate had higher recoveries with comparable chromatography for *Condition 2* compared to the Ostro plate, so it was selected for sample preparation.

To improve chromatographic performance and reduce interference, a post-extraction dilution step was implemented. This step was designed to adjust both the organic composition of the sample to better match the initial LC conditions and the pH to improve chromatographic separation. The variables optimized included the pH of the protein precipitation step, the pH of the post-phospholipid removal dilution solvent, and the dilution ratio (**Table A.10)**. Among the conditions evaluated, *Condition 8* (0.2% formic acid precipitation; 1.5% formic acid post-preparation dilution; 1:2 sample to dilution mix) and *Condition 18* (0.2% formic acid precipitation; 5% ammonium hydroxide post-preparation dilution; 1:1 sample to dilution mix) were selected as the optimized acidic and basic dilution conditions, respectively.

The acidic dilution condition improved chromatographic performance for most analytes; however, pimelic acid, 1,4-cyclohexanedicarboxylic acid, and N-isovalerylglycine exhibited significantly better performance under the basic dilution condition (plasma dilution selection listed in **Table A.11**). Pimelic acid demonstrated a change in ion ratio between undiluted prepared plasma and stock injections (**Figure A.1A–B**). Resolution was not achieved using a 1:1

dilution in 1.8% formic acid after phospholipid removal but was achieved using a 1:1 dilution with 5% ammonium hydroxide in acetonitrile (**Figure A.1C–D**). 1,4-Cyclohexanedicarboxylic acid exhibited similar behavior, while N-isovalerylglycine showed improved chromatographic performance under basic dilution (**Figure 2.1**).

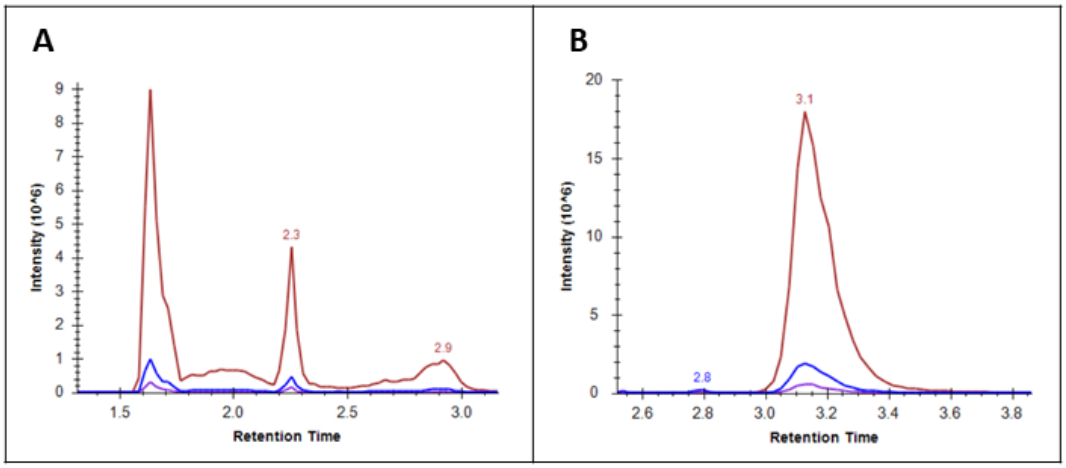

Figure 2.1. Effect of pH on N-isovalerylglycine. Plasma spiked with endogenous N-isovalerylglycine, diluted 1:1 in 1% FA in ACN following filtration (A), showed poor chromatography, whereas dilution 1:1 in 5% AmOH in ACN (B) resulted in improved chromatography.

Both acidic and basic dilution conditions were initially carried forward; however, the basic condition was later excluded following preliminary sample analysis. Pimelic acid and 1,4-cyclohexanedicarboxylic acid were not reliably detectable in patient samples (see section 4.1.1), and the additional preparation and instrument time required for the basic condition was not justified given the limited benefit, as only N-isovalerylglycine showed improvement. The final method is summarized in **Figure 3.1**.

2.4.2. Urine

The previously reported method utilized solid-phase extraction (SPE) of urine samples with two sorbent chemistries: a hydrophilic-lipophilic balance (HLB) plate (Oasis HLB 96-well Plate, 30 mg; Waters PN: WAT058951) and a mixed cation exchange (MCX) plate (Oasis MCX 96-well

Plate, 30 mg; Waters PN: 186000248). This method was subsequently optimized and expanded to improve analytical sensitivity and chromatographic performance.

In the starting method, 20 µL of urine was added to two separate plates. Each sample was diluted with 980 µL of formic acid in water, at concentrations of 0.2% (HLB workflow) and 2% (MCX workflow). The 0.2% formic acid solution was transferred to an HLB extraction plate that had first been primed with 1 mL of conditioning solution (40% methanol and 60% acetonitrile) and equilibrated with 1 mL diluent (0.2% formic acid in water), using a positive pressure manifold. The 2% formic acid solution was transferred to an MCX extraction plate, after the MCX plate had been primed with 1 mL of conditioning solution (40% methanol and 60% acetonitrile) and equilibrated with 1 mL of diluent (2% formic acid in water). Each plate was washed with 1 mL of diluent (HLB: 0.2% formic acid in water; MCX: 2% formic acid in water), and the analytes were eluted (HLB elution: 1 mL of 40% methanol and 60% acetonitrile; MCX elution: twice with 500 µL 5% concentrated ammonium hydroxide in 38% methanol and 57% acetonitrile) into new 96-well plates.

2.4.2.1. HLB Method Development

Further method development focused on the HLB sorbent due to its prior success. The HLB phase provides mixed-mode retention of both hydrophilic and lipophilic compounds and remains stable across a wide pH range (0–14), making it well suited for this application.[73]

Optimization efforts focused on improving chromatographic resolution by modifying the elution solvent to better match the initial LC-MS/MS mobile phase conditions (0.1% formic acid / 2% water / 3% methanol / 95% acetonitrile) and the plasma extraction composition (0.1% formic acid / 12.5% water / 87.4% acetonitrile). The original method did not achieve adequate separation for all analytes. The dilution and wash solvents (0.2% formic acid in water) were

retained, while the original HLB elution solvent was compared against a series of alternative solvents with varying pH and organic content (**Table A.12A**).

An Oasis PRiME HLB μElution plate (3 mg; Waters PN: 186008052), which does not require conditioning or equilibration, was also evaluated. Four conditions were tested (**Table A.12B**), incorporating a post-elution dilution step to adjust pH and better match LC-MS/MS starting conditions.

Among all conditions, *Condition 4* (1% formic acid/12.5% water/87.4% acetonitrile; **Table A.12A**) provided the best overall chromatographic performance across the analyte panel. However, pimelic acid did not achieve adequate separation from an interfering compound under this condition (**Figure A.1E**). In contrast, this condition yielded the best resolution and sensitivity for 4-hydroxyphenylacetic acid and 2-hydroxyphenylacetic acid, which were not well resolved under other conditions (**Figure A.2**).

2.4.2.2. Ion-Exchange SPE Plates

Additional SPE chemistries employing ion-exchange mechanisms were evaluated using an Oasis Method Development μElution plate (3 mg; Waters PN: 186004475). The sorbent types investigated included mixed cation exchange (MCX), weak anion exchange (WAX), mixed anion exchange (MAX), and weak cation exchange (WCX). MCX and MAX provide strong ion-exchange functionality, WAX and WCX provide weak ion-exchange interactions, and all types exhibit mixed-mode retention similar to HLB.

The initial experiment followed the manufacturer's protocol, which incorporated a neutral elution intended to capture uncharged analytes, and an acid/base elution intended to capture charged molecules. Post-elution dilution conditions were applied to adjust solvent composition to either

LC-MS/MS starting conditions or plasma matrix injection conditions (**Table A.13,** Experiment 1). Analyte performance under each condition was evaluated using a scoring system (0–3) to assess extraction efficiency and chromatographic quality. Across analytes, acid/base elution conditions significantly outperformed neutral elution.

A second experiment (**Table A.13,** Experiment 2) excluded neutral elution and replaced methanol with acetonitrile in the acid/base elution to improve chromatographic behavior. However, this modification did not yield substantial improvements.

Overall, the MCX µElution sorbent demonstrated the best performance across the analyte panel. However, it did not outperform the 30 mg MCX plate used in the original method. Therefore, the MCX 30 mg plate was retained for further method development.

The analyte 6′-sialyl-N-acetyllactosamine did not achieve sufficient sensitivity with any of the evaluated sorbents and was excluded from method development at this stage.

2.4.2.3. SPE Method Optimization

The HLB and MCX sorbent plate methods were employed in tandem to achieve the required chromatographic performance, resolution, and analytical sensitivity. These methods were subsequently optimized to streamline the sample preparation workflow.

Method optimization included evaluating the necessity of conditioning and equilibration steps (**Table A.14,** Conditions 1–3). For the HLB method, omission of both conditioning and equilibration steps did not adversely affect sensitivity or chromatographic performance; therefore, these steps were excluded from the final protocol. For the MCX method, omission of the conditioning step did not impact performance; however, the equilibration step was found to improve sensitivity and was therefore retained in the final sample preparation procedure.

The wash step was further optimized by increasing the organic content to enhance sample cleanup. The original aqueous wash solution was compared to wash solutions containing 10%, 20%, and 30% organic solvent (**Table A.14,** Conditions 4–6). However, the original aqueous wash condition provided the best overall performance for both MCX and HLB sorbents and was therefore maintained.

The final urine SPE method developed in this project incorporated both HLB and MCX sorbent plates, using the optimized conditions described above. The allocation of analytes to each sorbent is provided in **Table A.11**, and summaries of the finalized workflows are shown in **Figure 3.1 and Figure 3.2**.

2.4.3. Resolution of 3-Methylcrotonylglycine and Tiglylglycine

Among the analytes included in this assay, 3-methylcrotonylglycine and tiglylglycine are isobaric compounds with identical molecular weights and highly similar chemical structures (**Figure 2.2A**). When analytical standards were injected individually into the LC-MS/MS system, these compounds exhibited distinct transition ion ratios for both endogenous and internal standards **(Figure 2.2B–E**). However, in extracted matrix samples, chromatographic separation was not achieved in either plasma or urine extracts.

In plasma extracts, partial resolution was obtained by modifying the protein precipitation conditions. When acetonitrile alone was used (**Table A.15**, Condition 1), no separation between the two analytes was observed. In contrast, the addition of 1.1% formic acid to the precipitation solvent (**Table A.15,** Condition 2) resulted in partial chromatographic resolution of 3-methylcrotonylglycine and tiglylglycine (**Figure 2.2F–G**).

For urine samples, no resolution was observed when using the MCX plate, which may be attributed to the basic elution conditions (5% ammonium hydroxide in 38% methanol and 57% acetonitrile) (**Figure 2.2H**). In contrast, partial resolution was achieved using the HLB solid-phase extraction plate, likely due to the acidic conditions of the elution solvent (1% formic acid in 12.5% water and 87.5% acetonitrile) (**Figure 2.2I**).

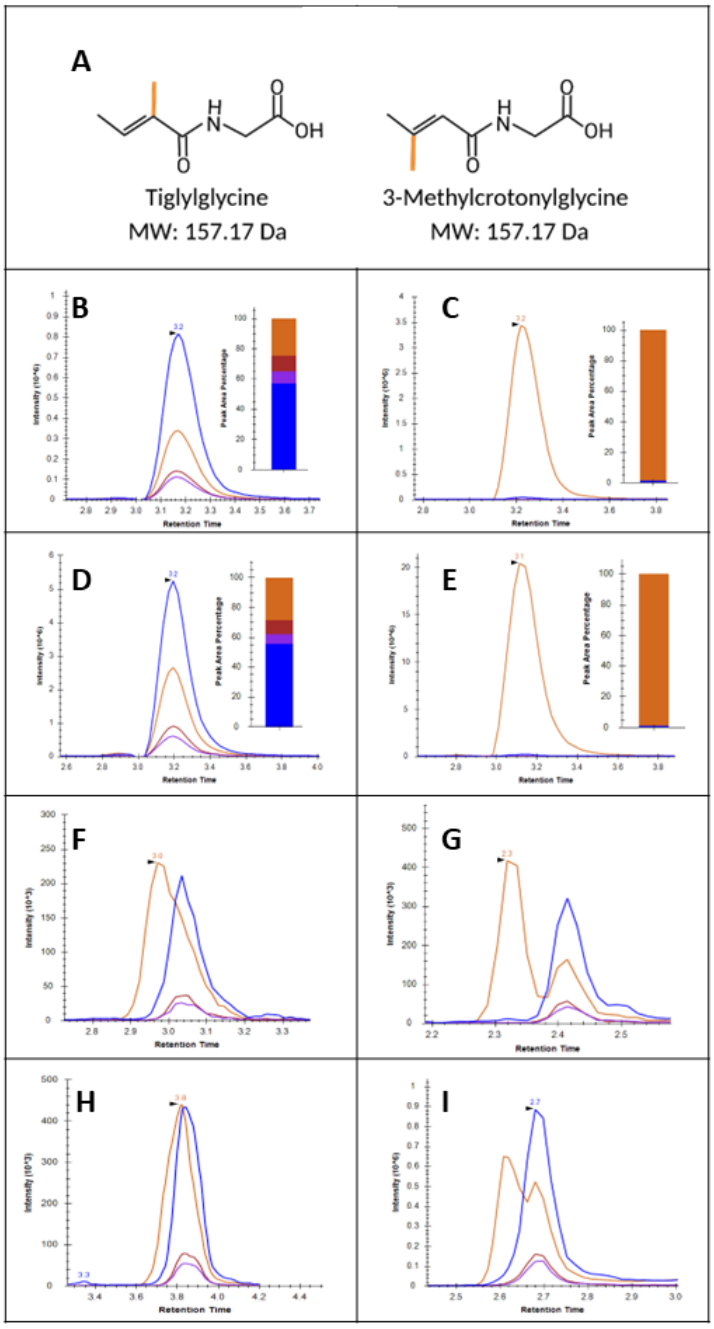

Figure 2.2. Chromatographic resolution of tiglylglycine and 3-methylcrotonylglycine. The compounds share the same molecular weight but differ in the position of the methyl substituent (highlighted in orange) (A). Representative chromatograms and transition ion ratio bars are shown for stock injections of unlabeled (B) and labeled (D) tiglylglycine, and unlabeled (C) and labeled (E) 3-methylcrotonylglycine. Unspiked plasma diluted 1:3 in ACN (F) did not resolve the analytes, whereas dilution 1:3 in 1% FA in ACN (G) improved resolution. Urine samples eluted from the MCX sorbent plate (5% AmOH / 38% MeOH / 57% ACN) (H) showed no resolution, while samples eluted from the HLB sorbent plate (1% FA / 12% H_2O / 88% ACN) (I) demonstrated improved, but incomplete, resolution.

2.4.3.1. Post-Acquisition Data Analysis

Because complete chromatographic resolution was not achieved in either matrix, a post-acquisition data processing approach was implemented to enable separate quantification of each analyte. Stock solutions were injected in triplicate, and the resulting peak areas were averaged for each of the four monitored transitions for both light and heavy standards (transitions listed in **Table A.3 and Table A.4**). The resulting ion ratios are summarized in **Table 2.1** and **Figure 2.2B–E**.

Table 2.1. Transition ion ratios for tiglylglycine and 3-methylcrotonylglycine. Product ion amounts (expressed as a percentage of the total ion signal) are shown for four transitions for both unlabeled (top) and isotopically labeled (bottom) forms of tiglylglycine and 3-methylcrotonylglycine. The two compounds share an identical precursor ion (156.1 *m/z* unlabeled; 159.1 *m/z* labeled). The purple/yellow transition ratio (110.2/74.3 for unlabeled; 112/77 for labeled) was calculated for tiglylglycine; this ratio was not applicable for 3-methylcrotonylglycine.

Transition	Tiglylglycine	3-Methylcrotonylglycine
156.1 / 112.3 (blue)	57.0%	1.3%
156.1 / 110.2 (purple)	7.9%	0.0%
156.1 / 96.3 (red)	10.2%	0.1%
156.1 / 74.3 (yellow)	24.8%	98.6%
Purple/Yellow Ratio	0.319	--
Transition	**Tiglylglycine ($^{13}C_2$, ^{15}N)**	**3-Methylcrotonylglycine ($^{13}C_2$, ^{15}N)**
159.1 / 114 (blue)	55.4%	1.0%
159.1 / 112 (purple)	6.6%	0.0%
159.1 / 98 (red)	9.6%	0.1%
159.1 / 77 (yellow)	28.4%	98.9%
Purple/Yellow Ratio	0.230	--

For tiglylglycine, the transitions at *m/z* 156.1→110.2 and 159.1→112.0 (purple**, Figure 2.2**) were selected as quantifier ions, as these were not observed in 3-methylcrotonylglycine. In contrast, 3-methylcrotonylglycine did not exhibit any unique transition ions. Therefore, the shared transition (yellow, **Figure 2.2**) was used for its quantification through a correction-based calculation.

Specifically, the contribution of tiglylglycine to the shared transitions at *m/z* 156.1→74.3 and 159.1→77.0 (yellow) was first estimated. This was accomplished by determining the ratio of the unique (purple) transitions to the shared (yellow) transitions for tiglylglycine using stock injections (**Table 2.1**). The contribution of tiglylglycine to the shared transition signal in each sample was then calculated as the ratio of the measured purple transition signal to the experimentally determined unique-to-shared transition ratio. Accordingly, the corrected signal for 3-methylcrotonylglycine was calculated as:

$$A_{\mathrm{MCG}} = A_{\mathrm{shared,total}} - \left(\frac{A_{\mathrm{uniqueTGG,sample}}}{R_{\mathrm{unique/shared}}} \right)$$

where A_{MCG}represents the corrected signal for 3-methylcrotonylglycine, $A_{\mathrm{shared,total}}$is the total measured signal of the shared (yellow) transition, $A_{\mathrm{uniqueTGG,sample}}$is the measured tiglylglycine-specific (purple) transition signal in the sample, and $R_{\mathrm{uniqueTGG/shared}}$is the transition ion ratio of purple/yellow for tiglylglycine determined from stock injections. This calculated tiglylglycine contribution was subtracted from the total shared transition signal, yielding the corrected signal attributable to 3-methylcrotonylglycine, which was used for quantification. The same approach was applied to both light and heavy isotopologues.

2.5. Possible misidentification of 2-[(4-Aminobenzoyl)-amino]acetic acid

The untargeted method used to generate the ranked list of candidate analytes identified 2-[(4-aminobenzoyl)-amino]acetic acid. This compound corresponds to the IUPAC name for para-aminohippurate (PAH; also known as aminohippuric acid), a diagnostic agent used to measure renal plasma flow. PAH is freely filtered and actively secreted by the kidneys, with minimal reabsorption, making it a well-established marker of renal function.[74]

This analyte was included in assay development but was only occasionally detected in patient samples, likely in individuals administered PAH. Although analytically interesting, PAH is not suitable as a potential biomarker of renal secretion, as it is not endogenously produced and is not present in most patients; therefore, it was excluded from the final assay.

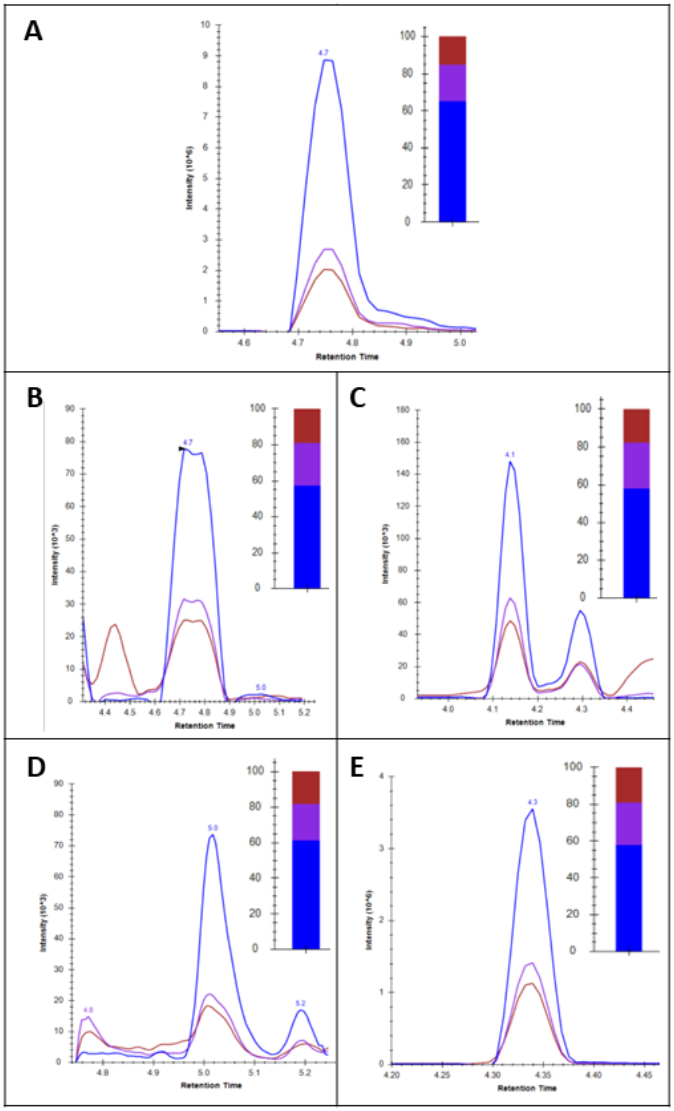

Figure 2.3. Potential misidentification of 2-[(4-aminobenzoyl)amino]acetic acid (PAH). Comparison of stock PAH (A) with serum SPC (B) and urine SPC (D) shows matching transition ion ratios and retention times. An unknown peak observed in serum (C) and urine (E) exhibited similar transition ion ratios but eluted approximately 30 seconds earlier than authentic PAH in both matrices.

During assay development, an unknown peak with the same precursor mass and fragment ions as PAH was observed, eluting approximately 30 seconds earlier in both plasma and urine (plasma: PAH 4.7 min, unknown 4.1 min; urine: PAH 5.0 min, unknown 4.35 min) (**Figure 2.3**). In untargeted metabolomics, features are commonly identified by matching mass spectrometric data to reference databases, where a shared precursor mass and fragmentation pattern is typically

considered sufficient evidence for a confident identification.[75] However, retention time is an important additional piece of information that is not always accounted for in database matching. The approximately 30-second difference in retention time between the observed peak and authentic PAH in both plasma and urine suggests that this peak may represent a structural isomer or a different compound with similar mass spectrometric properties. Its consistent presence across all patient samples in both matrices further supports the possibility that the original feature assignment to PAH in the untargeted analysis was incorrect.

2.6. Summary

A targeted LC-MS/MS assay was developed for the simultaneous quantification of 24 analytes in plasma, serum, and urine. Following chromatographic and sample preparation optimization, a HILIC column was selected for separation, with acetonitrile-based protein precipitation and phospholipid removal for plasma and serum, and tandem HLB and MCX solid-phase extraction for urine. Three analytes were excluded from the method during development. Isobaric overlap between 3-methylcrotonylglycine and tiglylglycine was addressed through a post-acquisition signal correction approach. The optimized method was then carried forward for validation.

3. CHAPTER 3 - METHODS, DATA PROCESSING, AND ASSAY VALIDATION

Following assay development, the finalized extraction protocols and LC-MS/MS conditions were applied to clinical samples. Calibration strategy, sample preparation procedures, and validation studies were performed across both matrices to confirm the method is fit for clinical use. Representative chromatographs from a serum single-point calibrator are shown in **Figure A.3 and Figure A.4**.

3.1. Internal standard mix

All internal standards were combined in a small volume of 0.2% formic acid and 5% acetonitrile in water, and the volume was brought to 10 mL. The mix was combined for 10 minutes on a tube rocker and stored in aliquots at -80 °C. Internal standard stocks were stored at -20°C. The concentration of each internal standard stock and working internal standard concentration is detailed in **Table A.16**.

3.2. Extraction from plasma and serum

Secretion analytes were extracted from plasma and serum samples by protein precipitation with an organic solvent, followed by phospholipid removal and pH adjustment. In a filter plate (96-well Acroprep Advance 045µm; Pall PN: 8148), 300 µL of 0.2% formic acid in acetonitrile was added to 100 µL of serum or plasma and 10 µL of internal standard. The plate was agitated on a multitube vortexer for 10 minutes and then spun down at 3000 rpm for 10 minutes. The filtrate was transferred to a phospholipid removal plate (Phree, 30 mg; Phenomenex PN: 8E-S133-TGB) and placed on a positive pressure manifold (Biotage, Pressure+96) for filtration. The filtrate was diluted 1:1 (v/v) in 1.8% formic acid in acetonitrile, transferred to a 96-well V-bottom microplate

(Greiner PN: 651201), and sealed with an adhesive seal (Waters PN: 186006336). A summary of the plasma and serum extraction is shown in **Figure 3.1**.

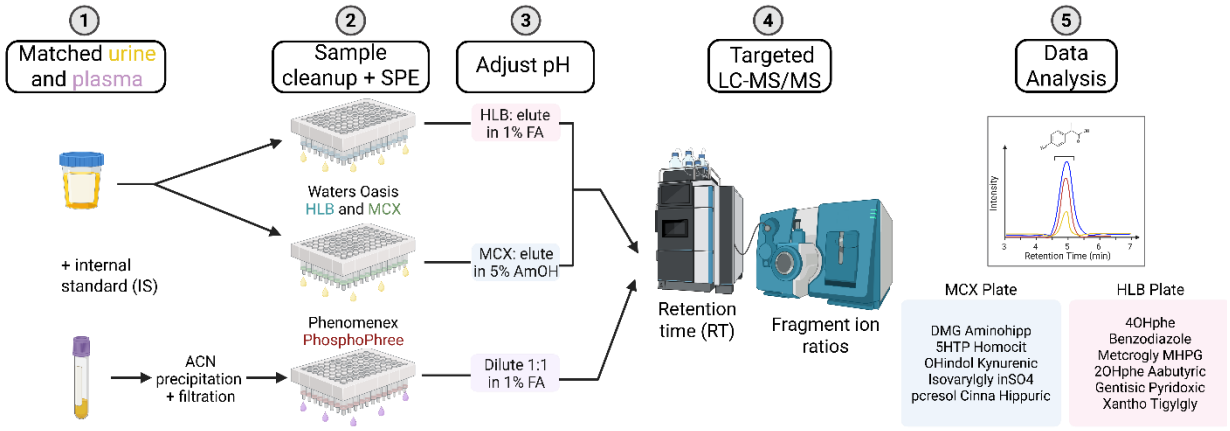

Figure 3.1. Renal secretion method overview. Matched urine and plasma samples were spiked with isotopically labeled internal standards (IS) before sample preparation (Step 1). Urine samples underwent solid-phase extraction (SPE) cleanup using Waters Oasis HLB and MCX sorbent plates, with HLB fractions eluted in 1% formic acid (FA) and MCX fractions eluted in 5% ammonium hydroxide (AmOH) (Steps 2–3). Plasma samples were prepared by acetonitrile (ACN) precipitation followed by filtration using a Phenomenex PhosphoPhree plate and dilution in 1% FA (Steps 2–3). All samples were analyzed by targeted liquid chromatography-tandem mass spectrometry (LC-MS/MS), with analytes identified using retention time (RT) and fragment ion ratios (Step 4). Data analysis was performed, with analytes distributed across HLB and MCX plates according to their chromatographic behavior (Step 5). Created with BioRender.com

3.3. Extraction from urine

Secretion analytes were extracted from urine samples using two SPE methods (the analytes eluted by each SPE method are listed in **Table A.11**). In two separate 96-well Deep Well Masterblock plates (Greiner PN: 780270), 20 µL of urine and 10 µL of internal standard were added. A volume of 970 µL of 0.2% formic acid in water was added to one plate and 970 µL of 2% formic acid in water to the other. The 0.2% formic acid solution was transferred to a hydrophilic-lipophilic binding (HLB) extraction plate (Oasis HLB 96-well Plate, 30 mg; Waters PN: WAT058951) and placed on a positive pressure manifold (Biotage, Pressure+96) for sample loading. The 2% formic acid solution was transferred to a mixed cation exchange (MCX)

extraction plate (Oasis MCX 96-well Plate, 30 mg; Waters PN: 186000248), after the MCX plate had been primed with diluent (2% formic acid in water). Each plate was washed with 1 mL of diluent (HLB: 0.2% formic acid in water; MCX: 2% formic acid in water), and the analytes were eluted (HLB elution: 1 mL of 1% formic acid in 12.4% water and 86.6% acetonitrile; MCX elution: twice with 500 µL 5% concentrated ammonium hydroxide in 38% methanol and 57% acetonitrile) into new 96-well Deep Well Masterblock plates (Greiner PN: 780270). Each plate was sealed with an adhesive seal (Waters PN: 186006336). A summary of the urine extraction is shown in **Figure 3.1 and Figure 3.2.**

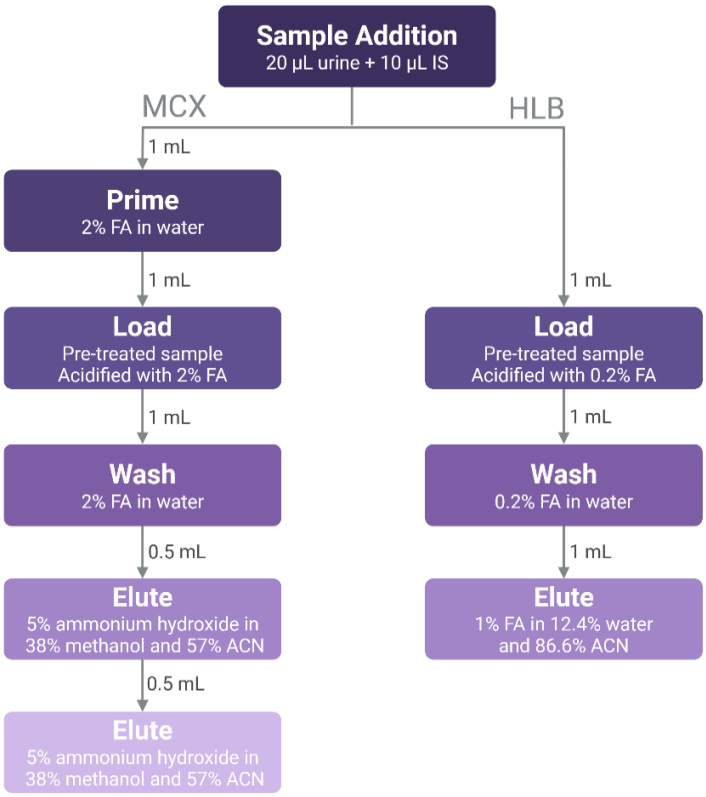

Figure 3.2. Urine solid-phase extraction (SPE) method overview. A total of 20 µL of urine was combined with 10 µL of internal standard (IS) and processed in parallel on MCX and HLB sorbent plates. For the MCX plate, samples were primed with 1 mL of 2% formic acid (FA) in water, loaded after acidification with 2% FA, washed with 1 mL of 2% FA in water, and eluted twice with 0.5 mL of 5% ammonium hydroxide in 38% methanol and 57% acetonitrile (ACN). For the HLB plate, samples were loaded after acidification with 0.2% FA, washed with 1 mL of 0.2% FA in water, and eluted with 1 mL of 1% FA in 12.4% water and 86.6% ACN. Created with BioRender.com

3.4. Liquid chromatography-tandem mass spectrometry

Eluted samples were injected into a liquid chromatography-tandem mass spectrometry system (Shimadzu LC-40 coupled to a Sciex 6500+) at a volume of 40 µL or 20 µL (plasma or serum and urine, respectively). Separation was achieved using an Atlantis Premier BEH Z-HILIC chromatographic column (BEH Z-HILIC 1.7µm 2.1 x 150mm; Waters PN: 186009983) operated under a gradient elution program (**Table A.17 and Table A.18**). The column eluate was directed to the mass spectrometer for analysis (**Table A.2–Table A.4**). Data were acquired using either unscheduled or scheduled MRMs (60-second window around the retention times specified in **Table A.11**). Endogenous peak areas (analyzed in Skyline) were normalized to the corresponding internal standard peak areas when isotopically labeled analogs were available (reported as peak area ratios). Two isotopes, 3-methylcrotonylglycine and tiglylglycine, were quantified using the method specified above. To minimize inter-run variability, peak area ratios (PARs) from study samples were normalized to the mean peak area ratio obtained from five replicates of a matrix-matched single-point calibrator included in each batch (NPARs). The normalized values were then multiplied by the estimated concentration of each analyte in the calibrator to determine the analyte concentration in study samples. Two matrix-matched control materials were included in every batch and carried through the full workflow to verify process consistency. Data processing was performed using Skyline, Microsoft Excel, and RStudio.[76]

3.5. Calibrators and quality control materials

Calibrators and quality control (QC) materials were prepared by pooling discarded human serum samples, followed by aliquoting and storage at -80°C. The low QC material was generated from a serum pool with low creatinine concentration (0.49 mg/dL), and the high QC material was

prepared from a serum pool with elevated creatinine (7.09 mg/dL) and further spiked with a concentrated high-level spike mixture.

The single-point calibrator (SPC) was prepared from a separate serum pool with a final creatinine concentration of 0.82 mg/dL and subsequently spiked with a low-level spike mixture to achieve analyte concentrations representative of average patient values.

3.5.1. Single-point calibrator concentration assignment

Analyte concentrations for the SPC were assigned by multiplying the known concentration of the internal standard (IS) added to each sample by the corresponding peak area ratio (SPC peak area divided by IS peak area), as determined using Skyline software. Measurements were conducted over three days with five replicates per day for serum samples, and on a single day with five replicates for urine samples.

For analytes without a matched isotopically labeled internal standard, structurally similar surrogate internal standards were selected and applied using the same calculation approach (**Table A.19**).

3.6. Method validation

3.6.1. Precision

Inter- and intra-assay variability were assessed by analyzing four sample types (SPC, HiQC, LoQC, and either an unspiked gold-top serum sample or a discarded urine sample), with five replicates of each sample measured over five consecutive days.

For each analyte, between-day and within-day variability were calculated, and the total percent coefficient of variation (%CV) was determined using the following equation:

$$\text{Total } \%CV = \sqrt{(\text{between-day } \%CV)^2 + (\text{within-day } \%CV)^2}$$

The total %CV values obtained for the four sample types were averaged to obtain the final reported variability (**Table 3.1**).

Table 3.1. Total percent coefficient of variation (%CV) for all analytes across serum and urine matrices. Inter- and intra-assay variability were assessed by analyzing five replicates of four sample types (SPC, HiQC, LoQC, and an unspiked matrix sample) over five consecutive days. Between-day and within-day variability were calculated for each analyte, and the total %CV was determined and averaged across all four sample types for each matrix.

Compound	Serum (Total %CV)	Urine (Total %CV)
4-Hydroxyphenylacetic acid	10%	10%
N2,N2-Dimethylguanosine	11%	4%
5-Fluoro-1-methyl-1H-1,3-benzodiazole[a]	6%	5%
Pimelic acid	10%	5%
3-Methylcrotonylglycine	12%	7%
3-Methoxy-4-hydroxyphenylglycol sulfate	12%	11%
2-[(4-Aminobenzoyl)-amino]acetic acid[a]	7%	7%
6'-Sialyl-N-acetyllactosamine[b]	--	--
2-Hydroxyphenylacetic acid	6%	7%
1,4-Cyclohexanedicarboxylic acid[a]	27%	24%
5-Hydroxytryptophan	35%	12%
4-Acetamidobutyric acid	11%	27%
L-Homocitrulline	11%	5%
Gentisic acid	8%	5%
5-Hydroxy-3-indoleacetic acid	20%	15%
Kynurenic acid	11%	6%
4-Pyridoxic acid	14%	5%
N-Isovalerylglycine	6%	4%
Indoxyl sulfate	11%	8%
P-cresol sulfate	7%	17%
Xanthosine	13%	7%
Tiglylglycine	16%	8%
N-Cinnamoylglycine	15%	6%
Hippuric acid	18%	8%

[a] LoQC and low patient sample %CVs were excluded from the average because the analyte was not detected in these samples.
[b] 6′-Sialyl-N-acetyllactosamine was excluded from the assay prior to validation.

3.6.2. Linearity and limits of quantification

Linearity was evaluated by gravimetrically mixing a high-concentration spiked sample with a low-concentration sample across seven mixing levels (12.5–87.5%) in both serum and urine over three days. Linearity was assessed by calculating the coefficient of determination (R^2) and the percent bias at each mixing level relative to the gravimetrically assigned concentrations. Precision was determined as the mean %CV from three replicates analyzed over three days. Results are summarized in **Table B.1 and Table B.2**.

Overall, linearity was acceptable across both matrices, with most analytes achieving $R^2 \geq 0.95$ and bias within 85–115%. Analytes lacking matched internal standards, including 4-acetamidobutyric acid and 1,4-cyclohexanedicarboxylic acid, showed elevated %CV and bias deviations, particularly at lower mixing levels.

The LLOQ was determined by diluting a high-concentration sample with a matrix-matched blank (water for urine; Mass Spect Gold (MSG) 3000 for serum) to 20–80% of the original concentration in triplicate, with acceptance criteria of |bias| ≤20% and %CV ≤20% (**Table B.3 and Table B.4**). Most analytes met criteria at the 20% dilution level in both matrices. In urine, 3-methoxy-4-hydroxyphenylglycol sulfate, 2-[(4-aminobenzoyl)-amino]acetic acid, 5-hydroxytryptophan, and 4-acetamidobutyric acid failed to meet acceptance criteria at any dilution level so a LLOQ was not determined. In serum, 5-fluoro-1-methyl-1H-1,3-benzodiazole, 2-[(4-aminobenzoyl)-amino]acetic acid, 5-hydroxytryptophan, and tiglylglycine failed to meet criteria at any dilution level so a LLOQ was not determined.

3.6.3. Interference

Interference studies were performed in serum and urine using a spike-recovery approach. For urine, specimens with elevated total protein, increased specific gravity, and hemolysis were evaluated by comparing with a normal control specimen (**Figure B.1**). Each specimen type was spiked with both low- and high-concentration analyte mixtures and analyzed in triplicate across two independent patient samples (P1 and P2). For each spike level, the change in response was calculated by subtracting the mean signal of the three unspiked replicates from each individual spiked replicate. Spike recovery under each interferent condition was then compared to recovery in the corresponding normal control specimen. For serum, specimens with elevated bilirubin (38–39 mg/dL), creatinine (15–18 mg/dL), severe hemolysis, triglycerides (388–460 mg/dL), and total protein (8.6–9.1 g/dL) were compared with a normal control specimen using the same spike-recovery methodology (**Figure B.2**).

Overall, the majority of analytes demonstrated acceptable recovery in the presence of each interferent in both matrices, with the greatest susceptibility to interference observed in analytes lacking a matched internal standard. In serum, 4-acetamidobutyric acid showed interference from elevated bilirubin and creatinine, 3-methoxy-4-hydroxyphenylglycol sulfate was affected by hemolysis in P1, and 2-[(4-aminobenzoyl)-amino]acetic acid showed apparent ion suppression across all interferent conditions. In urine, 3-methoxy-4-hydroxyphenylglycol sulfate showed notably reduced recovery in the high specific gravity specimen (P2) at both concentration levels. Gentisic acid showed reduced recovery under hemolysis conditions in P1, and 4-acetamidobutyric acid demonstrated increased variability at the high concentration level, though no single interferent resulted in complete failure.

3.6.4. Stability

Stability was evaluated by subjecting urine and serum single point calibrator (SPC) samples to multiple stress conditions: room temperature for 24 hours (RT 24hr), refrigeration at 4°C for 24 hours (4°C 24hr), and one, two, and three freeze-thaw cycles (FT ×1, FT ×2, FT ×3) (**Figure B.3 and Figure B.4**). Following each condition, samples were prepared and analyzed in quintuplicate and compared with a freshly thawed SPC control stored at -80°C. Stability was assessed by comparing each condition to the fresh control mean ± 2SD.

Overall, the majority of analytes demonstrated acceptable stability across all conditions in both matrices. In urine, 4-acetamidobutyric acid showed elevated recovery under the RT 24hr condition, while 5-hydroxy-3-indoleacetic acid exhibited increased variability following FT ×1. Lower recovery was observed for 4-pyridoxic acid across freeze-thaw cycles, and high variability across all conditions was noted for p-cresol sulfate and xanthosine. In serum, gentisic acid showed reduced recovery following RT 24hr storage, and N2,N2-dimethylguanosine showed elevated recovery following 4°C 24hr storage.

3.7. Summary

The finalized method employed protein precipitation with phospholipid removal for plasma and serum, and tandem HLB and MCX solid-phase extraction for urine, with all samples analyzed by HILIC LC-MS/MS. Analyte concentrations were determined using a single-point calibrator, with batch-to-batch normalization and matrix-matched quality controls included in every run. Validation studies encompassing precision, linearity, interference, and stability were performed across both matrices to confirm that the method is fit for clinical use.

4. CHAPTER 4 – PRELIMINARY CHARACTERIZATION OF TUBULAR SECRETORY FUNCTION IN HEALTHY ADULTS AND CKD PATIENTS

Having developed and validated the TSS assay, it was next applied in a clinical population, including patients with CKD, to evaluate the ability of the assay to measure proximal tubular secretory function. Previous research utilized the Proximal Tubular Clearance of Renal Medication (PROCLAIM) study cohort, in which participants were recruited across a spectrum of estimated glomerular filtration rate (eGFR; 21–140 ml/min/1.73 m^2) to investigate this relationship.[47] Participants received single doses of furosemide and famciclovir (which is metabolized to penciclovir), two medications primarily cleared via tubular secretion. Timed urine collections and sequential plasma samples spanning the urine collection were obtained to calculate renal clearance. For the present analysis, the tubular secretory solute (TSS) assay was implemented for 48 PROCLAIM participants. Per participant, this included three to four plasma samples collected between baseline and 10 hours post-dose, along with a paired timed urine sample collected from the time of dose administration to 10 hours post-dose. These measurements enabled comparison of furosemide and famciclovir clearance with TSS clearance. A schematic overview of the study design is presented in **Figure 4.1.**

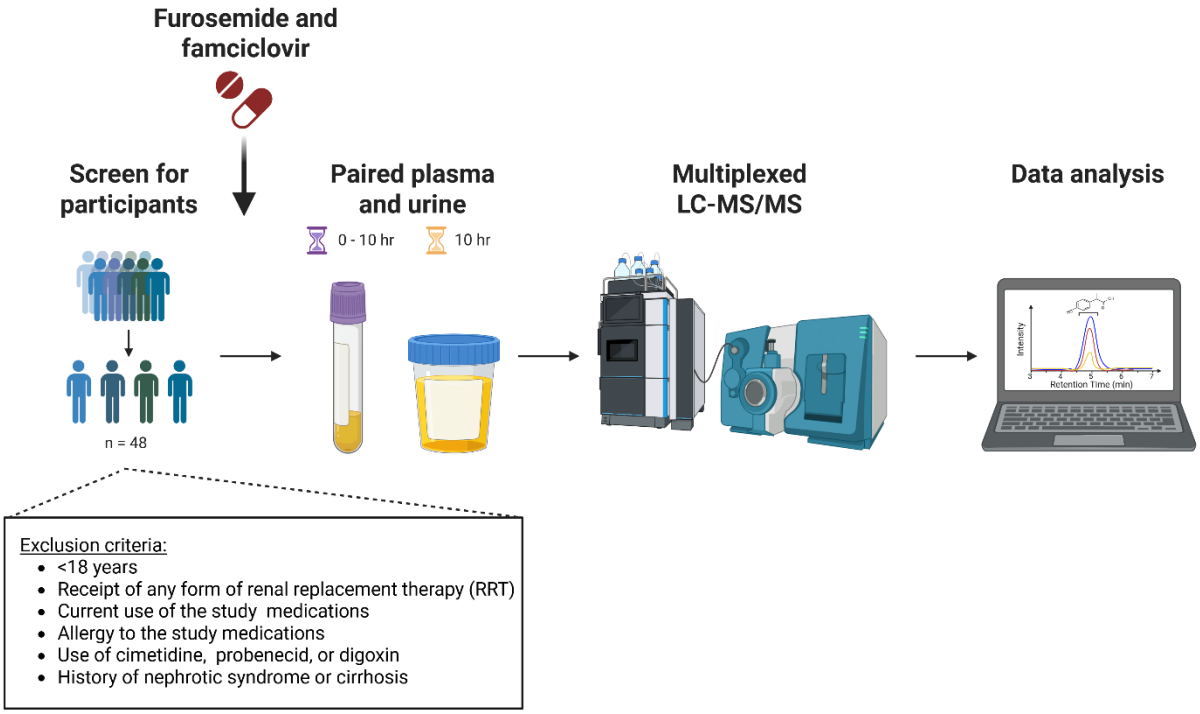

Figure 4.1. PROCLAIM study design. Participants (n = 48) were screened for eligibility and administered single doses of furosemide and famciclovir. Sequential plasma samples were collected between 0 and 10 hours post-dose, and a paired timed urine sample was collected over the same 10-hour period. Plasma and urine samples were measured using the TSS assay. Exclusion criteria included age <18 years, receipt of any form of renal replacement therapy, current use of or allergy to the study medications, use of cimetidine, probenecid, or digoxin, and history of nephrotic syndrome or cirrhosis. Created with BioRender.com

4.1. Solute characteristics

Each TSS was evaluated using multiple criteria: calculated clearance, plasma biological and assay variability (expressed as percent coefficient of variation [%CV] across all plasma measurements), and degree of protein binding (percentage values derived from prior studies[42,49]) (**Table 4.1**). Calculated clearance ranged from 3 to 439 mL/min; within-patient plasma variability ranged from 9% to 72% CV, and the degree of protein binding ranged from 6% to 95%. Clearance exceeding eGFR indicates that solutes likely undergo tubular secretion in addition to filtration. Low plasma variability is desirable for biomarker selection, and higher

protein binding suggests a greater reliance on tubular secretion, as protein-bound solutes do not easily pass through the glomerular basement membrane.

Table 4.1. PROCLAIM solute characteristics. Solute plasma variability (percent coefficient of variation [%CV]), degree of protein binding (%), and clearance (mL/min) in the PROCLAIM cohort. Percent coefficient of variation (%CV) reflects inter-individual variability in plasma concentrations across the cohort, protein binding (%) reflects the fraction of each solute bound to plasma proteins, and clearance (mL/min) reflects the rate of solute removal. Solutes are ordered by ascending sum of R^2 as reported in Table 4.2.

Solute	CV (%)	Protein Bound (%)	Clearance (mL/min)
Aminohippuric acid	72	72	45
Benzodiazole	31	22	3
1,4-Cyclohexanedicarboxylic acid	58	15	55
Pimelic acid	39	12	16
5-Hydroxytryptophan	24	34	12
Hippuric acid	56	68	340
3-Methylcrotonylglycine	48	17	439
Homocitrulline	20	11	40
Cinnamoylglycine	33	91	137
P-cresol sulfate	13	97	7
Isovalerylglycine	29	6	425
Gentisic acid	24	64	68
Indoxyl sulfate	20	97	45
3-Methoxy-4-hydroxyphenylglycol	16	18	106
2-Hydroxyphenylacetic acid	13	54	43
4-Hydroxyphenylacetic acid	22	50	258
Xanthosine	18	11	211
Pyridoxic acid	25	83	175
Tiglylglycine	34	33	416
5-Hydroxy-3-indoleacetic acid	31	45	299
4-Acetamidobutyric acid	9	18	108
Kynurenic acid	18	97	159
N2,N2-Dimethylguanosine	12	29	274

4.2. Solute associations with medication clearance in the proximal tubule

Associations between each solute and tubular secretion were assessed by correlating solute measures with furosemide and penciclovir clearance, quantified using the Pearson coefficient of determination (R^2) from linear regression models. For each solute, four relationships were evaluated: solute clearance versus furosemide clearance, solute clearance versus penciclovir

clearance, mean plasma solute concentration versus furosemide clearance, and mean plasma solute concentration versus penciclovir clearance (**Table 4.2**). Correlation with solute clearance reflects the extent of proximal tubular secretion, whereas correlation with mean plasma concentration suggests potential utility for simplified, plasma-based applications that may be more feasible in clinical settings.

Table 4.2. PROCLAIM solute R^2 relationships with proximal tubule medication clearance. Coefficient of determination (R^2) values for four relationships evaluated per solute: solute clearance vs. furosemide clearance, solute clearance vs. penciclovir clearance, plasma solute concentration vs. furosemide clearance, and plasma solute concentration vs. penciclovir clearance. The sum of R^2 across all four relationships is shown. Solutes are ordered by ascending sum of R^2. Cells are color-coded: green = $R^2 \geq 0.5$, red = $R^2 < 0.5$; sum of R^2: green ≥ 2.0, red < 2.0. CL = clearance; PL = plasma concentration.

PROCLAIM Solute R^2 Relationships

Sorted by sum of R^2 (ascending). R^2: green ≥0.5, red <0.5. CL = clearance; PL = plasma concentration.

Solute	R^2				
	Furosemide CL – Solute CL	Penciclovir CL – Solute CL	Furosemide CL – Solute PL	Penciclovir CL – Solute PL	Sum R^2
Aminohippuric acid	0.01	0.02	0.01	0.02	0.06
Benzodiazole	0.01	0.01	0.07	0.10	0.19
1,4-Cyclohexanedicarboxylic acid	0.05	0.01	0.05	0.08	0.19
Pimelic acid	0.17	0.20	0.07	0.05	0.49
5-Hydroxytryptophan	0.31	0.40	0.14	0.17	1.02
Hippuric acid	0.39	0.48	0.14	0.14	1.15
3-Methylcrotonylglycine	0.42	0.65	0.03	0.08	1.18
Homocitrulline	0.34	0.35	0.28	0.30	1.27
Cinnamoylglycine	0.58	0.67	0.02	0.06	1.33
P-cresol sulfate	0.55	0.68	0.04	0.12	1.39
Isovalerylglycine	0.50	0.70	0.07	0.12	1.39
Gentisic acid	0.60	0.70	0.08	0.07	1.45
Indoxyl sulfate	0.60	0.67	0.12	0.14	1.53
3-Methoxy-4-hydroxyphenylglycol	0.42	0.53	0.42	0.41	1.78
2-Hydroxyphenylacetic acid	0.51	0.65	0.33	0.30	1.79
4-Hydroxyphenylacetic acid	0.54	0.73	0.26	0.27	1.80
Xanthosine	0.45	0.54	0.42	0.40	1.81
Pyridoxic acid	0.69	0.81	0.16	0.18	1.84
Tiglylglycine	0.53	0.70	0.30	0.31	1.84
5-Hydroxy-3-indoleacetic acid	0.62	0.72	0.37	0.41	2.12
4-Acetamidobutyric acid	0.40	0.57	0.56	0.69	2.22
Kynurenic acid	0.70	0.82	0.50	0.29	2.31
N2,N2-Dimethylguanosine	0.61	0.80	0.55	0.65	2.61

Several solutes had strong associations across these evaluation metrics (**Table 4.1 and Table 4.2**). Notably, N2,N2-dimethylguanosine, kynurenic acid, and 4-acetamidobutyric acid had robust associations across all four secretion-related measures and showed low plasma variability. Additional solutes, including 5-hydroxy-3-indoleacetic acid, tiglylglycine, pyridoxic acid, xanthosine, 4-hydroxyphenylacetic acid, 2-hydroxyphenylacetic acid, and 3-methoxy-4-hydroxyphenylglycol also performed well overall, although their correlations based solely on plasma measurements were comparatively weaker. In contrast, several analytes demonstrated limited performance across the evaluated metrics and were not prioritized for further investigation. These included 1,4-cyclohexanedicarboxylic acid and pimelic acid (see Section 2.4.1), 2-[(4-aminobenzoyl)-amino]acetic acid (see Section 2.5), 5-fluoro-1-methyl-1H-1,3-benzodiazole, hippuric acid, 5-hydroxytryptophan, and 3-methylcrotonylglycine.

4.3. Summary

Overall, these findings support several candidate biomarkers of proximal tubular secretion with potential use across a range of kidney function. Analytes with strong associations with proximal tubule medication clearance, low inter-individual variability, and higher endogenous clearances emerged as the most promising candidates for further evaluation. However, this study was limited to healthy adults and individuals with CKD, and with a small sample size, it remains unclear how these biomarkers perform in more acute clinical settings. The next phase of this work aimed to evaluate these candidate tubular secretory biomarkers in critically ill patients, particularly in the context of acute kidney injury (AKI).

5. CHAPTER 5 – ANALYSIS OF TUBULAR SECRETORY FUNCTION IN CRITICALLY ILL PATIENTS

Acute kidney injury (AKI) is a major complication in many critically ill patients, contributing to increased mortality, longer hospitalizations, and a greater likelihood of requiring dialysis.[77] This disease can lead to the development of CKD and end-stage renal disease and causes ~1.7 million deaths every year.[9] Although diagnosis of AKI commonly relies on rising serum creatinine as a proxy for GFR, this approach does not fully capture the underlying cellular damage that often targets the proximal tubular epithelium.[78,79] Additionally, clinical AKI is a heterogeneous syndrome that can result from a range of processes, including volume depletion, hemodynamic instability, tubular damage, or medication effects, and a creatinine-based diagnosis does not distinguish between these underlying mechanisms.[80]

The goal of the present study was to characterize tubular secretory solute (TSS) clearance in critically ill patients at ICU admission and to evaluate associations between TSS clearance and creatinine clearance, and adverse clinical outcomes including incident AKI and major adverse kidney events at 30 days (MAKE30). The Role of Kidney Tubular Secretion in Critical Illness (ROKIT) cohort consists of critically ill adults admitted to intensive care units (ICUs) at Harborview Medical Center and Vanderbilt University Medical Center. Timed plasma and urine samples were collected on ICU days 1, 2, 3, and 8, with an additional collection at day 90 when available. Per day, this included two plasma samples collected at baseline and 4 hours, along with a paired timed urine sample collected over 4 hours. These samples were analyzed using the targeted renal secretion assay, measuring 16 TSS prioritized in the PROCLAIM cohort. An overview of the study design and enrollment criteria is presented in **Figure 5.1**.

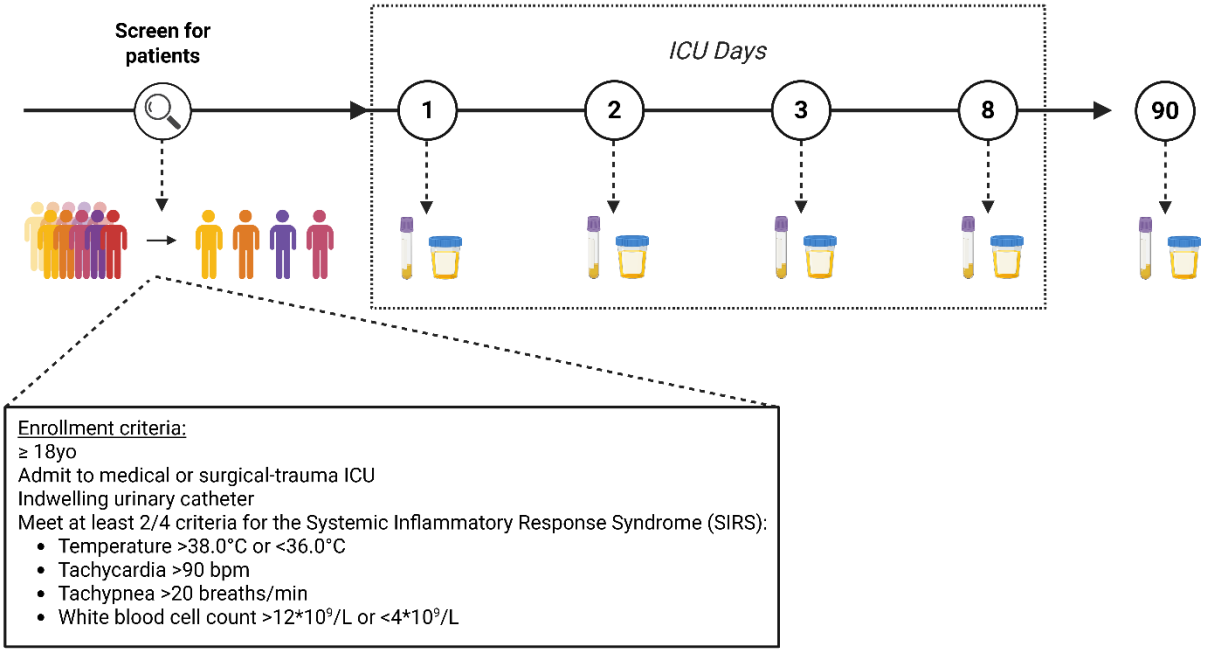

Figure 5.1. ROKIT enrollment criteria and sample collection timeline. Patients were screened for eligibility and enrolled at intensive care unit (ICU) admission. Enrollment required age ≥18 years, admission to a medical or surgical-trauma ICU, presence of an indwelling urinary catheter, and meeting at least 2 of 4 criteria for the Systemic Inflammatory Response Syndrome (SIRS): temperature >38.0°C or <36.0°C, tachycardia >90 bpm, tachypnea >20 breaths/min, or white blood cell count >12×10⁹/L or <4×10⁹/L. Plasma and timed urine samples were collected over four hours at ICU days 1, 2, 3, 8, and 90. Created with BioRender.com

5.1. Study characteristics

The study population consisted of 246 participants with a median age of 58 years (IQR, 43.7–66.3), of whom 39% were female, and 87% were white (**Table 5.1**). At baseline, the median serum creatinine concentration was 0.9 mg/dL (IQR, 0.8–1.1); 34% of participants had sepsis, 43% were receiving mechanical ventilation, 37% were receiving vasopressors, and 25% had diabetes mellitus. The median APACHE II score was 12 (IQR, 8–19) and the median SOFA score was 5 (IQR, 1–10), indicating moderate baseline illness severity with evidence of organ dysfunction and heterogeneity across the cohort.

Table 5.1. Baseline characteristics of the ROKIT study cohort. Baseline demographic and clinical characteristics of all enrolled patients (n = 246). Values are median (Q1, Q3) for continuous variables and n (%) for categorical variables.

Table 1. Baseline characteristics (n = 246)

Characteristic	N = 246[1]
Age, years	58.1 (44.0, 66.3)
Sex	
Male	151 (61%)
Female	95 (39%)
Race	
White	212 (87%)
Black or African American	25 (10%)
Other	7 (2.9%)
BMI, kg/m²	29.0 (24.0, 35.6)
APACHE II score	12.0 (8.0, 18.0)
SOFA score	5.0 (1.0, 9.0)
Sepsis at baseline	83 (34%)
Mechanical ventilation	106 (43%)
Vasopressor use	90 (37%)
Diabetes mellitus	61 (25%)
Baseline creatinine, mg/dL	0.9 (0.8, 1.1)

[1] Median (Q1, Q3); n (%)

5.2. Solute panel and creatinine clearance

To establish the relationship between TSS clearances and creatinine clearance as a marker of glomerular filtration, average per-patient clearances across ICU days 1, 2, 3, 8, and 90 (as available) for 16 urinary solutes were correlated with average creatinine clearance across 244 patients (**Figure 5.2**); three patients were excluded for implausibly high creatinine or solute clearances. All pairwise correlations were statistically significant at $p < 0.001$. Clearances of 14 of the 16 solutes were moderately to strongly correlated with creatinine clearance (Pearson $r \geq 0.5$), while 3-methoxy-4-hydroxyphenylglycol ($r = 0.32$) and p-cresol sulfate ($r = 0.38$) showed

weaker associations (**Figure 5.2 and Figure 5.3**). 4-Hydroxyphenylacetic acid, N2,N2-dimethylguanosine, and homocitrulline had the strongest overall correlations with creatinine clearance (r = 0.76, r = 0.75, and r = 0.75, respectively).

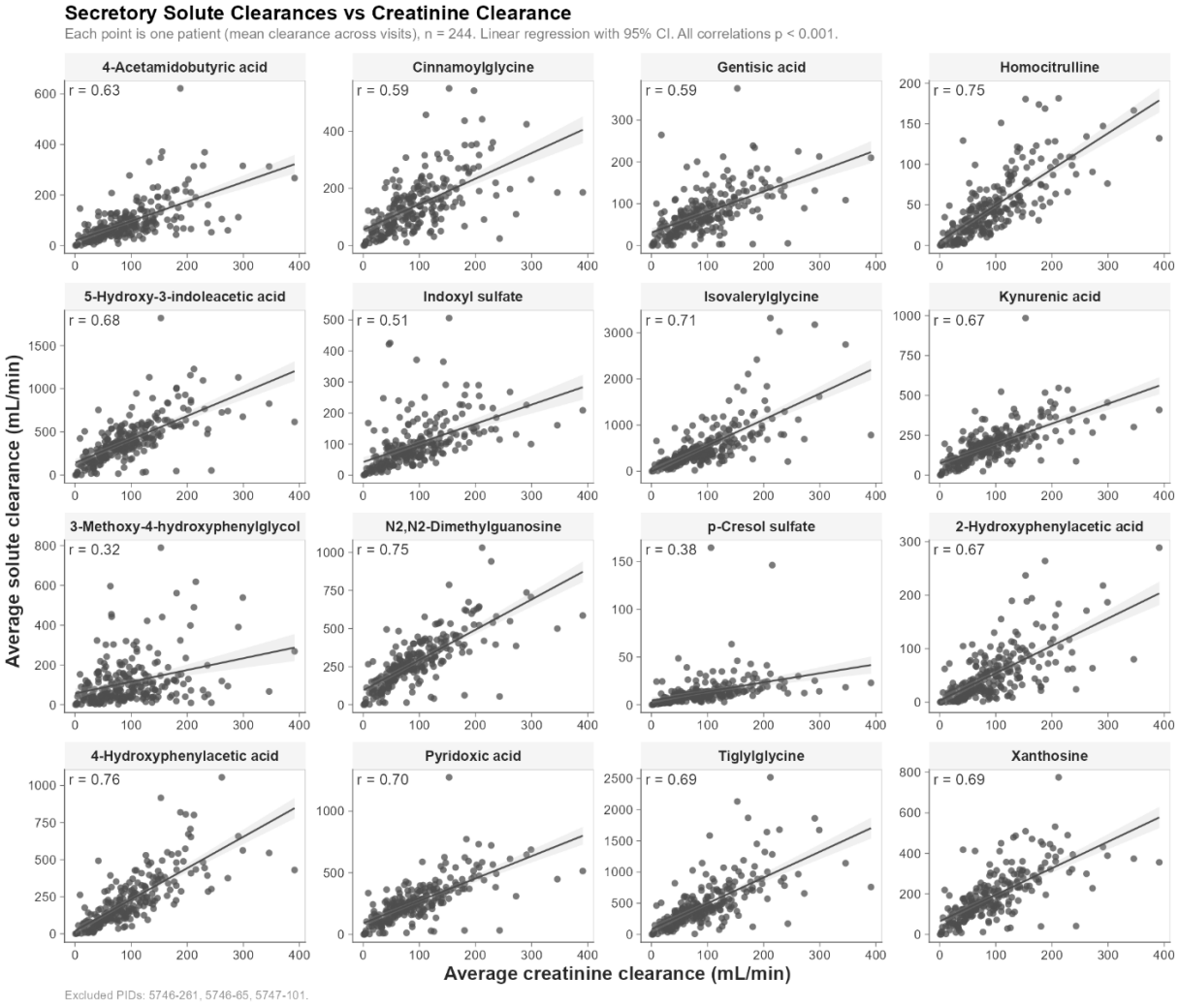

Figure 5.2. Correlations between average solute clearance and average creatinine clearance across 16 tubular secretory solutes. Scatter plots show the relationships between average solute clearance (y-axis) and average creatinine clearance (x-axis) across 16 tubular secretion solutes, with linear regression and Pearson correlation coefficients. Each panel represents an individual solute, with each point corresponding to a participant's average value across available measurements. Solid lines indicate linear regression fit with shaded 95% confidence intervals. Pearson correlation coefficients (r) are displayed within each panel. The x-axis represents average creatinine clearance (mL/min), and the y-axis represents average solute clearance (mL/min), with scales varying by solute. Three data points were excluded for implausibly high creatinine or solute clearances.

5.2.1. DMG as a panel-wide correlate

N2,N2-dimethylguanosine (DMG) stood out as the most broadly correlated solute across the panel, ranking among the top three correlates for the majority of other solutes (indicated by diamonds in **Figure 5.3**). With over half of the pairwise Pearson r values exceeding 0.80, DMG may act as a proxy for the clearance of many other analytes in the panel. However, not all pairwise relationships appear linear (**Figure 5.2**). Non-linearity was assessed visually using LOESS curves and the Ramsey RESET test with comparison of linear and quadratic model fit; isovalerylglycine and tiglylglycine showed the clearest evidence of non-linearity, with quadratic models providing a meaningfully better fit for these two solutes.

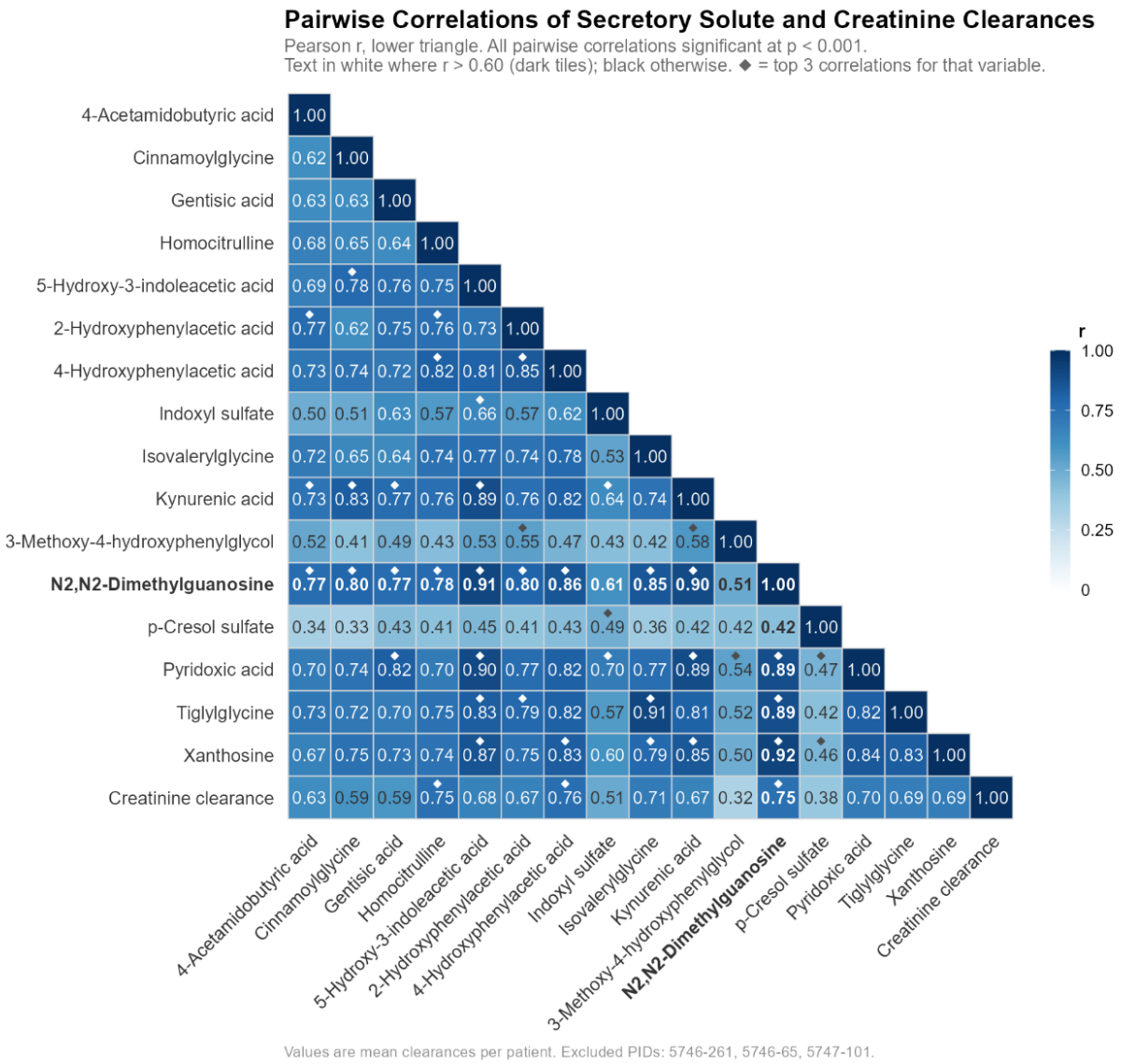

Figure 5.3. Pairwise Pearson correlations of secretory solute and creatinine clearances. Heatmap showing pairwise Pearson r values for average per-patient clearances of 16 secretory solutes and creatinine clearance (n = 244). Values represent mean clearances across all available study visits (ICU days 1, 2, 3, 8, and 90). All pairwise correlations were statistically significant at $p < 0.001$. Tile color represents the magnitude of the correlation coefficient, ranging from white (r = 0) to dark blue (r = 1). Correlation values are displayed in white where r > 0.60 and in black otherwise, and diamond markers (◆) indicate the top three correlations for each variable. Three patients were excluded for implausibly high creatinine or solute clearances.

The correlation between DMG and creatinine clearance (r = 0.75) displayed more scatter than many of the inter-solute correlations, indicating substantial variability between these two biomarkers despite their moderate overall association (**Figure C.1**). This suggests that DMG and

creatinine clearance are not redundant measures, and that DMG may capture aspects of tubular secretory function that are not fully reflected by creatinine-based filtration markers.

5.3. Solute panel and clinical outcome associations

Although timed urine collection for solute clearance measurement is feasible in research settings, plasma-based measurements would be more practical for routine clinical screening, as they require only a single blood draw and do not depend on accurate urine collection. A plasma-based secretory solute biomarker that does not require timed urine collection, analogous to eGFR for filtration, would be a more clinically accessible tool. Both baseline clearances (from ICU Day 1) and plasma concentrations of the TSS panel were analyzed for associations with incident AKI and MAKE30 outcomes, with a focused analysis on DMG.

5.3.1. Full panel outcome associations

Baseline clearances of all 16 solutes were associated with both MAKE30 and incident AKI outcomes, defined as the absence of AKI at enrollment with development of AKI during hospitalization. Adjusted odds ratios (ORs) and 95% confidence intervals (CIs) were estimated using separate logistic regression models for each analyte, adjusted for baseline creatinine, creatinine clearance, age, sex, and SOFA score. Raw p-values and Benjamini-Hochberg FDR-adjusted p-values were calculated across all analytes within each outcome panel, including filtration markers (**Figure 5.4A and C, Table C.1A and Table C.2A**). For incident AKI, 13 of 16 solute clearances remained significant after FDR correction, with ORs per 1-SD increase in log-transformed clearance ranging from 0.35 to 0.79, indicating that higher clearance at baseline was associated with lower odds of developing AKI. All 16 solute clearances remained significant after FDR correction for MAKE30, with ORs ranging from 0.23 to 0.49.

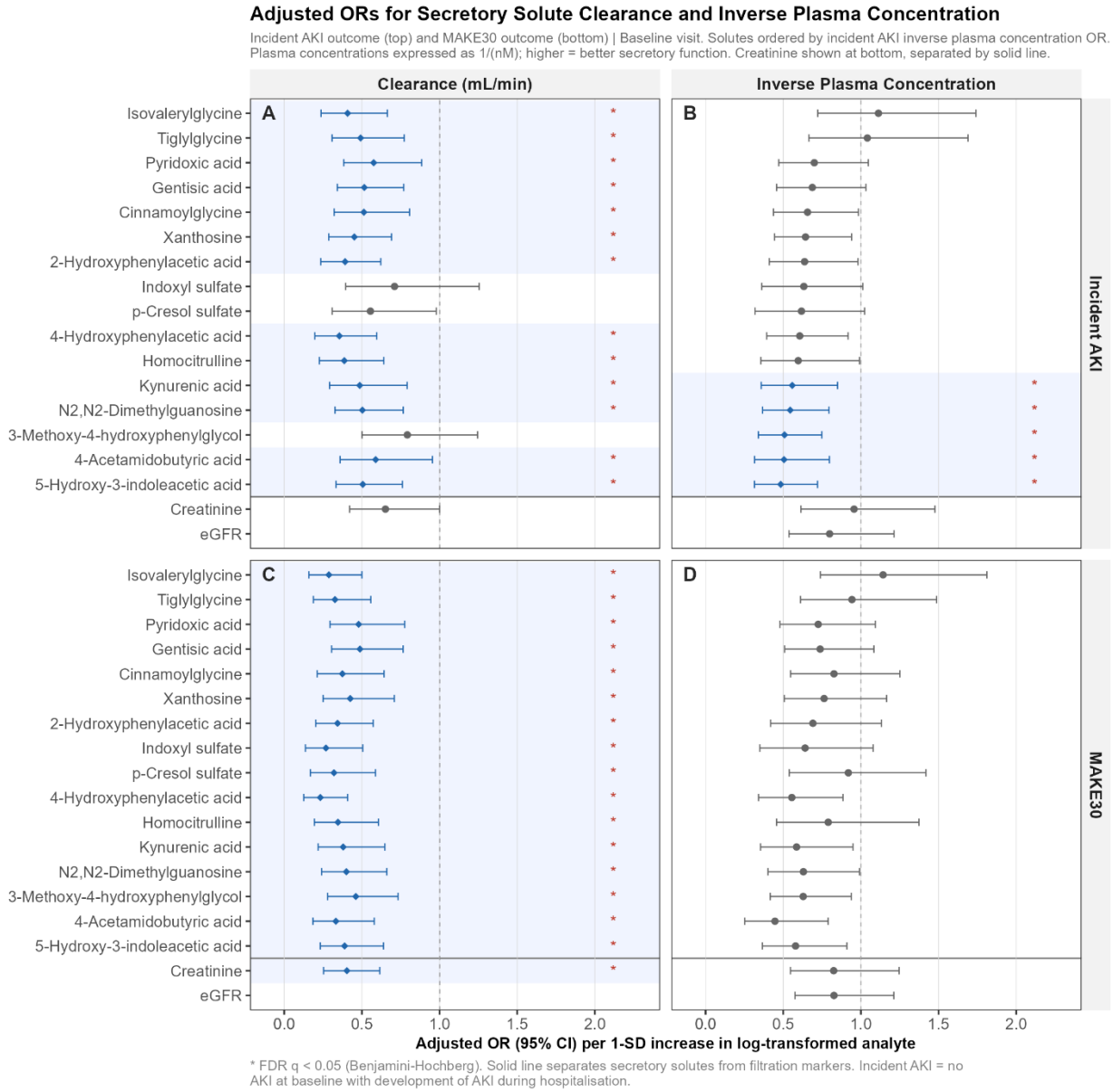

Figure 5.4. Adjusted odds ratios for secretory solute clearance and inverse plasma concentration in relation to incident AKI and MAKE30 outcomes at baseline. Panels A and C show adjusted ORs for solute clearance (mL/min); panels B and D show adjusted ORs for inverse plasma concentration (1/nM), where higher values indicate better secretory function. Filtration markers (creatinine clearance in A/C; inverse-creatinine concentration and eGFR in B/D) are shown below the solid horizontal line for comparison. Each point represents the adjusted OR per 1-SD increase in the log-transformed analyte for one solute; horizontal bars are 95% confidence intervals. Blue points and shading indicate FDR-significant associations ($q < 0.05$, Benjamini-Hochberg); grey indicates non-significant associations. Red asterisks (*) denote FDR $q < 0.05$. Secretory solute models were adjusted for baseline creatinine, creatinine clearance, age, sex, and SOFA score. Creatinine clearance was adjusted for baseline creatinine, age, sex, and SOFA score; inverse-creatinine and eGFR were adjusted for creatinine clearance, age, sex, and SOFA score. All analyte predictors were log-

transformed and standardized before modelling. Solutes are ordered by incident AKI inverse plasma concentration OR and this ordering is consistent across all panels. Incident AKI was defined as the development of AKI after enrollment in patients without AKI at baseline.

Baseline inverse plasma concentrations were significantly associated with incident AKI for five analytes after FDR correction: 4-acetamidobutyric acid, 5-hydroxy-3-indoleacetic acid, kynurenic acid, 3-methoxy-4-hydroxyphenylglycol, and N2,N2-dimethylguanosine (**Figure 5.4B, Table C.1B**). Plasma concentrations were expressed on the inverse scale (1/[plasma concentration]) because inverse values are directionally proportional to kidney secretory function. ORs per 1-SD increase in log-transformed inverse plasma concentration ranged from 0.48 to 0.69, indicating that lower inverse concentration (reflecting higher raw plasma concentration and impaired secretory function) was associated with higher odds of incident AKI. For MAKE30, six analytes showed nominally significant associations but none survived FDR correction, with ORs ranging from 0.45 to 0.83 (**Figure 5.4D, Table C.2B**). With the exception of 4-hydroxyphenylacetic acid, the analytes reaching significance for incident AKI were the same as those showing nominal associations for MAKE30, suggesting a consistent signal that may reach statistical significance in future studies with larger sample sizes or a narrower analyte panel.

Baseline creatinine clearance was significantly associated with MAKE30 (adjusted OR 0.40, $p < 0.001$) but did not survive FDR correction for incident AKI (OR 0.65, $p = 0.047$, FDR $q = 0.053$). Neither inverse creatinine concentration nor eGFR was significantly associated with either outcome after FDR correction (**Table C.1 and Table C.2**). Secretory solute clearances remained significantly associated with both outcomes after adjustment for creatinine clearance, suggesting that tubular secretory function captures prognostic information that is at least partially independent of glomerular filtration. Together, these findings suggest that secretory solute

clearance and conventional filtration-based markers are complementary rather than redundant, with each reflecting distinct aspects of kidney function.

5.3.2. DMG plasma concentration and clinical outcomes

DMG was selected for focused analysis based on its broad correlation with other solutes in the panel and its association with creatinine clearance, suggesting it may serve as a representative marker of overall secretory function (**Figure 5.3 and Figure C.1**). Baseline plasma DMG concentration was compared across the maximum AKI stage reached during hospitalization and by MAKE30 status.

Baseline inverse-DMG concentration differed significantly across the maximum AKI stage reached during hospitalization (Kruskal-Wallis test with Dunn post-hoc pairwise comparisons, Bonferroni-corrected; **Figure 5.5A–B**). Patients with no AKI had substantially higher inverse-DMG than those with AKI Stage 1, Stage 2, or Stage 3 (all $p < 0.001$), reflecting progressive plasma DMG accumulation with worse kidney injury. A similar pattern was observed for DMG clearance, which was significantly lower in patients with AKI Stage 1, Stage 2, and Stage 3 compared to those without AKI (all $p < 0.001$; **Figure C.2A–B**). A significant difference was also observed between AKI Stage 1 and Stage 3 ($p < 0.05$), suggesting that DMG clearance reflects the continuum of kidney injury severity across the full spectrum of AKI.

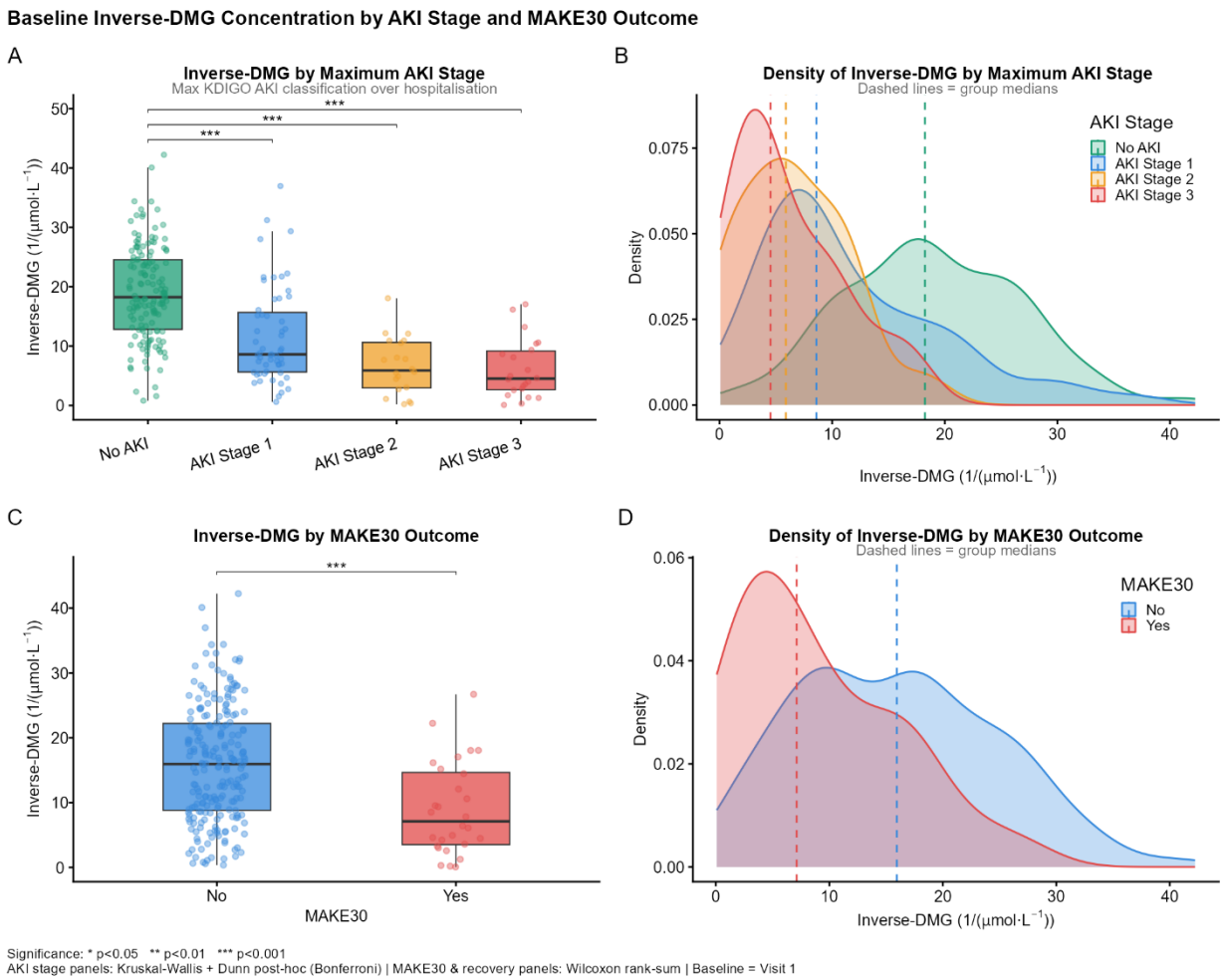

Figure 5.5. Baseline inverse-DMG plasma concentration stratified by maximum AKI severity and 30-day kidney outcome. Box plots with individual data points showing baseline inverse plasma DMG concentration (1/plasma DMG; 1/µmol·L⁻¹) stratified by (A) maximum AKI stage over the course of hospitalization (KDIGO criteria) and (C) MAKE30 outcome (No vs. Yes). Density plots illustrating the distribution of 1/plasma DMG by (B) maximum AKI stage and (D) MAKE30 outcome; dashed vertical lines indicate group medians. In panels A and B, groups were compared using the Kruskal-Wallis test with Dunn post-hoc correction (Bonferroni). In panel C, groups were compared using the Wilcoxon rank-sum test. Box plots display median with IQR. * p<0.05, ** p<0.01, *** p<0.001.

Patients who experienced a MAKE30 event (MAKE30-positive) had significantly lower baseline inverse DMG concentration compared to MAKE30-negative patients (p<0.001, Wilcoxon rank-sum) (**Figure 5.5C–D**). The MAKE30-positive group exhibited a distribution shifted toward lower values and a narrower spread compared to the MAKE30-negative group. The same pattern

was observed for DMG clearance (**Figure C.2C–D**), suggesting that impaired tubular secretory function at enrollment is associated with worse 30-day kidney outcomes.

Neither inverse DMG nor DMG clearance at baseline differed significantly between patients who achieved AKI recovery and those who did not (both not significant, Wilcoxon rank-sum) (**Figure C.2E–F**), suggesting that a single early measurement of tubular secretory function may not be sufficient to distinguish patients who recover from those who do not.

Taken together, these findings indicate that baseline DMG plasma concentration reflects the severity of kidney injury and is associated with short-term clinical outcomes. As a secretory solute, DMG relies on active proximal tubular transport rather than glomerular filtration alone, which may make it a more sensitive early indicator of functional tubular impairment than conventional filtration-based markers such as serum creatinine.

5.4. DMG reference range analysis

A preliminary reference range analysis was performed using baseline DMG plasma concentration as a proposed kidney secretory biomarker. Concentrations were characterized in patients who had no AKI at admission and never developed AKI during the study period, and were compared to baseline creatinine values in the same population.

Baseline inverse-DMG plasma concentrations in the no-AKI cohort (n = 150) demonstrated a left-skewed distribution with a median of 18.9 $1/(\mu mol \cdot L^{-1})$ (IQR 13.63–24.91), and a 2.5th–97.5th percentile reference interval of 4.7–34.37 $1/(\mu mol \cdot L^{-1})$ (**Figure 5.6A**). Four patients (2.7%) had baseline inverse-DMG concentrations falling below the lower reference limit of 4.7 $1/(\mu mol \cdot L^{-1})$. A clinical outcomes analysis of these four patients revealed substantially longer ICU and hospital stays compared to the remaining no-AKI cohort (median ICU LOS 10.6 vs 2.6

days, p = 0.007; median hospital LOS 33.6 vs 9.7 days, p = 0.008) (**Table 5.2A**). ICU readmission was observed in one of the four patients below the lower reference limit (25%), compared to 4.8% in the remaining cohort, though this did not reach statistical significance (p = 0.199). No events were observed for MAKE30 or in-hospital mortality in this group; however, given the sample size of n = 4, the absence of these outcomes is uninformative and should not be interpreted as evidence of no effect. The prolonged hospital course in these patients, despite the absence of formally staged AKI, suggests that low inverse-DMG may identify a subclinical kidney secretory dysfunction not captured by conventional AKI staging.

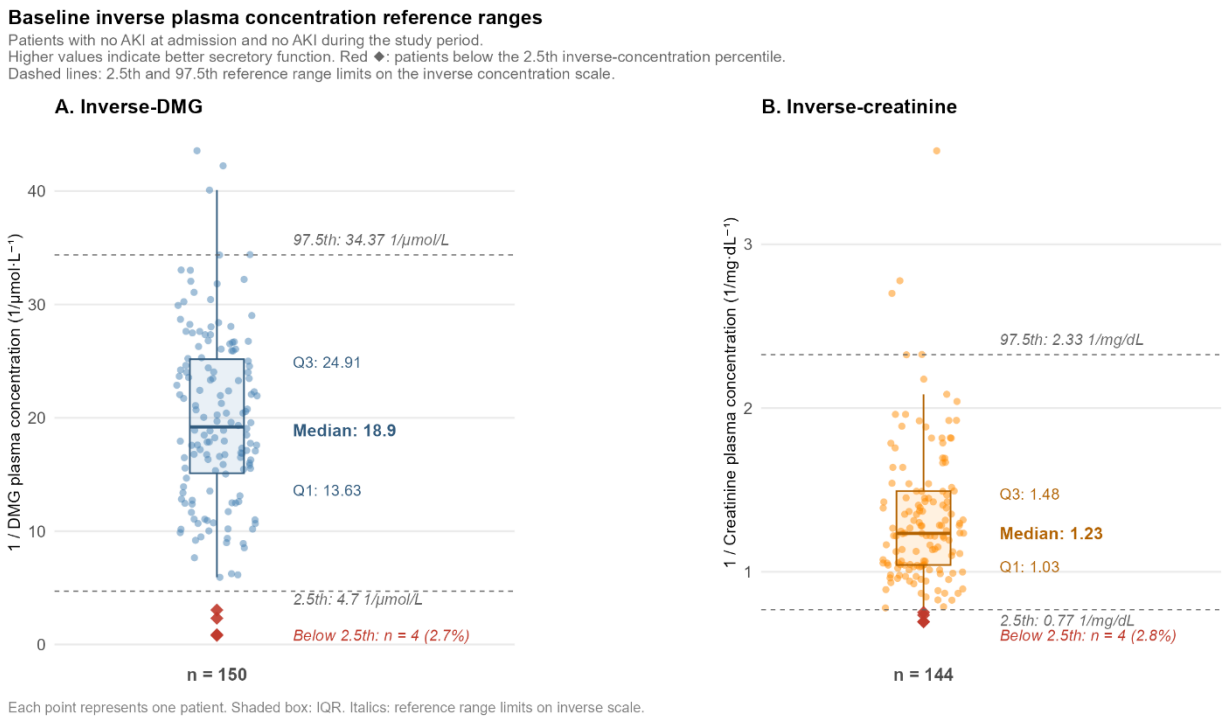

Figure 5.6. Baseline inverse plasma concentration reference ranges for DMG and creatinine in patients without AKI. Panel A shows baseline inverse-DMG plasma concentration ($1/\mu mol \cdot L^{-1}$) and Panel B shows baseline inverse-creatinine plasma concentration ($1/mg \cdot dL^{-1}$) at admission in patients with no AKI at admission and no AKI during the study period. Higher values indicate better kidney secretory function. Each point represents one patient. The box represents the interquartile range with the median line. Dashed lines indicate the 2.5th and 97.5th percentile reference range limits on the inverse scale, derived from the 97.5th and 2.5th concentration percentiles, respectively. Red diamonds (◆) indicate patients whose baseline concentration fell below the 2.5th inverse percentile. Panels have independent y-axes.

In contrast, baseline inverse-creatinine (1/[creatinine plasma concentration]) (n = 144) was more symmetrically distributed, with a median of 1.23 $1/(mg \cdot dL^{-1})$ (IQR 1.03–1.48) and a cohort-derived reference interval of 0.77–2.33 $1/(mg \cdot dL^{-1})$ (**Figure 5.6B**). This interval is consistent with established clinical reference ranges for serum creatinine, supporting the use of this no-AKI cohort as an exploratory reference population[81]. Four patients (2.8%) exceeded the cohort-derived lower inverse-creatinine reference limit of 0.77 $1/(mg \cdot dL^{-1})$. Unlike the DMG outliers, these patients showed no meaningful difference in ICU or hospital length of stay compared to the remaining cohort (median ICU LOS 2.3 vs 2.7 days, p = 0.947; median hospital LOS 9.9 vs 9.8 days, p = 0.775), and no events were observed for any binary outcome (**Table 5.2B**). There was no overlap between the patients identified as exceeding the upper reference limit by DMG and those identified by creatinine, suggesting these biomarkers may be identifying different subpopulations with different clinical trajectories.

Table 5.2. Clinical outcomes for patients below the 2.5th inverse percentile reference range limit compared to those within the reference range. Panel A shows outcomes for patients stratified by baseline inverse-DMG plasma concentration relative to the 2.5th inverse percentile reference range limit; Panel B shows the same comparison for baseline inverse-creatinine plasma concentration. Groups were defined on the inverse concentration scale, where values below the 2.5th percentile reflect impaired kidney secretory function. Reference ranges were determined from patients with no AKI at admission and no AKI during the study. Continuous variables are presented as median (IQR) and compared using the Wilcoxon rank-sum test. Binary variables are presented as n (%) and compared using Fisher's exact test. FDR correction was applied using the Benjamini-Hochberg method across all comparisons within each panel. * $p<0.05$, ** $p<0.01$, *** $p<0.001$.

A. Inverse-DMG (1/(µmol·L^{-1}))

No AKI at admission and no AKI during study period. 2.5th inverse percentile threshold = 5.14 1/(µmol·L^{-1}). Groups defined on inverse concentration scale.[1]

Variable		Overall (n=150)	Below 2.5th (n=4)	Above 2.5th (n=146)	p-value	FDR q
ICU LOS (days)	Median (IQR)	2.7 (1.7–3.9)	10.6 (8–13)	2.6 (1.7–3.8)	**0.007****	**0.019***
Hospital LOS (days)	Median (IQR)	9.8 (5.2–17.7)	33.6 (18.7–51.5)	9.7 (5.2–17.3)	**0.008****	**0.019***
MAKE30, n (%)	n (%)	2 (1.3%)	0 (0%)	2 (1.4%)	1.000	1.000
In-hospital death, n (%)	n (%)	4 (2.7%)	0 (0%)	4 (2.7%)	1.000	1.000
ICU readmission, n (%)	n (%)	8 (5.3%)	1 (25%)	7 (4.8%)	0.199	0.331

[1] Continuous: median (IQR); Wilcoxon rank-sum. Binary: n (%); Fisher's exact. FDR: Benjamini-Hochberg. Below 2.5th percentile = impaired secretory function on inverse scale. Significant p/q shown in bold red. * p<0.05 ** p<0.01 *** p<0.001.

B. Inverse-creatinine (1/(mg·dL^{-1}))

No AKI at admission and no AKI during study period. 2.5th inverse percentile threshold = 0.77 1/(mg·dL^{-1}). Groups defined on inverse concentration scale.[1]

Variable		Overall (n=144)	Below 2.5th (n=4)	Above 2.5th (n=140)	p-value	FDR q
ICU LOS (days)	Median (IQR)	2.7 (1.7–3.9)	2.3 (1.8–4)	2.7 (1.7–3.9)	0.947	1.000
Hospital LOS (days)	Median (IQR)	9.8 (5.2–17.8)	9.9 (3.9–18.5)	9.8 (5.2–17.8)	0.775	1.000
MAKE30, n (%)	n (%)	2 (1.4%)	0 (0%)	2 (1.4%)	1.000	1.000
In-hospital death, n (%)	n (%)	4 (2.8%)	0 (0%)	4 (2.9%)	1.000	1.000
ICU readmission, n (%)	n (%)	8 (5.6%)	0 (0%)	8 (5.7%)	1.000	1.000

[1] Continuous: median (IQR); Wilcoxon rank-sum. Binary: n (%); Fisher's exact. FDR: Benjamini-Hochberg. Below 2.5th percentile = impaired secretory function on inverse scale. Significant p/q shown in bold red. * p<0.05 ** p<0.01 *** p<0.001.

To assess whether this signal extended across the full distribution rather than exclusively being driven by the four outlier patients, a continuous unadjusted Spearman correlation analysis was performed across the no-AKI cohort (**Figure C.3**). Inverse-DMG was significantly negatively correlated with hospital length of stay (rho = −0.27, p = 0.001) but not ICU length of stay (rho = −0.09, p = 0.266), while inverse-creatinine was not significantly associated with either outcome (rho = −0.05 and −0.01, respectively), further supporting the specificity of the DMG signal across the full distribution of values.

Together, these findings suggest that elevated baseline DMG in patients without conventionally defined AKI may represent a more clinically meaningful deviation from normal kidney secretory function than creatinine elevation alone. The association between inverse-DMG and hospital

length of stay was consistent across both the threshold-based and continuous analyses, and was absent for inverse-creatinine in both approaches. Given the small sample sizes involved, all findings should be interpreted with caution and warrant investigation in larger cohorts.

5.4.1. Stratified reference range analysis

Reference range values for DMG were stratified by sex and age group and compared to creatinine to assess whether these demographic factors influenced baseline plasma concentrations in the no-AKI cohort (n = 144).

Baseline inverse-DMG plasma concentrations did not differ significantly between female (n = 57) and male (n = 87) patients (median 19.57 1/(μmol·L^{-1}) [IQR 6.18–32.11] vs 18.48 1/(μmol·L^{-1}) [IQR 13.25–24.51]; p = 0.647), suggesting that sex does not meaningfully influence DMG plasma concentration in patients with preserved kidney function (**Table 5.3**). The inverse-DMG reference intervals were similar between sexes (female: 6.18–32.11 1/(μmol·L^{-1}); male: 3.48–34.17 1/(μmol·L^{-1})), with a slightly wider lower reference limit in males. In contrast, inverse-creatinine plasma concentrations were significantly higher in females compared to males (median 1.41 1/(mg·dL^{-1}) [IQR 1.16–1.79] vs 1.12 1/(mg·dL^{-1}) [IQR 0.98–1.32]; p < 0.001), consistent with the well-established effect of lower muscle mass and reduced creatinine production in females.[32] The absence of a sex difference in DMG but the presence of one in creatinine suggests that DMG may be a less biologically variable biomarker across sexes, which is desirable for a clinical reference range.

Table 5.3. Baseline inverse-DMG and inverse-creatinine plasma concentration by sex. Median (IQR) and reference range (2.5th–97.5th percentile) for inverse-DMG (1/(μmol·L^{-1})) and inverse-creatinine (1/(mg·dL^{-1})) plasma concentrations at baseline in patients with no AKI at admission and no AKI during the study period. Values are stratified by sex (Female, Male) with the overall cohort shown for reference. Statistical comparison between sexes was

performed using the Wilcoxon rank-sum test on the inverse-concentration scale; effect size is reported as the rank-biserial correlation coefficient (r). * p<0.05, ** p<0.01, *** p<0.001.

Baseline inverse plasma biomarker reference ranges by sex

No AKI at admission and no AKI during study period. Wilcoxon rank-sum test: Male vs Female.[1]

		Inverse-DMG (1/(μmol·L⁻¹))				Inverse-creatinine (1/(mg·dL⁻¹))			
Subgroup	**n**	**Median (IQR)**	**2.5th–97.5th**	**p-value**	**r**	**Median (IQR)**	**2.5th–97.5th**	**p-value**	**r**
Overall									
Overall	144	18.88 (13.5–24.57)	4.7–34.38	—	—	1.23 (1.03–1.48)	0.77–2.33	—	—
By Sex									
Female	57	19.57 (15.56–24.55)	6.18–32.11	—	—	1.41 (1.16–1.79)	0.89–2.55	—	—
Male	87	18.48 (13.25–24.51)	3.48–34.17	0.647	0.038	1.12 (0.98–1.32)	0.74–2.12	**<0.001*** **	0.398

[1] Baseline = Visit 1. Values on inverse concentration scale (higher = better function). IQR: interquartile range. 2.5th–97.5th = reference range interval on inverse scale. Significant p-values shown in bold red. * p<0.05 ** p<0.01 *** p<0.001. p-value and r reported on Male row (Male vs Female comparison). r = rank-biserial correlation. — = not applicable.

Baseline inverse-DMG concentrations showed a statistically significant decrease with age (Kruskal-Wallis p = 0.006), with median inverse-DMG of 22.66 1/(μmol·L⁻¹) (IQR 16.58–27.18) in patients aged <50, 18.06 1/(μmol·L⁻¹) (IQR 13.32–24.17) in those aged 50–64, and 16.49 1/(μmol·L⁻¹) (IQR 13.38–18.89) in those aged ≥65 (**Table 5.4**). Pairwise comparisons revealed a significant difference between the <50 and ≥65 groups (Dunn p = 0.005, BH-adjusted), while the <50 vs 50–64 (p = 0.073) and 50–64 vs ≥65 (p = 0.139) comparisons did not reach significance after correction for multiple comparisons. The reference interval narrowed with age on the inverse scale (4.4–38.9 for <50 vs 4.69–25.91 for ≥65), reflecting both a lower median and reduced upper limit in older patients, consistent with a progressive decline in tubular secretory capacity. Inverse-creatinine concentrations did not differ significantly across age groups (Kruskal-Wallis p = 0.425), with median values of 1.25, 1.28, and 1.16 1/(mg·dL⁻¹) for the <50, 50–64, and ≥65 groups respectively, and no significant pairwise differences.

Table 5.4. Baseline inverse-DMG and inverse-creatinine plasma concentration by age group. Median (IQR) and reference range (2.5th–97.5th percentile) for inverse-DMG (1/(μmol·L⁻¹)) and inverse-creatinine (1/(mg·dL⁻¹)) plasma concentrations at baseline in patients with no AKI at admission and no AKI during the study period. Values are stratified by age group (<50, 50–64, ≥65 years) with the overall cohort shown for reference. The Kruskal-Wallis omnibus p-value is reported in the table subtitle. Pairwise comparisons were performed

using Dunn's test with Benjamini-Hochberg correction for multiple comparisons, on the inverse concentration scale. * p<0.05, ** p<0.01, *** p<0.001.

Baseline inverse plasma biomarker reference ranges by age group

No AKI at admission and no AKI during study period. KW p (Inverse-DMG) = 0.006; KW p (Inverse-creatinine) = 0.425.*[1]

		Inverse-DMG (1/(μmol·L^{-1}))			Inverse-creatinine (1/(mg·dL^{-1}))		
Subgroup	**n**	**Median (IQR)**	**2.5th–97.5th**	**Dunn p (BH)**	**Median (IQR)**	**2.5th–97.5th**	**Dunn p (BH)**
Overall							
Overall	144	18.88 (13.5–24.57)	4.7–34.38	—	1.23 (1.03–1.48)	0.77–2.33	—
By Age Group							
<50	58	22.66 (16.58–27.18)	4.4–38.9	—	1.25 (1.04–1.51)	0.78–2.59	—
50-64	56	18.06 (13.32–24.17)	6.57–30.83	—	1.28 (1.03–1.5)	0.83–2.01	—
≥65	30	16.49 (13.38–18.89)	4.69–25.91	—	1.16 (1.03–1.37)	0.69–2.22	—
Pairwise comparisons (Dunn test, BH-adjusted)							
<50 vs 50-64	—	—	—	0.073	—	—	0.873
<50 vs ≥65	—	—	—	**0.005****	—	—	0.400
50-64 vs ≥65	—	—	—	0.139	—	—	0.400

[1] Baseline = Visit 1. Values on inverse concentration scale (higher = better function). IQR: interquartile range. 2.5th–97.5th = reference range interval on inverse scale. Significant p-values shown in bold red. * p<0.05 ** p<0.01 *** p<0.001. KW p = Kruskal-Wallis omnibus p-value (reported in subtitle). Dunn p = BH-adjusted pairwise p-value. — = not applicable.

Although creatinine clearance is known to decline with advancing age, creatinine concentration remains stable due to the parallel age-related reduction in muscle mass and creatinine production, which offsets the functional decline. DMG, which is not known to be influenced by muscle mass, may more directly reflect the age-associated decline in tubular secretory capacity. The age-related increase in DMG plasma concentration in the absence of any equivalent change in creatinine concentration further supports the potential sensitivity of DMG as a biomarker of kidney secretory function and suggests that age-stratified reference ranges may be warranted in clinical application.

5.5. Summary and Discussion

This study highlights the importance of tubular secretory function as a distinct and clinically relevant dimension of kidney physiology in critically ill patients. Data from the ROKIT cohort provided insights that extend beyond traditional measures such as creatinine clearance, serum

creatinine, and eGFR. The observed variability in TSS clearance during critical illness, along with its associations with adverse clinical outcomes, suggests that proximal tubular function is meaningfully impaired in this population and warrants further investigation as a clinical target.

TSS clearances had significant correlations with creatinine clearance, with the majority of solutes showing moderate to strong associations. DMG was particularly notable for ranking among the top correlates for most other solutes in the panel and having one of the strongest associations with creatinine clearance. However, the non-linear and somewhat scattered correlation between DMG and creatinine clearance also indicated the possibility that these two markers are not measuring kidney function similarly. Creatinine clearance reflects filtration, while TSS clearance aims to capture proximal tubular transport, and these two processes may be differentially impaired in critical illness.

Baseline TSS clearances were strongly and consistently associated with both incident AKI development and MAKE30 outcomes. Baseline plasma concentrations showed associations for a subset of analytes, most prominently for incident AKI outcomes. Although clearance is the more physiologically direct measure of tubular function, plasma concentration alone may still carry a significant outcome-related signal. The clinical use of plasma-based measurement will likely depend on the application. For screening or early risk stratification, a single plasma sample would be more practical than timed urine collection and may be sufficient to identify patients at risk. For diagnostic purposes or precise quantification of tubular secretory capacity, clearance-based measurement would be more appropriate. For drug dosing decisions, where accurate characterization of tubular elimination is needed, clearance is likely more practical. Notably, secretory solute clearances remained significantly associated with both outcomes after adjustment for creatinine clearance, suggesting that tubular secretory function captures

prognostic information that is at least partially independent of glomerular filtration. This is further supported by the observation that creatinine clearance was only significantly associated with MAKE30 after FDR correction, and did not survive correction for incident AKI, while the secretory solute panel showed robust associations with both outcomes. These findings suggest that secretory solute clearance and conventional filtration-based markers are complementary rather than redundant, with each reflecting distinct aspects of kidney function.

The focused DMG analysis demonstrated that baseline inverse-DMG plasma concentration tracks the severity of clinical AKI, with progressive decline across KDIGO AKI stages and significantly lower inverse-DMG concentrations in patients who later had MAKE30 events, consistent with accumulation of DMG when proximal tubular secretion is impaired. Importantly, this signal was present at ICU admission, before the full clinical trajectory of AKI had occurred, which suggests that DMG may have value as an early prognostic tool in the ICU.

These findings also suggest that DMG may detect a form of subclinical tubular secretory dysfunction that creatinine cannot capture. The divergence between DMG and creatinine outlier groups, with no patient overlap, implies these biomarkers are identifying distinct subpopulations with different underlying physiology. This raises the possibility that conventional AKI staging, which relies on creatinine and urine output, may underestimate the true burden of kidney dysfunction in some critically ill patients. To assess whether this signal extended beyond the four outlier patients, a continuous analysis across the full no-AKI cohort confirmed a significant negative association between inverse-DMG and hospital length of stay. These findings are preliminary and limited by sample size and should be investigated in a larger study population.

In the no-AKI cohort, DMG reference ranges did not differ significantly by sex, which is notable given that creatinine-based measures are known to require sex-specific adjustment due to

differences in muscle mass and creatinine production, contributing to disparities in AKI diagnosis and eGFR estimation across sexes.[82–84] A biomarker that does not require sex adjustment would be simpler to implement and less prone to diagnostic bias. The age-related increase in DMG concentration, reflected as a decline in inverse-DMG, in the absence of any equivalent age effect for creatinine concentration, may reflect the progressive decline in tubular secretory capacity known to accompany ageing.[85] While this suggests that age-stratified reference ranges may be warranted, it also indicates the possibility that DMG could serve as a more sensitive marker of kidney aging than creatinine, a question worth exploring in future studies in non-critically ill populations.

Together, these results support DMG as a promising kidney secretory biomarker with potential use both as a prognostic marker in critically ill patients and as a sensitive indicator of subclinical tubular dysfunction in those without overt AKI. The findings are preliminary and limited by sample size, but they provide a strong foundation for future prospective studies. Future work should aim to identify patient- and disease-specific factors associated with reductions in tubular secretory solute clearance and plasma concentrations. In particular, investigating whether impaired tubular secretory function predicts plasma concentrations of commonly administered drugs and their metabolites could have direct implications for drug dosing in critically ill patients. Further studies should also investigate whether tubular secretory dysfunction is associated with other adverse clinical outcomes not examined here. If validated in larger studies, DMG, and potentially other tubular secretory solutes, could serve as useful kidney function markers that capture tubular secretory dysfunction earlier than current standard-of-care tools, with potential implications for patient monitoring, drug dosing, and AKI risk stratification in the ICU.

6. CHAPTER 6 – CONCLUSION

This work aimed to develop and apply a multiplexed targeted LC-MS/MS assay for measuring proximal tubular secretory function using endogenous secretory solutes, and to evaluate its clinical relevance in two patient populations. A method was developed and validated for 21 of the 24 initial candidate analytes, with three excluded during assay development. In both the PROCLAIM healthy adult and CKD cohort and the ROKIT critical illness cohort, the tubular secretory solute panel showed meaningful associations with kidney function and clinical outcomes, suggesting that this approach captures a dimension of kidney physiology not fully reflected by conventional filtration-based markers.

In the PROCLAIM cohort, several solute clearances correlated well with the clearance of furosemide and famciclovir, two medications primarily eliminated by proximal tubular secretion, which supports the biological validity of the panel. Several analytes emerged as promising candidates based on their strong correlation with medication clearance, low inter-individual variability, and high endogenous clearance.

In the ROKIT cohort, baseline secretory solute clearances were consistently associated with both incident AKI and MAKE30 outcomes across the full 16-solute panel, and these associations remained significant after FDR correction and adjustment for creatinine clearance. This suggests that tubular secretory function at ICU admission provides prognostic information beyond conventional filtration markers. The focused DMG analysis showed that baseline inverse plasma DMG concentration reflects AKI severity, declines progressively across AKI stages, and may identify patients with subclinical secretory dysfunction not captured by standard AKI staging. These findings support DMG as a promising early biomarker of tubular secretory impairment in critical illness.

6.1. Limitations

There are several limitations to these findings. Both cohorts were relatively small, with n = 48 in the PROCLAIM analysis and n = 246 in the ROKIT cohort, which limits statistical power. The DMG reference range analysis was based on only four patients exceeding the lower reference limit and should be considered preliminary.

The ROKIT cohort was enrolled at two academic medical centers with a predominantly White patient population, which may limit generalizability to more diverse critically ill populations. Observed associations between tubular secretory function and clinical outcomes may be influenced by confounding factors not fully captured by the adjustment variables used, such as unmeasured comorbidities or medication exposure.

Finally, the potential misidentification of PAH during assay development is a reminder that feature annotation in untargeted metabolomics can be unreliable when based on database matching alone, and that confirmation using authentic reference standards is an important step in assay development.

6.2. Future Directions

There are several directions for future research based on these findings. First, the secretory solute panel should be validated in larger and more diverse critical illness cohorts to confirm the associations observed here and to determine whether they hold across patient subgroups such as those with pre-existing CKD, polycystic kidney disease, or those receiving renal replacement therapy.

Second, the use of plasma-based secretory solute measurements as a clinical screening tool should be further investigated. A single plasma draw at ICU admission is logistically feasible,

and future studies should examine whether plasma DMG or perhaps a composite plasma secretory score can identify patients at risk of adverse kidney outcomes earlier than creatinine or eGFR.

Third, the relationship between tubular secretory function and drug elimination in critically ill patients should be directly studied. Many medications commonly used in the ICU are cleared via proximal tubular secretion, meaning that impaired secretory function could lead to drug accumulation and potential toxicity. Measuring secretory solute clearance alongside pharmacokinetic data in this population could help inform more individualized drug dosing decisions.

Finally, the current iteration of the TSS panel represents a continuation rather than a definitive set of biomarkers. Future candidate solutes could be identified through untargeted metabolomics approaches similar to those used to develop the current panel, with the inclusion of a formal chemical identification step. The goal would be to refine the panel to include analytes that are most reproducible, biologically informative, and practically measurable in clinical settings.

A. APPENDIX A. METHOD DEVELOPMENT SUPPLEMENTAL FIGURES AND TABLES

Table A.1. Analyte vendors and stock concentrations. A panel of 24 endogenous compounds was selected for analysis, ranked by priority. Each analyte is listed with its abbreviation, commercial vendor and catalog number, stock concentration (mM) and solvent, and priority ranking.

Compound (endogenous)	Abbriviation	Vendor	Concentration (mM)	Solvent	Rank
4-Hydroxyphenylacetic acid	4OHphe	Sigma: H50004	10	DMSO	1
N2,N2-Dimethylguanosine	DMG	Sigma: AMBH2D6FF9F5	6.87	DMSO	2
5-Fluoro-1-methyl-1H-1,3-benzodiazole	Benzodiazole	Sigma: ENA458426045	10	DMSO	3
Pimelic acid	Pimelic	TRC: P445040	10	DMSO	4
3-Methylcrotonylglycine	Metcrogly	AdooQ Bioscience: A13619	10	DMSO	5
3-Methoxy-4-hydroxyphenylglycol sulfate	MHPG	Sigma: H8759	10	DMSO	6
2-[(4-Aminobenzoyl)-amino]acetic acid	Aminohipp	Sigma: A1422	10	DMSO	7
6'-Sialyl-N-acetyllactosamine	Lactosamine	Sigma: 37966	10	Water	8
2-Hydroxyphenylacetic acid	2OHphe	Sigma: H49804	10	DMSO	9
1,4-Cyclohexanedicarboxylic acid	CycCOOH	Thermo: AC406040050	10	DMSO	10
5-Hydroxytryptophan	5HTP	Sigma: 797103	6.01	DMSO	11
4-Acetamidobutyric acid	Aabutyric	Sigma: AMBH97F07A1F	10	DMSO	12
L-Homocitrulline	Homocit	Sigma: SML2645	10	0.05% AmOH in H2O	13
Gentisic acid	Gentisic	Thermo: AC165200050	10	DMSO	14
5-Hydroxy-3-indoleacetic acid	OHindol	Sigma: H8876	10	DMSO	15
Kynurenic acid	Kynurenic	Sigma: K3375	10	DMSO	16
4-Pyridoxic acid	Pyridoxic	Sigma: P9630	5	0.05% AmOH in H2O	17
N-Isovalerylglycine	Isovarylgly	TRC: I917600	10	DMSO	18
Indoxyl sulfate potassium salt	inSO4	Sigma: I3875	5	DMSO	19
P-cresol sulfate	pcresol	Cayman Chemicals: 29504	10	DMSO	20
Xanthosine Dihydrate	Xantho	TRC: X742100	10	DMSO	21
Tiglylglycine	Tigylgly	TRC: T440100	10	DMSO	22
N-Cinnamoylglycine	Cinna	TRC: C442120	10	DMSO	23
Hippuric acid	Hippuric	TRC: 112003	10	DMSO	24

Table A.2. Mass spectrometric parameters 1. Ion source settings applied to all analytes using a Turbo Spray IonDrive source. Curtain gas (CUR), collision gas (CAD), and ion source gases 1 and 2 (GS1, GS2) are reported in arbitrary units. IonSpray voltage (IS) was set to +4500 V in positive mode and −4500 V in negative mode. Source temperature (TEM) was set at 400 °C.

Ion Source	Turbo Spray IonDrive
Curtain Gas (CUR)	35
Collision Gas (CAD)	8
IonSpray Voltage (IS, pos)	4500 V
IonSpray Voltage (IS, neg)	-4500 V
Temperature (TEM) [°C]	400 °C
Ion Source Gas 1 (GS1)	50
Ion Source Gas 2 (GS2)	50

Table A.3. Mass spectrometric parameters 2. Optimized MS parameters for each analyte, including retention time (RT, min), declustering potential (DP, V), entrance potential (EP, V), collision cell exit potential (CXP, V), precursor ion (MS1, *m/z*), product ions (MS3, *m/z*), and collision energy (CE, V). Negative values indicate parameters optimized for negative ionization mode. Up to four product ions are listed per analyte, with the most abundant ion used for quantification.

Compound	RT	DP	EP	CXP	MS1	MS3	CE
4-Hydroxyphenylacetic acid[a]	0.0	-40	-10	-11	151.15	107.2, 79.3, 105.2	-15
N2,N2-Dimethylguanosine	4.8	40	10	10	312.29	180.3, 110.3, 135.3	26
5-Fluoro-1-methyl-1H-1,3-benzodiazole	1.1	80	10	10	151.15	83.3, 110.3, 57.3	42
Pimelic acid	3.7	-40	-10	-11	159.17	97.3, 95.3, 115.3	-18
3-Methylcrotonylglycine[b]	2.5	-30	-10	-11	156.17	112.3, 110.2, 74.3, 96.3	-15
3-Methoxy-4-hydroxyphenylglycol sulfate	6.0	-75	-10	-11	263.25	121.3, 150.3, 165.3	-50
2-[(4-Aminobenzoyl)-amino]acetic acid	4.7	35	10	10	195.19	120.3, 64.3, 92.3	23
6'-Sialyl-N-acetyllactosamine	0.0	55	10	10	675.6	138.3, 204.3, 366.4, 384.5	65
2-Hydroxyphenylacetic acid[a]	0.0	-40	-10	-11	151.15	107.2	-15
1,4-Cyclohexanedicarboxylic acid	3.8	-70	-10	-11	171.18	153.3, 109.3	-17
5-Hydroxytryptophan	7.0	40	10	10	221.22	204.4, 77.3, 134.3	16
4-Acetamidobutyric acid	1.9	28	10	10	146.16	86.3	18
L-Homocitrulline	7.3	30	10	10	190.21	173.3, 127.3, 84.3	31
Gentisic acid	5.3	-50	-10	-11	153.12	108.2, 81.3	-30
5-Hydroxy-3-indoleacetic acid	4.6	30	10	10	192.18	146.3, 91.3	25
Kynurenic acid	5.7	35	10	10	190.17	144.3, 89.3, 116.3	27
4-Pyridoxic acid	4.7	30	10	10	184.16	148.3, 65.3, 92.3	30
N-Isovalerylglycine[c]	3.6, 1.9	-40	-10	-11	158.18	74.2, 114.3, 98.3	-16
Indoxyl sulfate	5.6	-90	-10	-11	212.21	80.2, 81.2, 132.3	-26
P-cresol sulfate	4.4	-35	-10	-11	187.2	107.3, 80.2, 77.3	-27
Xanthosine	5.7	35	10	10	285.23	153.3, 136.3, 110.3	16
Tiglylglycine[b]	2.5	-30	-10	-11	156.17	112.3, 110.2, 74.3, 96.3	-15
N-Cinnamoylglycine	3.0	40	10	10	206.21	131.3, 103.3, 51.3	21
Hippuric acid	3.1	36	10	10	180.2	105.3, 77.3, 51.3	22

[a] Identical transitions were observed for 4-hydroxyphenylacetic acid and 2-hydroxyphenylacetic acid.

[b] Identical transitions were observed for 3-methylcrotonylglycine and tiglylglycine.

[c] Retention time differences were observed for N-Isovalerylglycine across different pH mobile injection conditions (FA: 3.6 min; AmOH: 1.9 min).

Table A.4. Mass spectrometric parameters 3. Optimized MS parameters for each isotopically labeled internal standard, including retention time (RT, min), declustering potential (DP, V), entrance potential (EP, V), collision cell exit potential (CXP, V), precursor ion (MS1, *m/z*), product ions (MS3, *m/z*), and collision energy (CE, V). Negative values indicate parameters optimized for negative ionization mode. Up to four product ions are listed per internal standard, with the most abundant ion used for quantification.

Compound	RT	DP	EP	CXP	MS1	MS3	CE
4-Hydroxyphenylacetic acid-d6 ($^{2}H_6$)	0	-70	-10	-11	157.18	85.1, 97.1	-25
2-(Dimethylamino)guanosine-d6 ($^{2}H_6$)	4.8	40	10	10	318.33	186.2, 110.1, 135.2	25
Pimelic Acid-d4 ($^{2}H_4$)	3.7	-45	-10	-11	163.19	100.1, 99.1, 97.2	-19
3-Methylcrotonylglycine ($^{13}C_2$,^{15}N)[a]	2.5	-18	-10	-11	159.10	114, 112, 98, 77	-15
5-Hydroxy-L-tryptophan-d3 ($^{2}H_3$)	7	50	10	10	224.24	164, 207.1, 78	29
L-Homocitrulline-d3 ($^{2}H_3$)	7.3	85	10	10	193.23	87.3, 176.3, 103.1	33
2,5-Dihydroxybenzoic Acid-d3 ($^{2}H_3$)	5.3	-80	-10	-11	156.14	111.1, 110.1	-30
5-Hydroxyindole-3-acetic acid ($^{13}C_6$)	4.6	115	10	10	198.14	152.2, 96.2, 122.3	25
Kynurenic acid-d5 ($^{2}H_5$)	5.7	45	10	10	195.10	149.2, 94.1, 121.2	27
4-Pyridoxic acid-d3 ($^{2}H_3$)	4.7	50	10	10	187.20	169.2, 150.2, 141.3	21
N-Isovalerylglycine-d2 ($^{2}H_2$)[b]	3.6, 1.9	-20	-10	-11	160.10	76.1, 99.9	-17
Indoxyl sulfate ($^{13}C_6$)	5.6	-90	-10	-11	218.00	80, 138.1, 83	-28
P-cresol sulfate-d7 ($^{2}H_7$)	4.4	-30	-10	-11	194.10	114, 112.1	-24
Xanthosine ($^{13}C_5$)	5.7	35	10	10	290.19	153.2, 136.2, 138.3	17
Tiglylglycine ($^{13}C_2$,^{15}N)	2.5	-18	-10	-11	159.10	114, 112, 98, 77	-15
N-Cinnamoylglycine-d2 ($^{2}H_2$)	3	115	10	10	208.10	131.2, 103.1, 77.1	20
Hippuric acid-d5 ($^{2}H_5$)	3.1	20	10	10	185.10	110.2, 82.1, 54.1	23

[a] Identical transitions were observed for 3-methylcrotonylglycine ($^{13}C_2$,^{15}N) and tiglylglycine ($^{13}C_2$,^{15}N).

[b] Retention time differences were observed for N-Isovalerylglycine-d2 across different pH mobile injection conditions (FA: 3.6 min; AmOH: 1.9 min).

Table A.5. LC column types and dimensions evaluated. Four column chemistries were assessed during method development, including hydrophilic interaction chromatography (HILIC), phenyl-hexyl, amide, and C18 stationary phases. All columns had a particle size of 1.7-1.8 µm and an internal diameter of 2.1 mm. Two column lengths (150 mm and 50 mm) were evaluated for HILIC and phenyl-hexyl columns, while the amide and C18 columns were tested at a single length of 150 mm and 50 mm, respectively.

Column Type	Particle Size (µm)	Diameter (mm)	Length (mm)
HILIC	1.7	2.1	150, 50
Phenyl-hexyl	1.7	2.1	150, 50
Amide	1.7	2.1	150
C18	1.8	2.1	50

Table A.6. Chromatographic conditions evaluated on a hydrophilic interaction chromatography (HILIC) column. Twelve conditions were evaluated, varying mobile phase A (MPA) and mobile phase B (MPB) compositions, gradient slope, and initial hold time. Condition 11 was selected for further development based on overall chromatographic performance.

Parameter	Condition 1	Condition 2	Condition 3	Condition 4
MPA	86% ACN / 14% H_2O / 19 mM ammonium formate	95% ACN / 5% H_2O / 0.1% FA	86% ACN / 14% H_2O / 19 mM ammonium formate	86% ACN / 14% H_2O / 19 mM ammonium formate
MPB	95% H_2O / 5% ACN / 20 mM ammonium formate	95% H_2O / 5% ACN / 20 mM ammonium formate	95% H_2O / 5% ACN / 20 mM ammonium formate	95% H_2O / 5% ACN / 20 mM ammonium formate
Hold time (min)	1	1	1	8
Starting conditions	100% MPA	100% MPA	100% MPA	100% MPA
Gradient	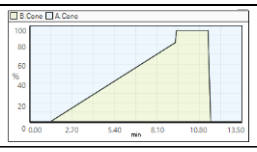	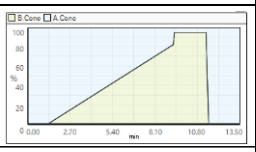		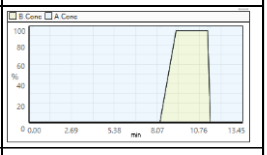
		Formic acid substituted for ammonium formate in MPA	Ammonium formate reintroduced in MPA; gradient slope reduced	Extended hold; shortened gradient
Parameter	**Condition 5**	**Condition 6**	**Condition 7**	**Condition 8**
MPA	100% ACN	86% ACN / 14% H_2O / 19 mM ammonium formate	86% ACN / 14% H_2O / 19 mM ammonium formate	95% ACN / 3% methanol / 2% H_2O
MPB	95% H_2O / 5% ACN / 100 mM ammonium formate	95% H_2O / 5% ACN / 100 mM ammonium formate	95% H_2O / 5% ACN / 100 mM ammonium formate	95% H_2O / 5% ACN / 100 mM ammonium formate
Hold time (min)	1	1	1	4
Starting conditions	100% MPA	100% MPA	100% MPA	100% MPA
Gradient	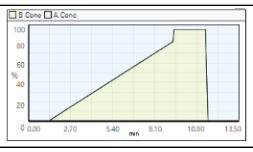	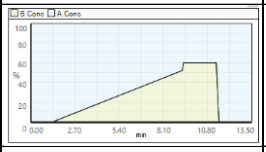	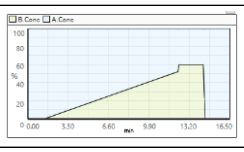	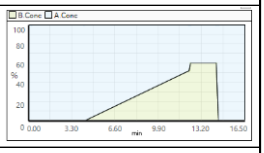
Notes	MPA composition modified to 100% ACN	No improvement; reverted composition; wash changed to 60% MPB	Gradient duration increased	MPA modified; initial hold time extended to 4 min
Parameter	**Condition 9**	**Condition 10**	**Condition 11**	**Condition 12**
MPA	95% ACN / 3% methanol / 2% H_2O / 0.1% FA	95% ACN / 3% methanol / 2% H_2O / 0.1% FA	95% ACN / 3% methanol / 2% H_2O / 0.1% FA	95% ACN / 3% methanol / 2% H_2O / 0.1% FA
MPB	95% H_2O / 5% ACN / 100 mM ammonium formate	95% H_2O / 5% ACN / 100 mM ammonium formate	95% H_2O / 5% ACN / 100 mM ammonium formate	95% H_2O / 5% ACN / 100 mM ammonium acxetate
Hold time (min)	4	1	2	2
Starting conditions	100% MPA	100% MPA	100% MPA	100% MPA
Gradient	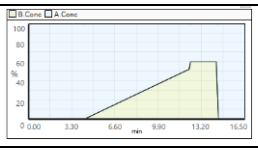	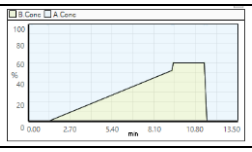	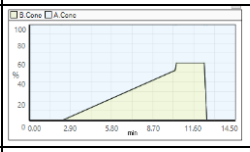	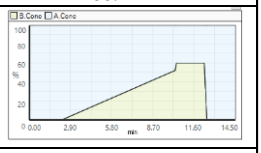
Notes	FA added to MPA	Initial hold time reduced	Initial hold time increased; **selected for further development**	Ammonium acetate used instead of ammonium formate

Table A.7. Chromatographic conditions evaluated on a phenyl-hexyl column under reversed-phase (A) and normal-phase (B) modes. Three reversed-phase conditions were evaluated in Panel A, varying starting mobile phase composition and gradient slope, with Condition 2 selected for further method development. Four normal-phase conditions were evaluated in Panel B, varying mobile phase A (MPA) and mobile phase B (MPB) compositions, initial hold time, and gradient duration.

A. Reversed-phase conditions

Parameter	Condition 1	Condition 2	Condition 3
MPA	95% H_2O / 5% ACN / 0.1% FA	95% H_2O / 5% ACN / 0.1% FA	95% H_2O / 5% ACN / 0.1% FA
MPB	95% ACN / 5% H_2O / 0.1% FA	95% ACN / 5% H_2O / 0.1% FA	95% ACN / 5% H_2O / 0.1% FA
Hold time (min)	1	1	1
Starting conditions	100% MPA	98% MPA	98% MPA
Gradient	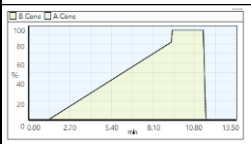	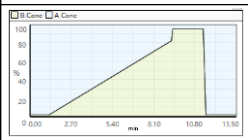	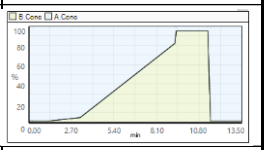
Notes		Starting mobile phase composition adjusted; **selected for further method development**	Initial gradient slope reduced to improve early analyte separation

B. Normal-phase conditions

Parameter	Condition 1	Condition 2	Condition 3	Condition 4
MPA	86% ACN / 14% H_2O / 19 mM ammonium formate	95% ACN / 5% H_2O / 0.1% FA	99.9% ACN / 0.1% FA	99.9% ACN / 0.1% FA
MPB	95% H_2O / 14% ACN / 19 mM ammonium formate	95% H_2O / 5% ACN / 20 mM ammonium formate	95% H_2O / 5% ACN / 20 mM ammonium formate	95% H_2O / 5% ACN / 20 mM ammonium formate
Hold time (min)	1	1	1	8
Starting conditions	100% MPA	100% MPA	100% MPA	100% MPA
Gradient	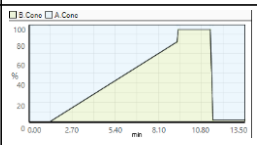	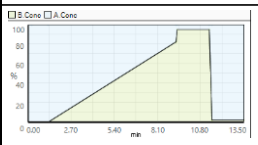	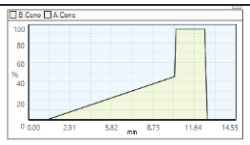	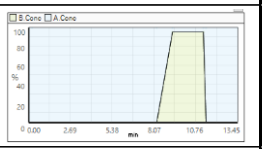
Notes		Formic acid used in MPA instead of ammonium formate	Water removed from MPA; gradient slope reduced	Initial hold time extended; gradient duration reduced

Table A.8. Chromatographic conditions evaluated on an amide column (A) and a C18 column (B). Six conditions were evaluated for the amide column in Panel A, varying mobile phase A (MPA) and mobile phase B (MPB) compositions, gradient slope, and initial hold time. A single condition was evaluated for the C18 column in Panel B using a reversed-phase mobile phase system with FA as the modifier.

A. Amide column chromatographic conditions

Parameter (Amide)	Condition 1	Condition 2	Condition 3
MPA	99.9% ACN / 0.1% FA	99.9% ACN / 0.1% FA	99.9% ACN / 0.1% FA
MPB	95% H_2O / 5% ACN / 0.1% FA	95% H_2O / 5% ACN / 20 mM ammonium formate	95% H_2O / 5% ACN / 20 mM ammonium formate
Hold time (min)	1	1	1
Starting conditions	100% MPA	100% MPA	100% MPA
Gradient	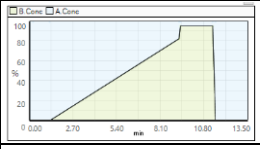	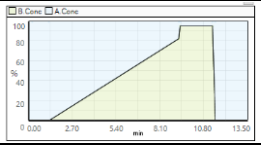	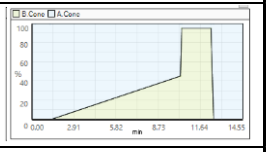
Notes		Ammonium formate substituted for formic acid in MPA	Gradient slope reduced
Parameter (Amide)	**Condition 4**	**Condition 5**	**Condition 6**
MPA	86% ACN / 14% H_2O / 19 mM ammonium formate	86% ACN / 14% H_2O / 19 mM ammonium formate	86% ACN / 14% H_2O / 19 mM ammonium formate
MPB	95% H_2O / 5% ACN / 20 mM ammonium formate	95% H_2O / 5% ACN / 20 mM ammonium formate	95% H_2O / 5% ACN / 20 mM ammonium formate
Hold time (min)	1	1	8
Starting conditions	100% MPA	100% MPA	100% MPA
Gradient	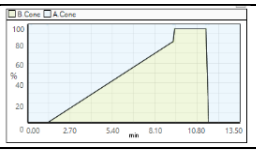	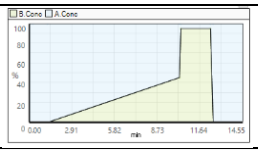	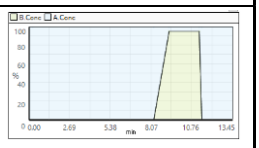
Notes	Water and ammonium formate added to MPA; gradient slope increased	Decreased gradient slope	Initial hold time extended; gradient duration reduced

B. C18 column chromatographic conditions

Parameter (C18)	Condition 1
MPA	95% H_2O / 5% ACN / 0.1% FA
MPB	95% ACN / 5% H_2O / 0.1% FA
Hold time (mins)	1
Starting conditions	98% MPA
Gradient	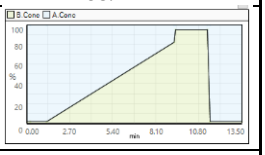
Notes	

Table A.9. Plasma protein precipitation conditions evaluated. Eight protein precipitation conditions were assessed during method development, varying organic solvent type, plasma-to-organic solvent ratio, and formic acid concentration. Acetonitrile (ACN) and methanol (MeOH) were evaluated as precipitating solvents at plasma:organic ratios of 1:3 and 1:4, each tested in the presence or absence of formic acid (1.1%).

Condition	Organic Solvent	Plasma:Organic Ratio	Formic Acid (%)
1	ACN	1:3	0
2	ACN	1:3	1.1
3	ACN	1:4	0
4	ACN	1:4	1.1
5	MeOH	1:3	0
6	MeOH	1:3	1.1
7	MeOH	1:4	0
8	MeOH	1:4	1.1

Table A.10. Evaluation of post-filtration acidic (A) and basic (B) dilution conditions for plasma sample preparation. Nineteen conditions were evaluated to optimize post-filtration dilution of protein-precipitated plasma samples. Panel A shows 13 acidic conditions using formic acid (FA) or acetic acid (AA), varying protein precipitation acid concentration (0.2% or 1.0% FA), post-preparation dilution mix composition (0–3% FA), and sample-to-dilution mix ratio (1:1 or 1:2). Panel B shows 6 basic conditions using ammonium hydroxide (AmOH), varying post-preparation dilution AmOH concentration (1.5–7.5%) and sample-to-dilution mix ratio (1:1 or 1:2), with either 0.2% FA or 0.2% AA used for protein precipitation.

A. Post-filtration acidic (FA) dilution

Condition	Protein Precipitation (% Acid)	Post-Prep Dilution Mix (% FA)	Dilution (Sample:Dilution Mix)
1	0.2% FA	1	1:2
2	0.2% FA	1.5	1:2
3	0.2% FA	2	1:2
4	0.2% FA	2.25	1:2
5	0.2% FA	3	1:2
6	0.2% FA	1	1:1
7	0.2% FA	1.5	1:1
8	0.2% FA	1.8	1:1
9	0.2% FA	1.95	1:1
10	1.0% FA	0	1:2
11	1.0% FA	0	1:1
12	1.0 % FA	1	1:1
13	0.2% AA	1.8	1:1

B. Post-filtration basic (AmOH) dilution

Condition	Protein Precipitation (% Acid)	Post-Prep Dilution Mix (% AmOH)	Dilution (Sample:Dilution Mix)
14	0.2% FA	1.5	1:2
15	0.2% FA	3	1:2
16	0.2% FA	5	1:2
17	0.2% FA	7.5	1:2
18	0.2% FA	5	1:1
19	0.2% AA	5	1:1

Table A.11. Mass spectrometric and analytical assay parameter summary. Compound-specific detection parameters for all 24 TSS analytes. Each compound is listed with its monoisotopic mass (Da), ionization mode (positive or negative), whether a matched isotopically labeled internal standard (IS) was available (Y/N), and chromatographic retention time (min). Sample preparation conditions are indicated for each compound, including plasma dilution solvent (formic acid, FA; ammonium hydroxide, AmOH) and the solid phase extraction (SPE) sorbent used for urine samples (HLB or MCX). Analytes are classified as scheduled or unscheduled for data acquisition.

Compound	Mass (Da)	Pos/Neg Mode	Matched IS (Y/N)	Retention Time (min)	Plasma Dilution	Urine SPE Plate	Un/Scheduled
4-Hydroxyphenylacetic acid	152.15	neg	Y	0	FA	HLB	Unscheduled
N2,N2-Dimethylguanosine	311.29	pos	Y	4.8	FA	MCX	Scheduled
5-Fluoro-1-methyl-1H-1,3-benzodiazole	150.15	pos	N	1.1	FA	HLB	Scheduled
Pimelic acid	160.17	neg	Y	3.7	AmOH	MCX	Scheduled
3-Methylcrotonylglycine	157.17	neg	Y	2.5	FA	HLB	Scheduled
3-Methoxy-4-hydroxyphenylglycol sulfate	264.25	neg	N	6	FA	HLB	Scheduled
2-[(4-Aminobenzoyl)-amino]acetic acid	194.19	pos	N	4.7	FA	MCX	Scheduled
6'-Sialyl-N-acetyllactosamine[a]	674.60	pos	N	0	FA	--	Unscheduled
2-Hydroxyphenylacetic acid	152.15	neg	N	0	FA	HLB	Unscheduled
1,4-Cyclohexanedicarboxylic acid	172.18	neg	N	3.8	AmOH	MCX	Scheduled
5-Hydroxytryptophan	220.22	pos	Y	7	FA	MCX	Scheduled
4-Acetamidobutyric acid	145.16	pos	N	1.9	FA	HLB	Scheduled
L-Homocitrulline	189.21	pos	Y	7.3	FA	MCX	Scheduled
Gentisic acid	154.12	neg	Y	5.3	FA	HLB	Scheduled
5-Hydroxy-3-indoleacetic acid	191.18	pos	Y	4.6	FA	MCX	Scheduled
Kynurenic acid	189.17	pos	Y	5.7	FA	MCX	Scheduled
4-Pyridoxic acid	183.16	pos	Y	4.7	FA	HLB	Scheduled
N-Isovalerylglycine[b]	159.18	neg	Y	3.6	FA	MCX	Scheduled
N-Isovalerylglycine[b]	159.18	neg	Y	1.9	AmOH	--	Scheduled
Indoxyl sulfate	251.30	neg	Y	5.6	FA	MCX	Scheduled
P-cresol sulfate	188.20	neg	Y	4.4	FA	MCX	Scheduled
Xanthosine	320.26	pos	Y	5.7	FA	HLB	Scheduled
Tiglylglycine	157.17	neg	Y	2.5	FA	HLB	Scheduled
N-Cinnamoylglycine	205.21	pos	Y	3.0	FA	MCX	Scheduled
Hippuric acid	179.17	pos	Y	3.1	FA	MCX	Scheduled

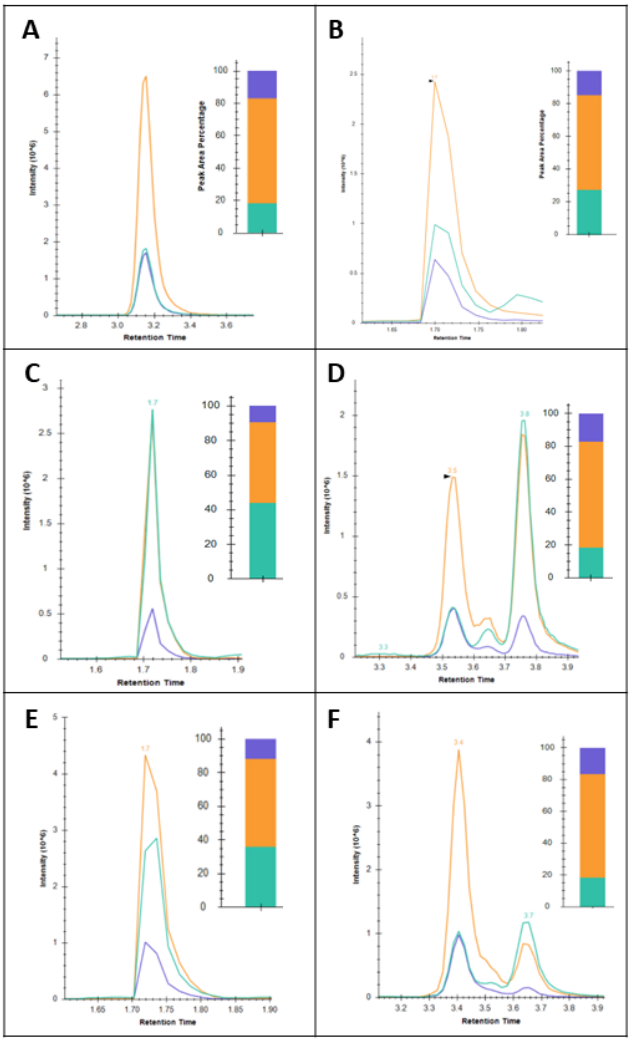

Figure A.1. Chromatographic separation of pimelic acid from an interferent by pH adjustment. Representative chromatograms and transition ion ratio bars are shown for stock injections of unlabeled pimelic acid (A) and unspiked plasma diluted 1:3 in 1% FA in ACN (B), highlighting differences in ion ratios. Dilution 1:1 of plasma in 1% FA in ACN following filtration (C) did not resolve pimelic acid from the interferent, whereas dilution 1:1 in 5% AmOH in ACN (D) achieved separation. Urine samples eluted from the HLB sorbent plate (1% FA / 12% H_2O / 88% ACN) (E) did not resolve pimelic acid, while elution from the MCX sorbent plate (5% AmOH / 38% MeOH / 57% ACN) (F) resulted in clear separation.

Table A.12. Elution and optimization conditions evaluated for HLB (A) and HLB PRiME µElution (B) solid-phase extraction sorbent plates. Panel A shows 12 elution conditions evaluated for the 2mL HLB sorbent plate, varying the composition of organic solvent (acetonitrile, ACN; methanol, MeOH), aqueous content (water, H_2O), and modifier (formic acid, FA; ammonium hydroxide, AmOH). Panel B shows 4 conditions evaluated for the HLB PRiME µElution plate, varying wash solvent composition, elution solvent composition, and post-elution dilution composition, using combinations of FA, MeOH, ACN, and H_2O.

A. HLB sorbent plate

Condition	Elution Solvent
1	40% MeOH / 60% ACN
2	0.1% FA / 99.9% ACN
3	0.1% FA / 12.5% H_2O / 87.4% ACN
4	1% FA / 12% H_2O / 87% ACN
5	1% FA / 5% H_2O / 94% ACN
6	1% FA / 99% ACN
7	1% AmOH / 99% ACN
8	5% AmOH / 95% ACN
9	1% AmOH / 40%MeOH / 59% ACN
10	5% AmOH / 38% MeOH / 57% ACN
11	1% AmOH/ 12% H_2O / 87% ACN
12	5% AmOH / 12% H_2O / 83% ACN

B. HLB PRiME µElution sorbent plate

Condition	Wash Solvent	Elution Solvent	Post-Elution Dilution Composition
13	0.2% FA / 99.8% H_2O	40% MeOH / 60% ACN	1% FA / 20% MeOH / 79% ACN
14	0.2% FA / 99.8% H_2O	40% MeOH / 60% ACN	1% FA / 12% H_2O / 20% MeOH / 67% ACN
15	5% MeOH / 95% H_2O	10% MeOH / 90% ACN	1% FA / 20% MeOH / 79% ACN
16	5% MeOH / 95% H_2O	10% MeOH / 90% ACN	1% FA / 12% H_2O / 20% MeOH / 67% ACN

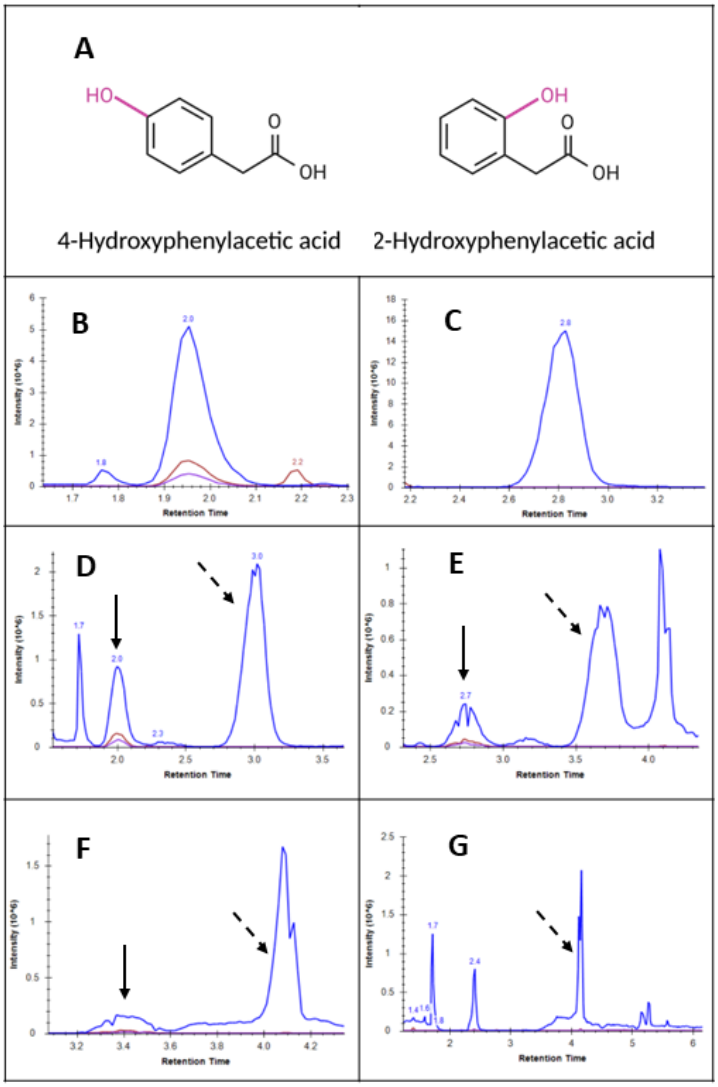

Figure A.2. Chromatographic resolution of 4-hydroxyphenylacetic acid (4OHphe) and 2-hydroxyphenylacetic acid (2OHphe) in urine. Chemical structures of 4OHphe and 2OHphe (A) show that the compounds share the same molecular weight but differ in the position of the hydroxyl substituent (highlighted in pink), indicating positional isomerism. Representative chromatograms and transition ion ratio bars are shown for high spikes of 4OHphe in plasma (B) and 2OHphe in plasma (C). Elution of urine samples from the HLB sorbent plate using 1% FA / 12% H_2O / 88% ACN (D) provided optimal separation and chromatographic performance for both 4OHphe (solid arrow) and 2OHphe (dashed arrow). Elution with 1% FA / 5% H_2O / 94% ACN (E) and 1% FA in ACN (F) resulted in poor chromatography and interference of 2OHphe with a co-eluting interferent. Elution with 1% AmOH / 12% H_2O / 88% ACN (G) resulted in interference of 2OHphe and loss of 4OHphe.

Table A.13. Ion-exchange SPE method development conditions evaluated for urine samples using MCX/WAX and MAX/WCX sorbent plates. Two experiments were performed to optimize the conditioning, equilibration, wash, elution, and post-elution dilution conditions for each sorbent type. In Experiment 1, methanol (MeOH) was used for conditioning and neutral elution, with acid or base modifiers applied for selective elution, and two post-elution dilution compositions were evaluated (1A and 1B). In Experiment 2, acetonitrile (ACN) was used for conditioning, and a single post-elution dilution condition was evaluated for each sorbent type.

Step	MCX / WAX	MAX / WCX
Sample Dilution Solvent	2% FA / 98% H_2O	2% FA / 98% H_2O
Wash Solvent	2% FA / 98% H_2O	5% AmOH / 95% H_2O
Experiment 1		
Conditioning Solvent	100% MeOH	100% MeOH
Equilibration Solvent	100% H_2O	100% H_2O
Neutral Elution	100% MeOH	100% MeOH
Acid/Base Elution	5% AmOH / 95% MeOH	2% FA / 98% MeOH
Post-Elution Dilution 1A	40% Elution Solvent / 60% ACN	40% Elution Solvent / 60% ACN
Post-Elution Dilution 1B	35% Elution Solvent / 12% H_2O / 53% ACN	35% Elution Solvent / 12% H_2O / 53% ACN
Experiment 2		
Conditioning Solvent	100% ACN	100% ACN
Equilibration Solvent	100% H_2O	100% H_2O
Acid/Base Elution	5% AmOH / 95% ACN	2% FA / 98% ACN
Post-Elution Dilution	50% Elution Solvent / 12% H_2O / 38% ACN	50% Elution Solvent / 12% H_2O / 38% ACN

Table A.14. Urine SPE method optimization conditions evaluated for MCX (A) and HLB (B) sorbent plates. Six conditions were evaluated for each sorbent type, with Condition 1 serving as the reference. For both sorbents, Condition 2 omitted the priming step, and Condition 3 omitted both the priming and equilibration steps, while all other parameters remained the same as Condition 1. Conditions 4–6 varied the wash solvent composition by increasing the organic solvent content (methanol, MeOH; acetonitrile, ACN) at the expense of water (H_2O), with formic acid (FA) or ammonium hydroxide (AmOH) included as modifiers.

A. MCX sorbent conditions

Condition	Prime	Equilibrate	Load Sample	Wash	Elute
1 (Reference)	40% MeOH / 60% ACN	2% FA / 98% H_2O	2% FA / 98% H_2O	2% FA / 98% H_2O	5% AmOH / 38% MeOH / 57%ACN
2	None	Same as Condition 1	Same as Condition 1	Same as Condition 1	Same as Condition 1
3	None	None	Same as Condition 1	Same as Condition 1	Same as Condition 1
4	Same as Condition 1	Same as Condition 1	Same as Condition 1	2% FA / 2.5% MeOH / 2.5% ACN / 88% H_2O	Same as Condition 1
5	Same as Condition 1	Same as Condition 1	Same as Condition 1	2% FA / 5% MeOH / 5% ACN / 78% H_2O	Same as Condition 1
6	Same as Condition 1	Same as Condition 1	Same as Condition 1	2% FA / 7.5% MeOH / 7.5% ACN / 68% H_2O	Same as Condition 1

B. HLB sorbent conditions

Condition	Prime	Equilibrate	Load Sample	Wash	Elute
1 (Reference)	1% FA / 12.5% H_2O / 87.5% ACN	0.2% FA / 99.8% H_2O	0.2% FA / 99.8% H_2O	0.2% FA / 99.8% H_2O	1% FA / 12.5% H_2O / 87.5% ACN
2	None	Same as Condition 1	Same as Condition 1	Same as Condition 1	Same as Condition 1
3	None	None	Same as Condition 1	Same as Condition 1	Same as Condition 1
4	Same as Condition 1	Same as Condition 1	Same as Condition 1	0.2% FA / 2.5% MeOH / 2.5% ACN / 89.8% H_2O	Same as Condition 1
5	Same as Condition 1	Same as Condition 1	Same as Condition 1	0.2% FA / 5% MeOH / 5% ACN / 79.8% H_2O	Same as Condition 1
6	Same as Condition 1	Same as Condition 1	Same as Condition 1	0.2% FA / 7.5% MeOH / 7.5% ACN / 69.8% H_2O	Same as Condition 1

Table A.15. Plasma protein precipitation conditions evaluated. Eight protein precipitation conditions were assessed during method development, varying organic solvent type, plasma-to-organic solvent ratio, and formic acid concentration. Acetonitrile (ACN) and methanol (MeOH) were evaluated as precipitating solvents at plasma:organic ratios of 1:3 and 1:4, each tested in the presence or absence of formic acid (1.1%).

Condition	Organic Solvent	Plasma:Organic Ratio	Formic Acid (%)
1	ACN	1:3	0
2	ACN	1:3	1.1
3	ACN	1:4	0
4	ACN	1:4	1.1
5	MeOH	1:3	0
6	MeOH	1:3	1.1
7	MeOH	1:4	0
8	MeOH	1:4	1.1

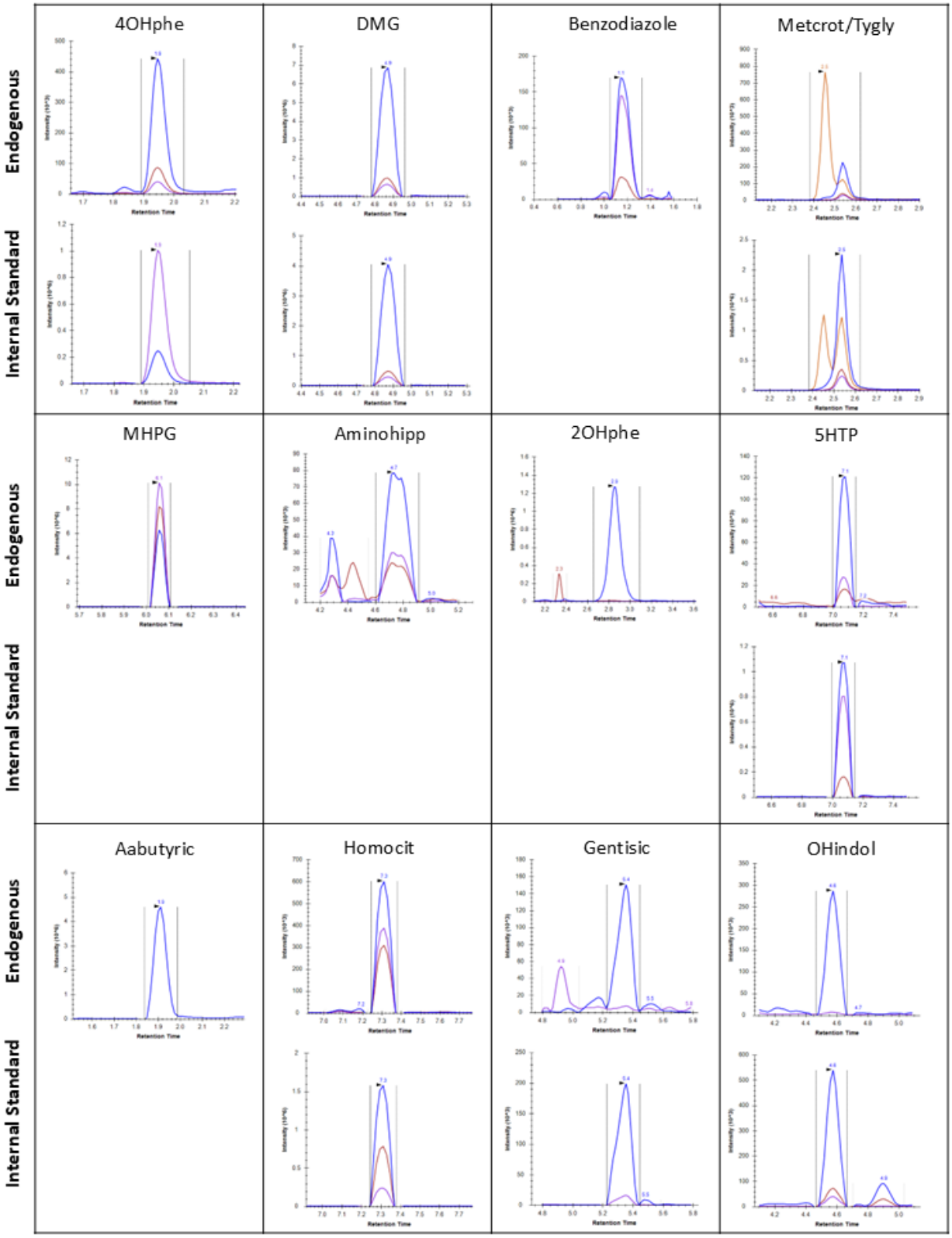
4OHphe
DMG
Benzodiazole
Metcrot/Tygly
MHPG
Aminohipp
2OHphe
5HTP
Aabutyric
Homocit
Gentisic
OHindol
Endogenous
Internal Standard
Endogenous
Internal Standard
Endogenous
Internal Standard
Retention Time

Figure A.3. Representative chromatograms from a serum single-point calibrator (SPC) 1. Chromatograms are shown for 12 analytes across three rows, displaying endogenous compound (top panel) and matched internal standard (IS, bottom panel) traces for each analyte where applicable. Multiple colored traces represent individual multiple reaction monitoring (MRM) transitions. Analyte abbreviations correspond to those defined in Table A.1.

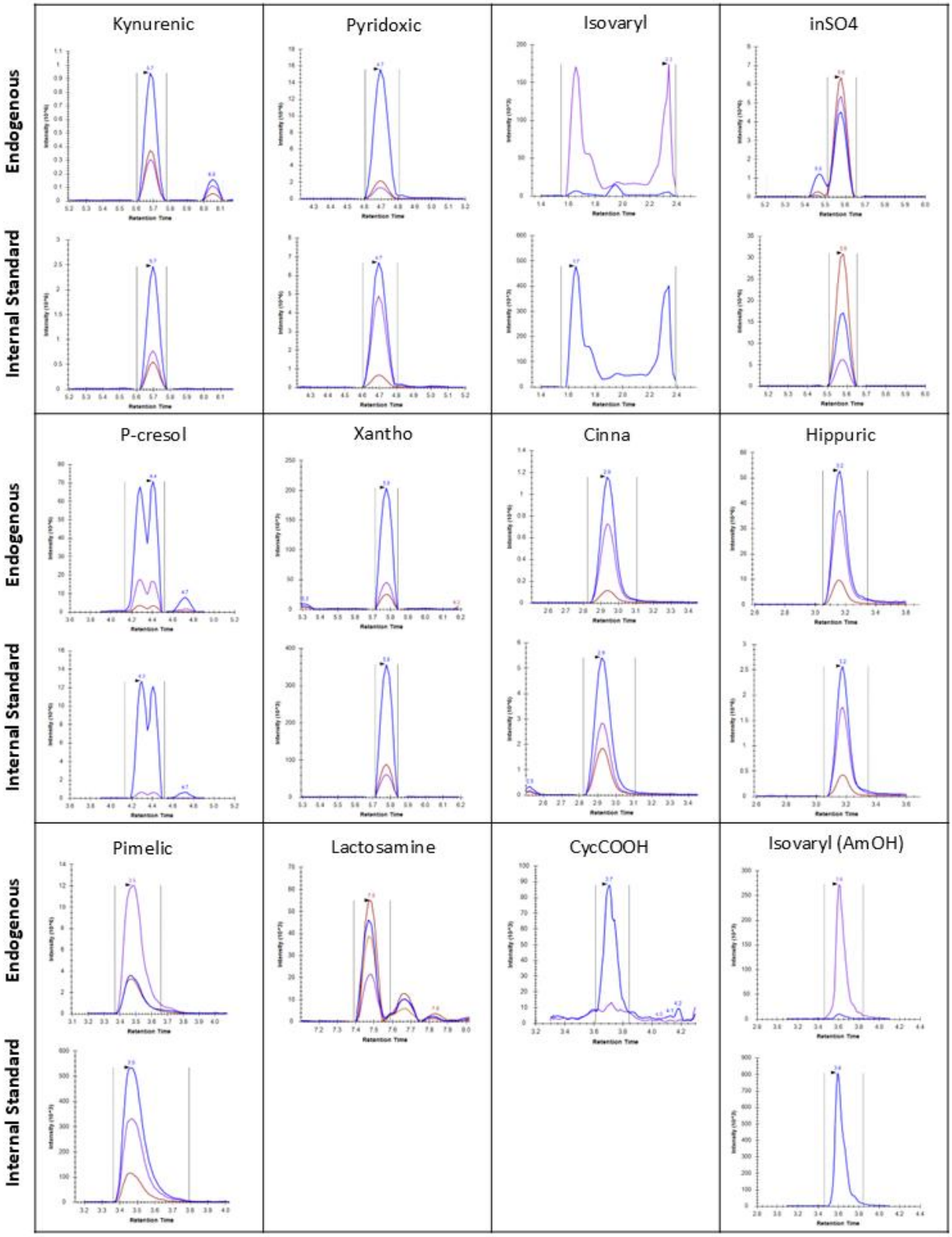
Endogenous
Internal Standard
Kynurenic
Pyridoxic
Isovaryl
inSO4
P-cresol
Xantho
Cinna
Hippuric
Pimelic
Lactosamine
CycCOOH
Isovaryl (AmOH)

Figure A.4. Representative ion chromatograms from a serum single-point calibrator (SPC) 2. Chromatograms are shown for 12 analytes across three rows, displaying endogenous compound (top panel) and matched internal standard (IS, bottom panel) signal for each analyte where applicable. Multiple colored traces represent individual multiple reaction monitoring (MRM) transitions. Analyte abbreviations correspond to those defined in Table 1. Isovaryl (AmOH) represents N-Isovalerylglycine diluted in basic solvent, shown separately from the formic acid condition.

Table A.16. Internal standard vendors and stock concentrations. A panel of 17 isotopically labeled internal standards was selected corresponding to the analytes of interest. Each internal standard is listed with its commercial vendor and catalog number, solvent, stock concentration (µM), and working concentration (µM).

Internal Standard	Vendor	Solvent	Stock Concentration (µM)	Working Concentration (µM)
4-Hydroxyphenylacetic acid-d6 ($^{2}H_{6}$)	MCE: HY-N1902S	DMSO	20000	300
2-(Dimethylamino)guanosine-d6 ($^{2}H_{6}$)	TRC: D460852	DMSO	6870	2
Pimelic Acid-d4 ($^{2}H_{4}$)	TRC: P445042	DMSO	10000	2
3-Methylcrotonylglycine ($^{13}C_{2}$,^{15}N)	TRC: M294542	DMSO	4780	1
5-Hydroxy-L-tryptophan-d3 ($^{2}H_{3}$)	CDN Isotopes: D-7154	DMSO	6010	24
L-Homocitrulline-d3 ($^{2}H_{3}$)	CDN Isotopes: D-7917	0.05% AmOH in H2O	10000	21
2,5-Dihydroxybenzoic Acid-d3 ($^{2}H_{3}$)	TRC: D451657	0.08% AmOH in H2O	5000	14
5-Hydroxyindole-3-acetic acid ($^{13}C_{6}$)	Cambridge Isotopes: CLM-9936-PK	DMSO	10000	15
Kynurenic acid-d5 ($^{2}H_{5}$)	TRC: K660502	DMSO	51512	13
4-Pyridoxic acid-d3 ($^{2}H_{3}$)	TRC: P99777	DMSO	5371	3
N-Isovalerylglycine-d2 ($^{2}H_{2}$)	CDN: D-6230	DMSO	31035	2
Indoxyl sulfate ($^{13}C_{6}$)	Sigma: 809780	DMSO	4564	46
P-cresol sulfate-d7 ($^{2}H_{7}$)	TRC: T536802	DMSO	10000	200
Xanthosine ($^{13}C_{5}$)	TRC: X742102	DMSO	10000	3
Tiglylglycine ($^{13}C_{2}$,^{15}N)	TRC: T440102	Methanol	6246	9
N-Cinnamoylglycine-d2 ($^{2}H_{2}$)	Medical Isotopes PN: D32615	Methanol	483	5
Hippuric acid-d5 ($^{2}H_{5}$)	TRC: H356702	DMSO	54321	5

Table A.17. Chromatographic parameters. Liquid chromatography conditions used for the separation of all analytes. Mobile phase A consisted of 95% acetonitrile (ACN)/3% methanol (MeOH)/2% water with 0.1% formic acid (FA), and mobile phase B consisted of 95% water/5% ACN with 100 mM ammonium formate. The needle wash solvent was composed of 25% ACN/25% MeOH/25% water/25% isopropanol (IPA). Separations were performed at a flow rate of 0.4 mL/min with the column oven maintained at 50 °C and the autosampler at 7 °C.

Mobile Phase A	95% ACN/3% MeOH/2% water + 0.1% FA
Mobile Phase B	95% water/5% ACN + 100mM Ammonium Formate
Needle Wash	25% ACN/25% MeOH/25% water/25% IPA
Flow Rate	0.4 mL/min
Autosampler Temperature	7 °C
Column Oven Temperature	50 °C

Table A.18. Chromatographic program. The liquid chromatography gradient and divert valve actions are listed as a function of run time (min). Mobile phase composition is expressed as percentage of solvent B, with the column re-equilibrated to initial conditions (0% B) following elution. The divert valve was directed to waste during the first 0.30 min and after 10.20 min of each run to minimize ion source contamination, with a total run time of 11.00 min.

Time (min)	Action
0.00	Divert to Waste
0.00	0% B
0.25	0% B
0.30	Divert to Instrument
0.75	0% B
7.90	46.5% B
8.00	60% B
9.50	60% B
9.65	0% B
10.15	0% B
10.20	Divert to Waste
11.00	End Run

Table A.19. Matched internal standards and surrogates used for estimating single-point calibrator (SPC) concentrations. Each analyte is paired with its corresponding isotopically labeled internal standard. Analytes marked with an asterisk (*) lacked a matched internal standard and were instead assigned a structurally or chromatographically similar surrogate internal standard, shown in bold. Two analytes, 6′-Sialyl-N-acetyllactosamine and 1,4-Cyclohexanedicarboxylic acid, were excluded from the assay before SPC quantification.

Compound	Internal Standards used to estimate SPC concentration
4-Hydroxyphenylacetic acid	4-Hydroxyphenylacetic acid-d6 ($^{2}H_{6}$)
N2,N2-Dimethylguanosine	2-(Dimethylamino)guanosine-d6 ($^{2}H_{6}$)
5-Fluoro-1-methyl-1H-1,3-benzodiazole*	**Kynurenic acid-d5 ($^{2}H_{5}$)**
Pimelic acid	Pimelic Acid-d4 ($^{2}H_{4}$)
3-Methylcrotonylglycine	3-Methylcrotonylglycine ($^{13}C_{2}$,^{15}N)
3-Methoxy-4-hydroxyphenylglycol sulfate*	**Indoxyl sulfate ($^{13}C_{6}$)**
2-[(4-Aminobenzoyl)-amino]acetic acid*	**5-Hydroxyindole-3-acetic acid ($^{13}C_{6}$)**
6'-Sialyl-N-acetyllactosamine*	--
2-Hydroxyphenylacetic acid*	**2,5-Dihydroxybenzoic Acid-d3 ($^{2}H_{3}$)**
1,4-Cyclohexanedicarboxylic acid*	--
5-Hydroxytryptophan	5-Hydroxy-L-tryptophan-d3 ($^{2}H_{3}$)
4-Acetamidobutyric acid*	**3-Methylcrotonylglycine ($^{13}C_{2}$,^{15}N)**
L-Homocitrulline	L-Homocitrulline-d3 ($^{2}H_{3}$)
Gentisic acid	2,5-Dihydroxybenzoic Acid-d3 ($^{2}H_{3}$)
5-Hydroxy-3-indoleacetic acid	5-Hydroxyindole-3-acetic acid ($^{13}C_{6}$)
Kynurenic acid	Kynurenic acid-d5 ($^{2}H_{5}$)
4-Pyridoxic acid	4-Pyridoxic acid-d3 ($^{2}H_{3}$)
N-Isovalerylglycine	N-Isovalerylglycine-d2 ($^{2}H_{2}$)
Indoxyl sulfate	Indoxyl sulfate ($^{13}C_{6}$)
P-cresol sulfate	P-cresol sulfate-d7 ($^{2}H_{7}$)
Xanthosine	Xanthosine ($^{13}C_{5}$)
Tiglylglycine	Tiglylglycine ($^{13}C_{2}$,^{15}N)
N-Cinnamoylglycine	N-Cinnamoylglycine-d2 ($^{2}H_{2}$)
Hippuric acid	Hippuric acid-d5 ($^{2}H_{5}$)

*No matched internal standard; surrogate internal standards indicated in bold

B. APPENDIX B. ASSAY VALIDATION SUPPLEMENTAL FIGURES AND TABLES

Table B.1. Urine linearity summary. Linearity was assessed by gravimetrically mixing a high- and low-concentration urine sample across seven mixing levels (12.5–87.5%) over three days (n = 9 per mixing level). Percent bias was calculated relative to the gravimetrically assigned concentration at each mixing level. The highest coefficient of variation (%CV) observed across all mixing levels and days is shown. R^2 was calculated by linear regression across all replicates. Cells are colour-coded as follows: green = bias 85–115%, %CV ≤15%, R^2 ≥0.95; yellow = bias 80–85% or 115–120%, %CV 15–20%, R^2 0.90–0.95; red = bias <80% or >120%, %CV >20%, R^2 <0.90. Solid phase extraction (SPE) plate used for extraction is indicated (HLB or MCX).

Urine Linearity Summary

Green = 85–115%; Yellow = 80–85% or 115–120%; Red = <80% or >120%. Max %CV: green ≤15%, red >15%. R^2: green ≥0.95, yellow 0.90–0.95, red <0.90

Compound	SPE	12.5%	25%	37.5%	50%	62.5%	75%	87.5%	Max %CV	R^2
4-Hydroxyphenylacetic acid	HLB	95%	98%	95%	98%	101%	97%	101%	13%	0.931
N2,N2-Dimethylguanosine	MCX	111%	105%	107%	103%	108%	104%	102%	7%	0.985
5-Fluoro-1-methyl-1H-1,3-benzodiazole	HLB	69%	68%	72%	75%	77%	84%	86%	14%	0.972
Pimelic acid	MCX	99%	95%	94%	96%	94%	96%	98%	5%	0.995
3-Methylcrotonylglycine	HLB	102%	98%	93%	100%	100%	103%	104%	9%	0.986
3-Methoxy-4-hydroxyphenylglycol sulfate	HLB	132%	111%	104%	96%	111%	96%	110%	12%	0.757
2-[(4-Aminobenzoyl)-amino]acetic acid	MCX	97%	97%	99%	100%	95%	98%	99%	50%	0.994
2-Hydroxyphenylacetic acid	HLB	106%	103%	102%	99%	102%	99%	107%	7%	0.956
1,4-Cyclohexanedicarboxylic acid	MCX	69%	70%	71%	72%	72%	77%	84%	115%	0.928
5-Hydroxytryptophan	MCX	102%	97%	96%	99%	99%	101%	101%	32%	0.940
4-Acetamidobutyric acid	HLB	122%	113%	107%	104%	111%	99%	121%	30%	0.558
L-Homocitrulline	MCX	101%	95%	97%	99%	98%	98%	100%	7%	0.991
Gentisic acid	MCX	99%	95%	96%	97%	96%	99%	99%	5%	0.994
5-Hydroxy-3-indoleacetic acid	MCX	98%	99%	107%	91%	93%	103%	100%	20%	0.924
Kynurenic acid	MCX	100%	97%	97%	95%	96%	100%	98%	5%	0.992
4-Pyridoxic acid	HLB	106%	102%	102%	102%	102%	104%	102%	7%	0.993
N-Isovalerylglycine	MCX	136%	126%	122%	116%	110%	108%	104%	4%	0.992
Indoxyl sulfate	MCX	98%	102%	92%	99%	98%	93%	95%	18%	0.925
P-cresol sulfate	MCX	100%	98%	99%	99%	98%	104%	98%	9%	0.980
Xanthosine	HLB	100%	97%	96%	94%	98%	95%	97%	13%	0.938
Tiglylglycine	HLB	99%	95%	95%	95%	96%	96%	98%	8%	0.983
N-Cinnamoylglycine	MCX	106%	97%	97%	100%	91%	92%	93%	16%	0.963
Hippuric acid	MCX	112%	117%	109%	116%	102%	116%	106%	23%	0.780

Table B.2. Serum linearity summary. Linearity was assessed by gravimetrically mixing a high- and low-concentration serum sample across seven mixing levels (12.5–87.5%) over three days (n = 9 per mixing level). Percent bias was calculated relative to the gravimetrically assigned concentration at each mixing level. The highest coefficient of variation (%CV) observed across all mixing levels and days is shown. R^2 was calculated by linear regression across all replicates. Cells are colour-coded as follows: green = bias 85–115%, %CV ≤15%, R^2 ≥0.95; yellow = bias 80–85% or 115–120%, %CV 15–20%, R^2 0.90–0.95; red = bias <80% or >120%, %CV >20%, R^2 <0.90.

Serum Linearity Summary

Green = 85–115%; Yellow = 80–85% or 115–120%; Red = <80% or >120%. Max %CV: green ≤15%, red >15%. R^2: green ≥0.95, yellow 0.90–0.95, red <0.90

Compound	12.5%	25%	37.5%	50%	62.5%	75%	87.5%	Max %CV	R^2
4-Hydroxyphenylacetic acid	103%	105%	106%	105%	108%	102%	102%	10%	0.956
N2,N2-Dimethylguanosine	119%	113%	105%	110%	107%	103%	99%	8%	0.975
5-Fluoro-1-methyl-1H-1,3-benzodiazole	101%	102%	104%	102%	96%	100%	102%	10%	0.991
Pimelic acid	126%	119%	115%	110%	107%	104%	100%	4%	0.989
3-Methylcrotonylglycine	104%	102%	101%	97%	96%	95%	94%	8%	0.961
3-Methoxy-4-hydroxyphenylglycol sulfate	154%	133%	124%	113%	101%	105%	100%	9%	0.942
2-[(4-Aminobenzoyl)-amino]acetic acid	144%	134%	128%	118%	110%	109%	105%	6%	0.978
2-Hydroxyphenylacetic acid	191%	162%	147%	129%	115%	111%	104%	6%	0.941
1,4-Cyclohexanedicarboxylic acid	190%	155%	134%	121%	108%	102%	101%	26%	0.853
5-Hydroxytryptophan	95%	103%	106%	109%	106%	106%	91%	24%	0.883
4-Acetamidobutyric acid	137%	131%	129%	120%	123%	105%	107%	9%	0.951
L-Homocitrulline	108%	104%	101%	103%	102%	104%	104%	7%	0.974
Gentisic acid	135%	129%	122%	118%	111%	106%	103%	5%	0.916
5-Hydroxy-3-indoleacetic acid	99%	110%	110%	95%	102%	105%	94%	17%	0.917
Kynurenic acid	102%	97%	96%	94%	99%	96%	99%	11%	0.977
4-Pyridoxic acid	105%	106%	102%	101%	100%	99%	105%	12%	0.988
N-Isovalerylglycine	163%	150%	137%	127%	118%	111%	104%	7%	0.947
Indoxyl sulfate	108%	105%	103%	103%	103%	102%	102%	7%	0.987
P-cresol sulfate	104%	105%	104%	100%	100%	98%	100%	7%	0.977
Xanthosine	103%	100%	99%	99%	99%	98%	97%	7%	0.980
Tiglylglycine	101%	101%	99%	96%	102%	101%	100%	11%	0.984
N-Cinnamoylglycine	111%	107%	107%	104%	102%	103%	98%	7%	0.955
Hippuric acid	103%	104%	107%	102%	100%	101%	100%	14%	0.964

Table B.3. Urine lower limit of quantification (LLOQ) summary. The LLOQ was determined by diluting a high-concentration urine sample with water to 20%, 40%, 60%, and 80% of the original concentration. Percent bias was calculated as the deviation from the expected peak area ratio at each dilution level. The LLOQ was defined as the lowest dilution level meeting acceptance criteria of |bias| ≤20% and %CV ≤20% across all replicates. Cells are color-coded: green = acceptable (|bias| ≤20%, %CV ≤20%); red = unacceptable. The LLOQ is reported in µM. Compounds that did not meet acceptance criteria at any dilution level are indicated as FAIL. Solid phase extraction (SPE) plate used for extraction is indicated (HLB or MCX).

Urine LLOQ Summary

Bias expressed as % deviation from expected. Acceptance criteria: |bias| ≤20%, CV ≤20%

		20%		40%		60%		80%		
Compound	SPE	20% Bias	20% CV	40% Bias	40% CV	60% Bias	60% CV	80% Bias	80% CV	LLOQ (µM)
4-Hydroxyphenylacetic acid	HLB	-2.8%	6.5%	-0.2%	6.4%	-1.3%	4.1%	2.9%	5.3%	256
N2,N2-Dimethylguanosine	MCX	1.9%	7.9%	1.7%	2.2%	1.5%	3.7%	-0.3%	6.2%	3.93
5-Fluoro-1-methyl-1H-1,3-benzodiazole	HLB	-1.5%	22.6%	2.3%	22.2%	4.5%	11.5%	-2.8%	7.8%	0.012
3-Methylcrotonylglycine	HLB	2.5%	4.3%	1.3%	5.6%	2.6%	4.6%	3%	7.5%	0.193
3-Methoxy-4-hydroxyphenylglycol sulfate	HLB	123.6%	10.2%	76.9%	8.4%	42.7%	8.7%	21.2%	13.7%	FAIL
2-[(4-Aminobenzoyl)-amino]acetic acid	MCX	5.2%	22.9%	-15.9%	38.3%	-18.5%	44.9%	6.6%	42.3%	FAIL
2-Hydroxyphenylacetic acid	HLB	47.2%	3.8%	23.5%	4.3%	13.2%	5.4%	20.2%	12.5%	69.1
5-Hydroxytryptophan	MCX	-12.8%	34.4%	-12.2%	9.1%	-8.4%	18%	0.6%	24.9%	FAIL
4-Acetamidobutyric acid	HLB	41.8%	10%	19.6%	24.1%	10.1%	11%	25.7%	21.5%	FAIL
L-Homocitrulline	MCX	-9%	11.2%	-5.6%	6.9%	-2.1%	25.2%	-3.3%	10.5%	10.4
Gentisic acid	HLB	-6.4%	5%	-5.7%	4%	-2.8%	2.5%	-1.3%	4.3%	4.99
5-Hydroxy-3-indoleacetic acid	MCX	-1.8%	11.7%	0.2%	6.6%	-0.3%	6.9%	0.9%	6.9%	9.69
Kynurenic acid	MCX	-14.3%	14%	-8%	19.6%	-6%	9.6%	-4.3%	8.5%	2.44
4-Pyridoxic acid	HLB	-5.3%	4.4%	-1.5%	4.4%	-2.6%	3.4%	-1.8%	4.6%	1.67
N-Isovalerylglycine	MCX	-8.9%	5.7%	-3.8%	1.9%	-2.9%	2.5%	-2.6%	1.7%	0.775
Indoxyl sulfate	MCX	-9.7%	7.1%	-0.6%	6.3%	-1.3%	2.1%	-0.9%	4.4%	30.3
P-cresol sulfate	MCX	-10.4%	5.7%	-5.2%	5.4%	-3.3%	4.2%	-3.2%	5.9%	88.6
Xanthosine	HLB	-3.5%	11.2%	-0.5%	12.9%	0.5%	11.9%	-3%	10.9%	1.09
Tiglylglycine	HLB	-9.4%	5.6%	-6.1%	5.8%	-3.9%	2.9%	-2.7%	6.4%	2.23
N-Cinnamoylglycine	MCX	-13%	5.9%	-6.7%	3.3%	-5.1%	5.6%	-5.5%	6.3%	0.999
Hippuric acid	MCX	19.8%	6.8%	15.4%	12.5%	6.6%	7%	3.8%	8.3%	328

Table B.4. Serum lower limit of quantification (LLOQ) summary. The LLOQ was determined by diluting a high serum sample with MassCheck Serum 3000 (MSG3000) to 20%, 40%, 60%, and 80% of the original concentration. Percent bias was calculated as the deviation from the expected peak area ratio at each dilution level. The LLOQ was defined as the lowest dilution level meeting acceptance criteria of |bias| ≤20% and %CV ≤20% across all replicates. Cells are color-coded as follows: green = acceptable (|bias| ≤20%, %CV ≤20%); red = unacceptable. The LLOQ is reported in nM. Compounds that did not meet acceptance criteria at any dilution level are indicated as FAIL.

Serum LLOQ Summary

Bias expressed as % deviation from expected. Acceptance criteria: |bias| ≤20%, CV ≤20%

	20%		40%		60%		80%		
Compound	20% Bias	20% CV	40% Bias	40% CV	60% Bias	60% CV	80% Bias	80% CV	LLOQ (nM)
4-Hydroxyphenylacetic acid	11%	5.4%	4.2%	5.2%	3.6%	5.4%	2.6%	3.5%	535
N2,N2-Dimethylguanosine	4.6%	9.8%	11%	4%	3.8%	10.6%	-1.3%	11.4%	6.72
5-Fluoro-1-methyl-1H-1,3-benzodiazole	9.9%	19%	29.2%	26.3%	24.3%	16.3%	26.4%	20.9%	FAIL
3-Methylcrotonylglycine	14.8%	45.1%	31.5%	12.8%	13.6%	19.8%	6.7%	16.1%	1.06
3-Methoxy-4-hydroxyphenylglycol sulfate	17.8%	8%	3%	15.9%	-0.5%	8.1%	2.9%	13%	6.83
2-[(4-Aminobenzoyl)-amino]acetic acid	-3.5%	30.9%	-19.3%	55.9%	-15.6%	60.7%	42.8%	68.6%	FAIL
2-Hydroxyphenylacetic acid	10.4%	6.4%	6.3%	7.3%	1.8%	5.5%	-0.5%	5.5%	574
5-Hydroxytryptophan	-25.6%	31.8%	-13.8%	30.4%	20.7%	23.9%	-2%	26.8%	FAIL
4-Acetamidobutyric acid	16.9%	15.2%	1.2%	3.4%	-0.2%	3.8%	4.7%	10.3%	15.5
L-Homocitrulline	6.5%	11.7%	2.8%	8.1%	-2%	6.7%	-2.8%	8.6%	112
Gentisic acid	-3.2%	6.5%	1.2%	7%	-0.8%	3.3%	-2%	6.4%	103
5-Hydroxy-3-indoleacetic acid	20.9%	22.7%	1.5%	22.5%	3.4%	14.4%	-4.1%	14.4%	67.3
Kynurenic acid	1.5%	8.2%	0.5%	4.6%	2.4%	4.7%	1.9%	8.8%	29
4-Pyridoxic acid	-0.8%	4.9%	2.6%	5.8%	2.7%	2.9%	2.2%	4.8%	4.34
N-Isovalerylglycine	-0.5%	7.1%	0.9%	4.5%	2.1%	4.8%	1.8%	5.6%	1.43
Indoxyl sulfate	3.2%	11.2%	7.2%	7.9%	0.3%	6.3%	5.9%	6.4%	441
P-cresol sulfate	9.8%	4.8%	7%	3.7%	-0.2%	2.8%	3.2%	3.1%	15400
Xanthosine	-6.5%	16.5%	2.9%	3.4%	-3.5%	8.1%	3.8%	7.6%	4.72
Tiglylglycine	-1.3%	30.2%	-26.6%	15%	-2.3%	33%	-4.5%	25.5%	FAIL
N-Cinnamoylglycine	5.3%	5.9%	11.6%	4.4%	1.3%	4.7%	7%	4.9%	3.53
Hippuric acid	4.8%	17.4%	-1.1%	8.5%	1.3%	9.5%	4.6%	13.1%	599

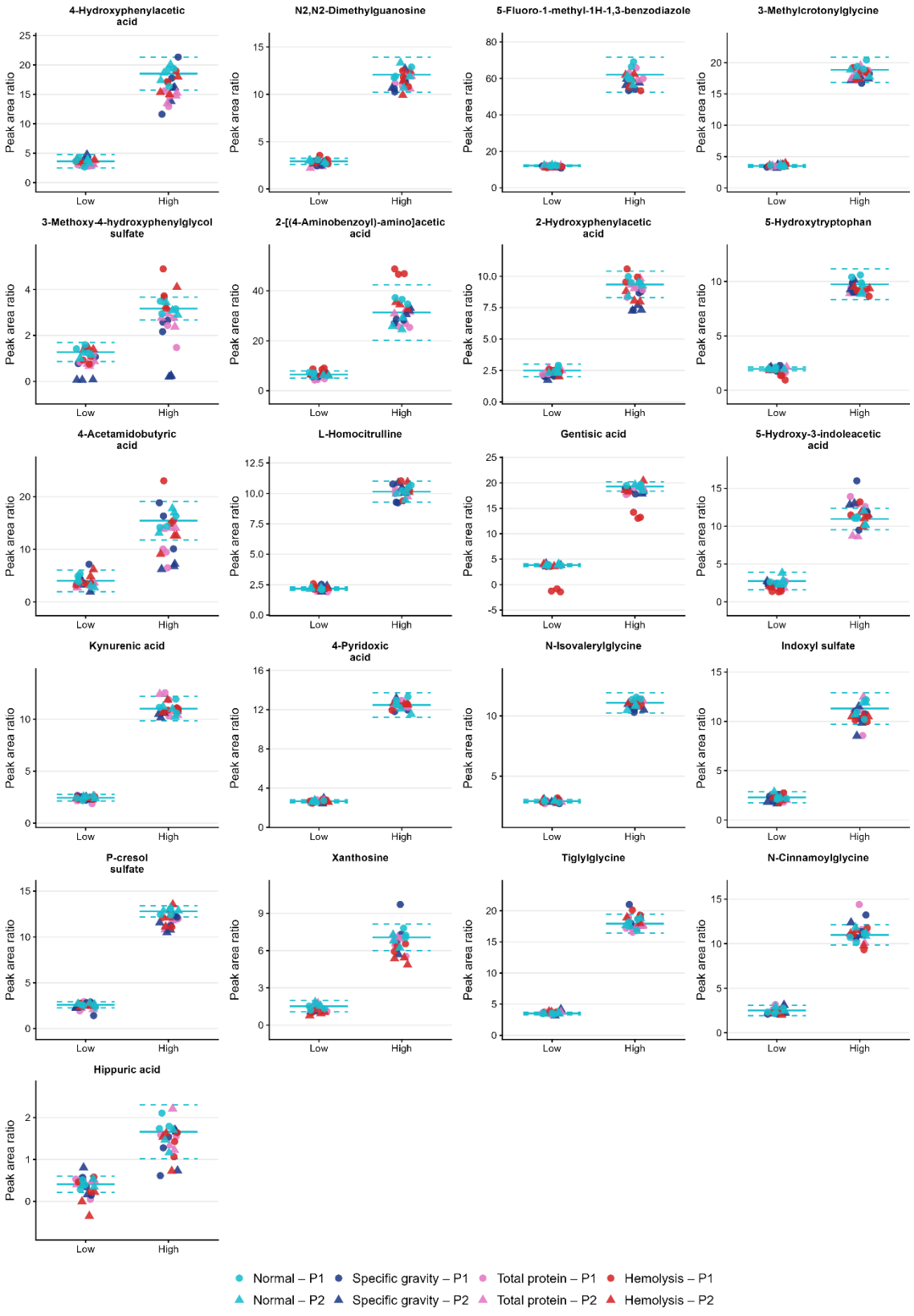
Urine Interference Analysis
Cyan line = Normal mean per level; dashed = mean ± 2SD
Circle = P1; triangle = P2
4-Hydroxyphenylacetic acid
N2,N2-Dimethylguanosine
5-Fluoro-1-methyl-1H-1,3-benzodiazole
3-Methylcrotonylglycine
3-Methoxy-4-hydroxyphenylglycol sulfate
2-[(4-Aminobenzoyl)-amino]acetic acid
2-Hydroxyphenylacetic acid
5-Hydroxytryptophan
4-Acetamidobutyric acid
L-Homocitrulline
Gentisic acid
5-Hydroxy-3-indoleacetic acid
Kynurenic acid
4-Pyridoxic acid
N-Isovalerylglycine
Indoxyl sulfate
P-cresol sulfate
Xanthosine
Tiglylglycine
N-Cinnamoylglycine
Hippuric acid
Peak area ratio
Low
High
Normal – P1
Specific gravity – P1
Total protein – P1
Hemolysis – P1
Normal – P2
Specific gravity – P2
Total protein – P2
Hemolysis – P2

Figure B.1. Urine interference analysis. Peak area ratios were measured for 21 urine metabolites across two concentration levels (Low and High) in the presence of three interferants: specific gravity (1.042–1.054), severe hemolysis (4+), and total protein (3+). Two individual patient urine samples (P1 and P2) were tested with each interferant. Cyan lines represent the mean of the normal (unmodified) urine samples at each concentration level; dashed lines represent the mean ± 2SD. Marker shape indicates patient sample (circle = P1; triangle = P2); color indicates interferant.

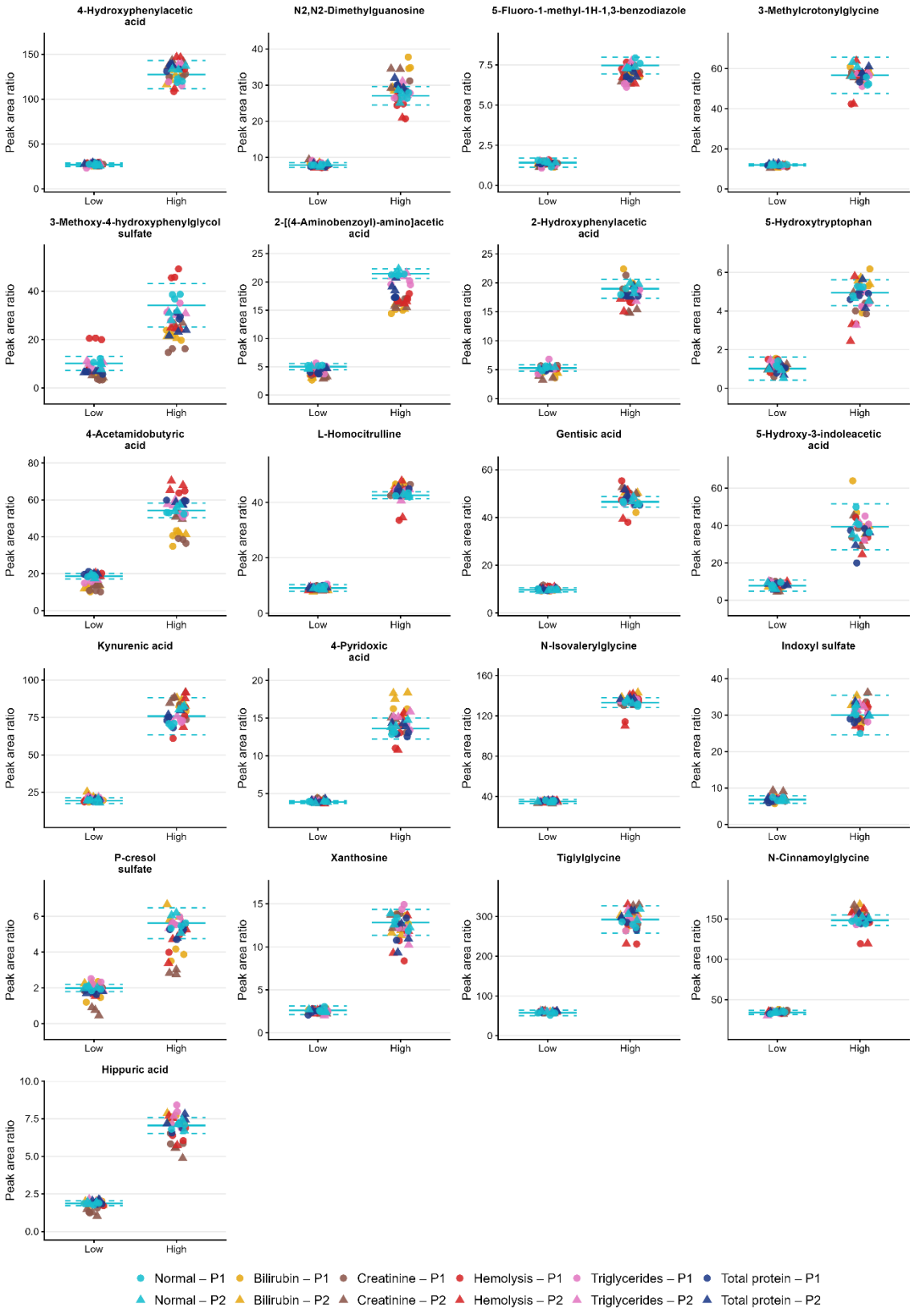
Serum Interference Analysis
Cyan line = Normal mean per level; dashed = mean ± 2SD
Circle = P1; triangle = P2
4-Hydroxyphenylacetic acid
N2,N2-Dimethylguanosine
5-Fluoro-1-methyl-1H-1,3-benzodiazole
3-Methylcrotonylglycine
3-Methoxy-4-hydroxyphenylglycol sulfate
2-[(4-Aminobenzoyl)-amino]acetic acid
2-Hydroxyphenylacetic acid
5-Hydroxytryptophan
4-Acetamidobutyric acid
L-Homocitrulline
Gentisic acid
5-Hydroxy-3-indoleacetic acid
Kynurenic acid
4-Pyridoxic acid
N-Isovalerylglycine
Indoxyl sulfate
P-cresol sulfate
Xanthosine
Tiglylglycine
N-Cinnamoylglycine
Hippuric acid
Peak area ratio
Low
High
Normal – P1
Bilirubin – P1
Creatinine – P1
Hemolysis – P1
Triglycerides – P1
Total protein – P1
Normal – P2
Bilirubin – P2
Creatinine – P2
Hemolysis – P2
Triglycerides – P2
Total protein – P2

Figure B.2. Serum interference analysis. Peak area ratios were measured for 21 serum metabolites across two concentration levels (Low and High) in the presence of five interferants: bilirubin (38–39 mg/dL), creatinine (15–18 mg/dL), severe hemolysis, triglycerides (388–460 mg/dL), and total protein (8.6–9.1 g/dL). Two individual patient serum samples (P1 and P2) were tested with each interferant. Cyan lines represent the mean of the normal serum samples at each concentration level; dashed lines represent the mean ± 2SD. Marker shape indicates patient sample (circle = P1; triangle = P2); color indicates interferant.

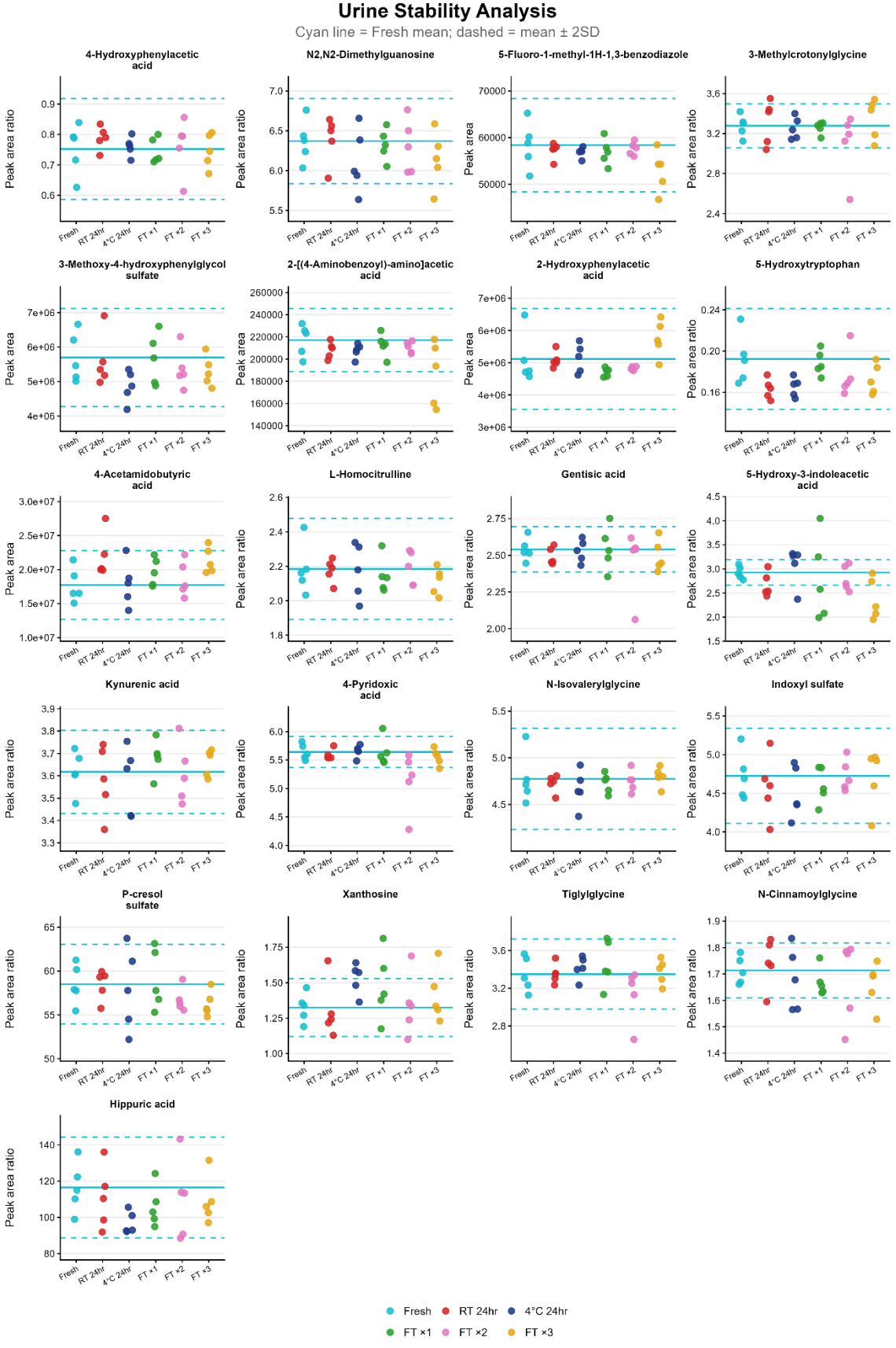
Urine Stability Analysis
Cyan line = Fresh mean; dashed = mean ± 2SD
4-Hydroxyphenylacetic acid
N2,N2-Dimethylguanosine
5-Fluoro-1-methyl-1H-1,3-benzodiazole
3-Methylcrotonylglycine
3-Methoxy-4-hydroxyphenylglycol sulfate
2-[(4-Aminobenzoyl)-amino]acetic acid
2-Hydroxyphenylacetic acid
5-Hydroxytryptophan
4-Acetamidobutyric acid
L-Homocitrulline
Gentisic acid
5-Hydroxy-3-indoleacetic acid
Kynurenic acid
4-Pyridoxic acid
N-Isovalerylglycine
Indoxyl sulfate
P-cresol sulfate
Xanthosine
Tiglylglycine
N-Cinnamoylglycine
Hippuric acid
Peak area ratio
Peak area
Fresh
RT 24hr
4°C 24hr
FT ×1
FT ×2
FT ×3

Figure B.3. Urine stability analysis. The stability of 21 urine metabolites was assessed in a single point calibrator (SPC) under four storage conditions: room temperature for 24 hours (RT 24hr), refrigeration at 4°C for 24 hours (4°C 24hr), and one, two, and three freeze-thaw cycles (FT ×1, FT ×2, FT ×3). Five replicates were analyzed per condition. The cyan line represents the mean of freshly thawed SPC samples; dashed lines represent the mean ± 2SD. Peak area ratio is shown for compounds with an internal standard; peak area is shown for compounds without.

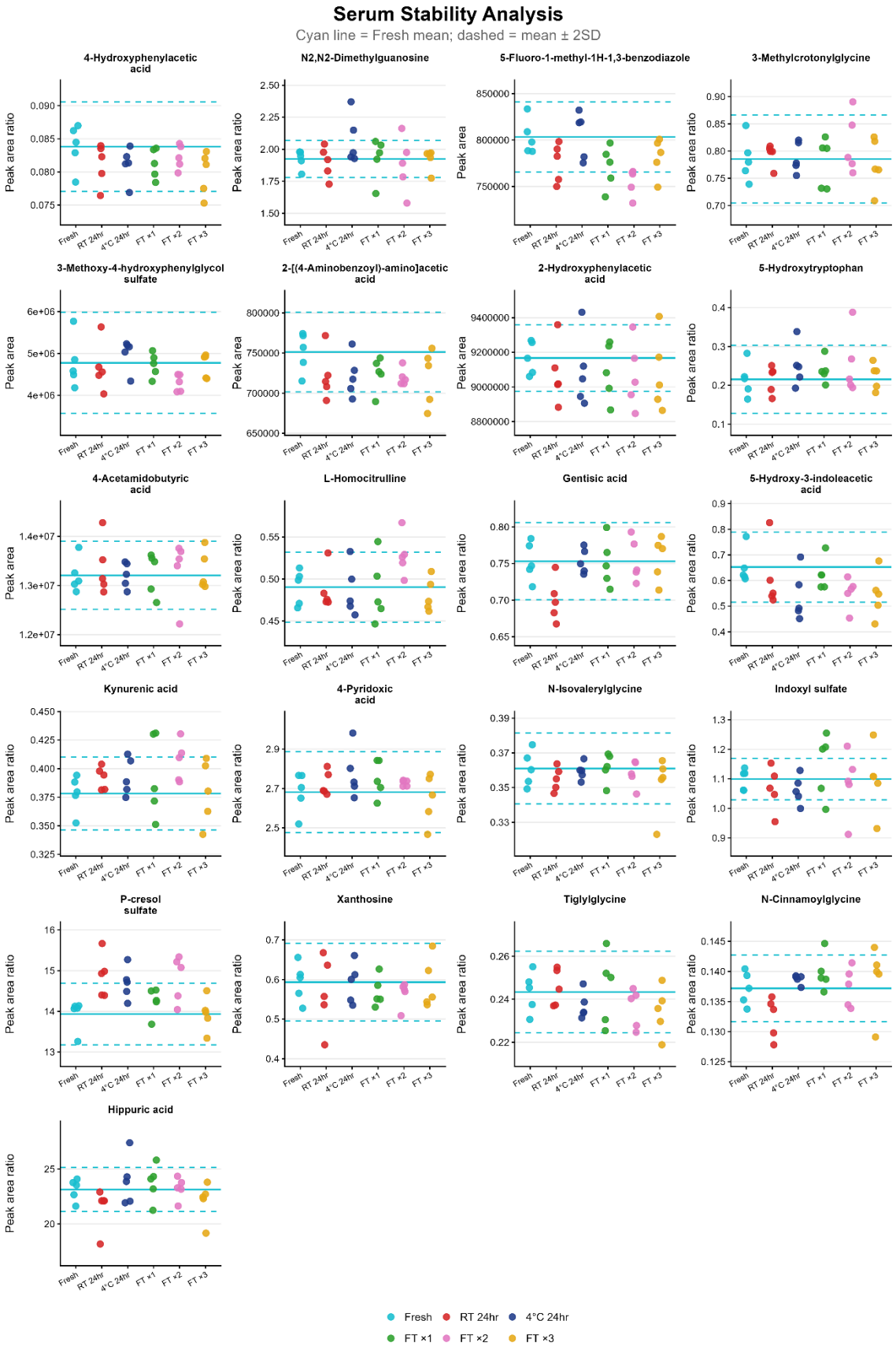
Serum Stability Analysis
Cyan line = Fresh mean; dashed = mean ± 2SD
4-Hydroxyphenylacetic acid
N2,N2-Dimethylguanosine
5-Fluoro-1-methyl-1H-1,3-benzodiazole
3-Methylcrotonylglycine
3-Methoxy-4-hydroxyphenylglycol sulfate
2-[(4-Aminobenzoyl)-amino]acetic acid
2-Hydroxyphenylacetic acid
5-Hydroxytryptophan
4-Acetamidobutyric acid
L-Homocitrulline
Gentisic acid
5-Hydroxy-3-indoleacetic acid
Kynurenic acid
4-Pyridoxic acid
N-Isovalerylglycine
Indoxyl sulfate
P-cresol sulfate
Xanthosine
Tiglylglycine
N-Cinnamoylglycine
Hippuric acid
Peak area ratio
Peak area
Fresh
RT 24hr
4°C 24hr
FT ×1
FT ×2
FT ×3

Figure B.4. Serum stability analysis. The stability of 21 serum metabolites was assessed in a single point calibrator (SPC) under four storage conditions: room temperature for 24 hours (RT 24hr), refrigeration at 4°C for 24 hours (4°C 24hr), and one, two, and three freeze-thaw cycles (FT ×1, FT ×2, FT ×3). Five replicates were analyzed per condition. The cyan line represents the mean of freshly thawed SPC samples; dashed lines represent the mean ± 2SD. Peak area ratio is shown for compounds with an internal standard; peak area is shown for compounds without.

C. APPENDIX C. RESULTS SUPPLEMENTAL FIGURES AND TABLES

Table C.1. Baseline secretory solute clearance and plasma concentration by incident AKI outcome. Panel A shows baseline solute clearances (mL/min) and Panel B shows baseline inverse plasma concentrations ($1/\mu mol \cdot L^{-1}$) by incident AKI status. Incident AKI was defined as the absence of AKI at enrollment with development of AKI during hospitalization. Values are median (IQR). Adjusted ORs are from logistic regression, one analyte at a time, adjusted for baseline creatinine, creatinine clearance, age, sex, and SOFA score; each analyte was log-transformed and standardized before modelling. Filtration markers (creatinine clearance in Panel A; inverse-creatinine concentration and eGFR in Panel B) are shown in italics and were adjusted for age, sex, and SOFA score only. FDR correction was applied within each panel across all analytes including filtration markers (Benjamini-Hochberg). Higher inverse plasma concentration values indicate better secretory function. * raw $p < 0.05$; † FDR $q < 0.05$. Significant values shown in bold red.

A. Baseline Solute Clearance (mL/min)

Solute	Incident AKI Yes Median (IQR) (n=30)	Incident AKI No Median (IQR) (n=151)	Adj-OR (95% CI)	Raw p-value*	FDR q-value†
4-Acetamidobutyric acid	66.7 (32.0-105.3)	77.5 (45.6-133.1)	0.59 (0.36, 0.95)	**0.031***	**0.040***
Cinnamoylglycine	86.7 (46.3-130.1)	143.7 (90.9-199.7)	0.51 (0.32, 0.81)	**0.004***	**0.006***
Gentisic acid	53.8 (33.1-69.0)	75.7 (52.1-110.4)	0.52 (0.34, 0.77)	**0.001***	**0.002***
Homocitrulline	14.7 (7.94-39.6)	46.3 (26.3-73.5)	0.39 (0.23, 0.64)	**<0.001***	**0.001***
5-Hydroxy-3-indoleacetic acid	318.5 (132.4-514.6)	426.8 (301.0-606.3)	0.51 (0.33, 0.76)	**<0.001***	**0.002***
2-Hydroxyphenylacetic acid	15.9 (4.84-27.1)	39.6 (19.9-73.7)	0.39 (0.24, 0.62)	**<0.001***	**0.001***
4-Hydroxyphenylacetic acid	100.6 (42.8-179.6)	208.8 (124.4-353.3)	0.35 (0.2, 0.6)	**<0.001***	**0.001***
Indoxyl sulfate	74.9 (54.0-111.5)	91.2 (66.1-134.7)	0.71 (0.4, 1.25)	0.242	0.257
Isovalerylglycine	332.2 (151.0-399.4)	502.7 (283.7-811.6)	0.41 (0.24, 0.66)	**<0.001***	**0.001***
Kynurenic acid	139.4 (80.8-231.6)	195.9 (142.9-264.0)	0.49 (0.29, 0.79)	**0.004***	**0.006***
3-Methoxy-4-hydroxyphenylglycol	37.5 (20.4-89.1)	60.0 (29.3-116.8)	0.79 (0.5, 1.25)	0.314	0.314
N2,N2-Dimethylguanosine	229.0 (103.9-371.6)	318.4 (221.2-427.5)	0.5 (0.33, 0.77)	**0.001***	**0.002***
p-Cresol sulfate	9.51 (6.35-11.5)	12.8 (8.37-17.0)	0.56 (0.31, 0.98)	**0.045***	0.053
Pyridoxic acid	215.4 (111.4-328.2)	278.4 (188.4-371.8)	0.58 (0.38, 0.89)	**0.008***	**0.012***
Tiglylglycine	309.5 (128.1-503.7)	439.8 (267.9-686.1)	0.49 (0.31, 0.77)	**0.002***	**0.004***
Xanthosine	126.8 (79.4-176.4)	211.5 (135.0-276.9)	0.45 (0.29, 0.69)	**<0.001***	**0.001***
Creatinine clearance	*81.5 (56.2-130.8)*	*107.6 (76.2-148.5)*	*0.65 (0.42, 0.99)*	***0.047****	*0.053*

[1] * raw p < 0.05; † q < 0.05. Filtration markers (*italics*) adjusted for age, sex, and SOFA score only.

B. Baseline Inverse Plasma Concentration (1/µmol·L^{-1})

Solute	Incident AKI Yes Median (IQR) (n=30)	Incident AKI No Median (IQR) (n=151)	Adj-OR (95% CI)	Raw p-value*	FDR q-value†
4-Acetamidobutyric acid	0.196 (0.114-0.360)	0.127 (0.0866-0.203)	0.51 (0.32, 0.8)	**0.003***	**0.016***
Cinnamoylglycine	0.0026 (0.0011-0.0093)	0.0021 (0.0011-0.0043)	0.66 (0.44, 0.98)	**0.041***	0.082
Gentisic acid	0.0599 (0.0289-0.237)	0.0455 (0.0255-0.0977)	0.69 (0.46, 1.03)	0.067	0.110
Homocitrulline	0.745 (0.549-1.03)	0.476 (0.352-0.696)	0.6 (0.36, 0.99)	**0.046***	0.083
5-Hydroxy-3-indoleacetic acid	0.164 (0.105-0.282)	0.105 (0.0698-0.144)	0.48 (0.32, 0.72)	**<0.001***	**0.006***
2-Hydroxyphenylacetic acid	3.72 (2.29-6.39)	2.60 (1.51-4.11)	0.64 (0.41, 0.98)	**0.041***	0.082
4-Hydroxyphenylacetic acid	4.78 (1.83-12.1)	2.09 (1.26-4.35)	0.61 (0.39, 0.92)	**0.020***	0.050
Indoxyl sulfate	1.98 (0.982-2.74)	1.08 (0.570-2.13)	0.63 (0.36, 1.01)	0.080	0.111
Isovalerylglycine	0.0052 (0.0034-0.0073)	0.0048 (0.0031-0.0091)	1.11 (0.72, 1.74)	0.631	0.710
Kynurenic acid	0.195 (0.108-0.362)	0.120 (0.0830-0.173)	0.56 (0.36, 0.85)	**0.007***	**0.027***
3-Methoxy-4-hydroxyphenylglycol	0.0564 (0.0289-0.102)	0.0276 (0.0194-0.0410)	0.51 (0.34, 0.75)	**<0.001***	**0.006***
N2,N2-Dimethylguanosine	0.0871 (0.0565-0.117)	0.0529 (0.0400-0.0739)	0.54 (0.37, 0.8)	**0.002***	**0.010***
p-Cresol sulfate	64.6 (41.7-119.2)	43.4 (22.0-78.0)	0.62 (0.32, 1.02)	0.101	0.130
Pyridoxic acid	0.0186 (0.0125-0.0246)	0.0121 (0.0080-0.0228)	0.7 (0.47, 1.05)	0.076	0.111
Tiglylglycine	0.0107 (0.0055-0.0199)	0.0106 (0.0070-0.0172)	1.04 (0.67, 1.69)	0.863	0.863
Xanthosine	0.0324 (0.0273-0.0433)	0.0234 (0.0181-0.0324)	0.64 (0.44, 0.94)	**0.019***	0.050
Creatinine (inverse)	*1.03 (0.883-1.30)*	*1.16 (0.941-1.37)*	*0.94 (0.6, 1.45)*	*0.774*	*0.819*
eGFR	*85.6 (70.7-102.8)*	*90.0 (78.6-103.8)*	*0.78 (0.52, 1.18)*	*0.221*	*0.265*

[1] * raw p < 0.05; † q < 0.05. Filtration markers (*italics*) adjusted for age, sex, and SOFA score only.

Incident AKI defined as no AKI at baseline with development of AKI. Values are median (IQR). Clearance in mL/min; inverse plasma in 1/(µmol/L) (higher = better secretory function). Inverse creatinine displayed in 1/(mg/dL). eGFR in mL/min/1.73m^2. Secretory solute ORs adjusted for baseline creatinine, creatinine clearance, age, sex, SOFA score. Filtration markers adjusted for age, sex, and SOFA score only. FDR: Benjamini–Hochberg across all analytes per panel (solutes + filtration markers). * raw p < 0.05; † q < 0.05. Significant values in bold red.

Table C.2. Baseline secretory solute clearance and plasma concentration by MAKE30 outcome. Panel A shows baseline solute clearances (mL/min) and Panel B shows baseline inverse plasma concentrations ($1/\mu mol \cdot L^{-1}$) by MAKE30 status. Values are median (IQR). Adjusted ORs are from logistic regression, one analyte at a time, adjusted for baseline creatinine, creatinine clearance, age, sex, and SOFA score; each analyte was log-transformed and standardized before modelling. Filtration markers (creatinine clearance in Panel A; inverse-creatinine concentration and eGFR in Panel B) are shown in italics and were adjusted for age, sex, and SOFA score only. FDR correction was applied within each panel across all analytes including filtration markers (Benjamini-Hochberg). Higher inverse plasma concentration values indicate better secretory function. MAKE30 = major adverse kidney events at 30 days. * raw $p < 0.05$; † FDR $q < 0.05$. Significant values shown in bold red.

A. Baseline Solute Clearance (mL/min)

Solute	MAKE30 Yes Median (IQR) (n=28)	MAKE30 No Median (IQR) (n=236)	Adj-OR (95% CI)	Raw p-value*	FDR q-value†
4-Acetamidobutyric acid	22.8 (7.27-45.0)	65.9 (36.7-111.8)	0.33 (0.18, 0.58)	**<0.001***	**<0.001***
Cinnamoylglycine	36.0 (18.5-80.7)	116.2 (65.4-181.1)	0.37 (0.21, 0.64)	**<0.001***	**<0.001***
Gentisic acid	20.2 (6.86-46.6)	61.4 (34.7-99.9)	0.49 (0.31, 0.77)	**0.002***	**0.002***
Homocitrulline	6.90 (1.64-15.3)	31.6 (14.5-60.1)	0.35 (0.19, 0.61)	**<0.001***	**<0.001***
5-Hydroxy-3-indoleacetic acid	121.3 (37.4-288.5)	359.8 (208.3-529.5)	0.39 (0.23, 0.64)	**<0.001***	**<0.001***
2-Hydroxyphenylacetic acid	2.33 (0.736-11.7)	25.8 (9.40-55.7)	0.34 (0.2, 0.57)	**<0.001***	**<0.001***
4-Hydroxyphenylacetic acid	22.2 (6.30-74.2)	152.9 (71.5-294.0)	0.23 (0.13, 0.41)	**<0.001***	**<0.001***
Indoxyl sulfate	37.8 (7.94-70.5)	77.9 (46.5-117.0)	0.27 (0.14, 0.51)	**<0.001***	**<0.001***
Isovalerylglycine	88.4 (41.8-247.2)	360.9 (195.9-603.2)	0.29 (0.16, 0.5)	**<0.001***	**<0.001***
Kynurenic acid	60.6 (31.7-156.1)	171.3 (101.8-239.5)	0.38 (0.22, 0.65)	**<0.001***	**<0.001***
3-Methoxy-4-hydroxyphenylglycol	16.3 (3.22-41.5)	52.0 (25.3-112.4)	0.46 (0.28, 0.73)	**0.002***	**0.002***
N2,N2-Dimethylguanosine	76.9 (35.3-263.6)	264.8 (153.7-384.4)	0.4 (0.24, 0.66)	**<0.001***	**<0.001***
p-Cresol sulfate	4.02 (1.43-9.78)	9.75 (6.04-15.1)	0.32 (0.17, 0.59)	**<0.001***	**<0.001***
Pyridoxic acid	95.1 (29.7-218.1)	228.9 (135.4-345.1)	0.48 (0.29, 0.78)	**0.003***	**0.003***
Tiglylglycine	86.8 (51.3-253.3)	356.9 (187.3-569.4)	0.33 (0.19, 0.56)	**<0.001***	**<0.001***
Xanthosine	54.4 (27.6-134.0)	152.7 (91.8-240.2)	0.43 (0.25, 0.71)	**0.001***	**0.001***
Creatinine clearance	*32.1 (14.7-86.4)*	*87.2 (54.6-130.5)*	*0.4 (0.26, 0.59)*	***<0.001****	***<0.001****

B. Baseline Inverse Plasma Concentration (1/µmol·L^{-1})

Solute	MAKE30 Yes Median (IQR) (n=28)	MAKE30 No Median (IQR) (n=236)	Adj-OR (95% CI)	Raw p-value*	FDR q-value†
4-Acetamidobutyric acid	0.334 (0.216-0.867)	0.163 (0.102-0.315)	0.45 (0.25, 0.79)	**0.006***	0.100
Cinnamoylglycine	0.0054 (0.0019-0.0121)	0.0027 (0.0013-0.0077)	0.83 (0.55, 1.25)	0.362	0.465
Gentisic acid	0.157 (0.0605-0.591)	0.0515 (0.0311-0.171)	0.74 (0.51, 1.08)	0.107	0.201
Homocitrulline	0.984 (0.629-2.19)	0.613 (0.409-1.07)	0.79 (0.46, 1.37)	0.396	0.475
5-Hydroxy-3-indoleacetic acid	0.278 (0.166-0.479)	0.123 (0.0855-0.198)	0.58 (0.37, 0.91)	**0.018***	0.107
2-Hydroxyphenylacetic acid	7.51 (3.00-12.2)	3.40 (1.88-5.88)	0.69 (0.42, 1.13)	0.143	0.214
4-Hydroxyphenylacetic acid	11.4 (4.68-19.1)	3.33 (1.49-8.57)	0.56 (0.34, 0.89)	**0.015***	0.107
Indoxyl sulfate	3.90 (1.09-7.93)	1.73 (0.799-2.86)	0.64 (0.35, 1.08)	0.122	0.201
Isovalerylglycine	0.0086 (0.0042-0.0176)	0.0059 (0.0035-0.0109)	1.14 (0.74, 1.81)	0.556	0.626
Kynurenic acid	0.412 (0.214-0.911)	0.156 (0.0940-0.302)	0.59 (0.35, 0.95)	**0.032***	0.117
3-Methoxy-4-hydroxyphenylglycol	0.0742 (0.0475-0.169)	0.0338 (0.0216-0.0636)	0.63 (0.42, 0.94)	**0.024***	0.110
N2,N2-Dimethylguanosine	0.142 (0.0683-0.285)	0.0637 (0.0454-0.117)	0.63 (0.4, 0.99)	**0.043***	0.130
p-Cresol sulfate	99.7 (63.9-181.7)	52.4 (29.8-100.3)	0.92 (0.54, 1.42)	0.729	0.772
Pyridoxic acid	0.0211 (0.0145-0.0698)	0.0152 (0.0094-0.0314)	0.73 (0.48, 1.09)	0.123	0.201
Tiglylglycine	0.0186 (0.0089-0.0462)	0.0130 (0.0086-0.0217)	0.94 (0.61, 1.49)	0.791	0.791
Xanthosine	0.0406 (0.0324-0.0779)	0.0280 (0.0211-0.0426)	0.76 (0.51, 1.17)	0.200	0.277
Creatinine (inverse)	*1.04 (0.828-1.25)*	*1.11 (0.926-1.33)*	*0.71 (0.48, 1.08)*	*0.105*	*0.201*
eGFR	*87.1 (66.1-90.2)*	*90.0 (74.5-102.0)*	*0.72 (0.51, 1.05)*	*0.067*	*0.173*

Values are median (IQR). n reflects dataset totals before per-analyte complete-case exclusions. Clearance in mL/min; inverse plasma in 1/(µmol/L); higher = better secretory function. Inverse creatinine displayed in 1/(mg/dL). eGFR in mL/min/1.73m^2. Secretory solute ORs adjusted for baseline creatinine, creatinine clearance, age, sex, SOFA score. Filtration markers (*italics*) adjusted for age, sex, and SOFA score only. FDR: Benjamini–Hochberg across all analytes per panel (solutes + filtration markers). MAKE30 = major adverse kidney events at 30 days. * raw p < 0.05; † q < 0.05. Significant values in bold red.

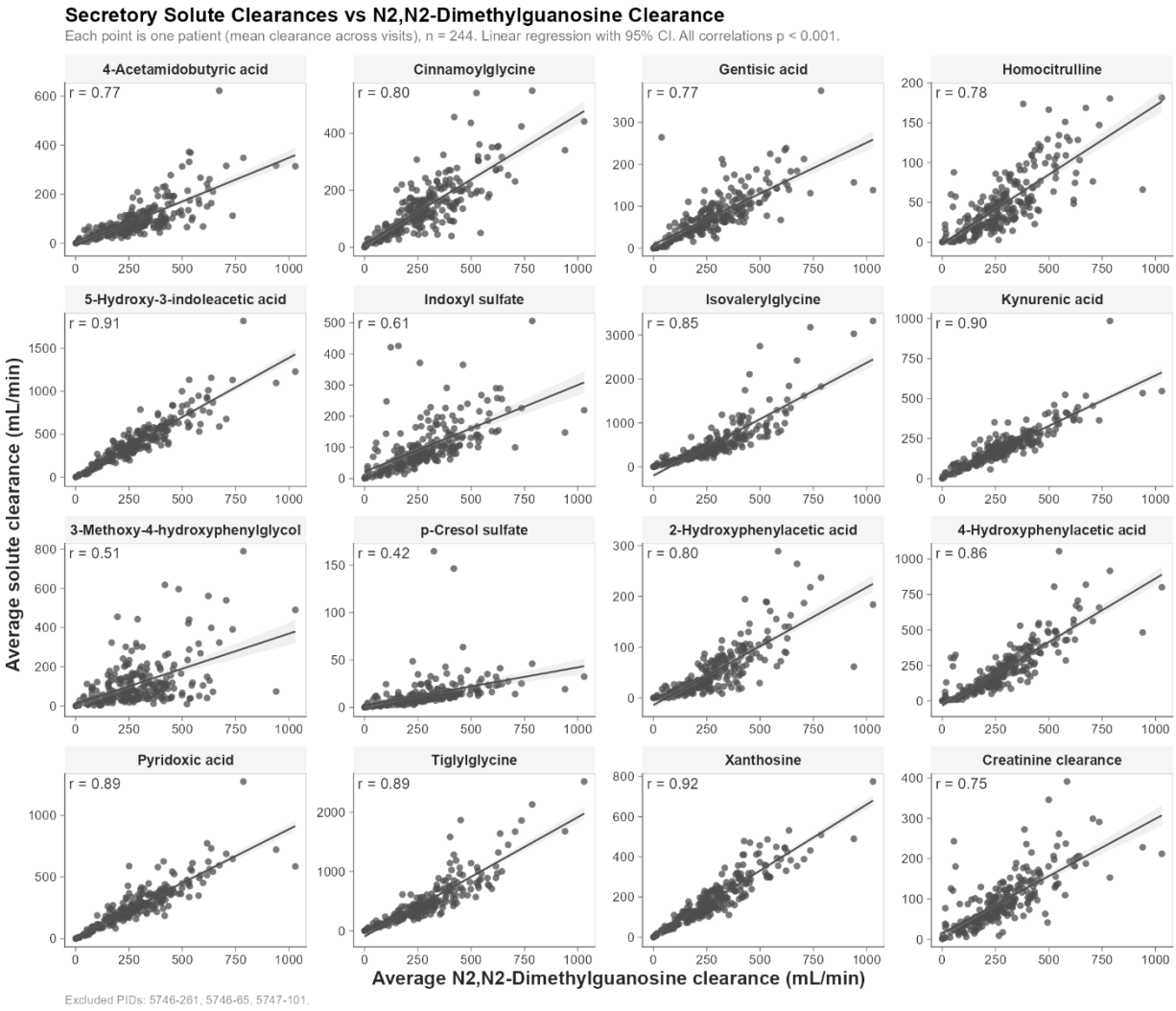

Figure C.1. Pairwise correlations of secretory solute clearances and creatinine clearance with N2,N2-dimethylguanosine (DMG) clearance. Each panel shows the relationship between average DMG clearance (x-axis) and average clearance of one secretory solute or creatinine (y-axis), where each point represents one patient (n = 244). The solid line represents a linear regression fit with a 95% confidence interval (shaded). Pearson correlation coefficients (r) are displayed within each panel. All correlations were statistically significant at $p < 0.001$. Values are mean clearances per patient averaged across all study visits. Three patients were excluded for implausibly high creatinine or solute clearances.

Baseline DMG Clearance by AKI Stage, MAKE30 Outcome, and AKI Recovery

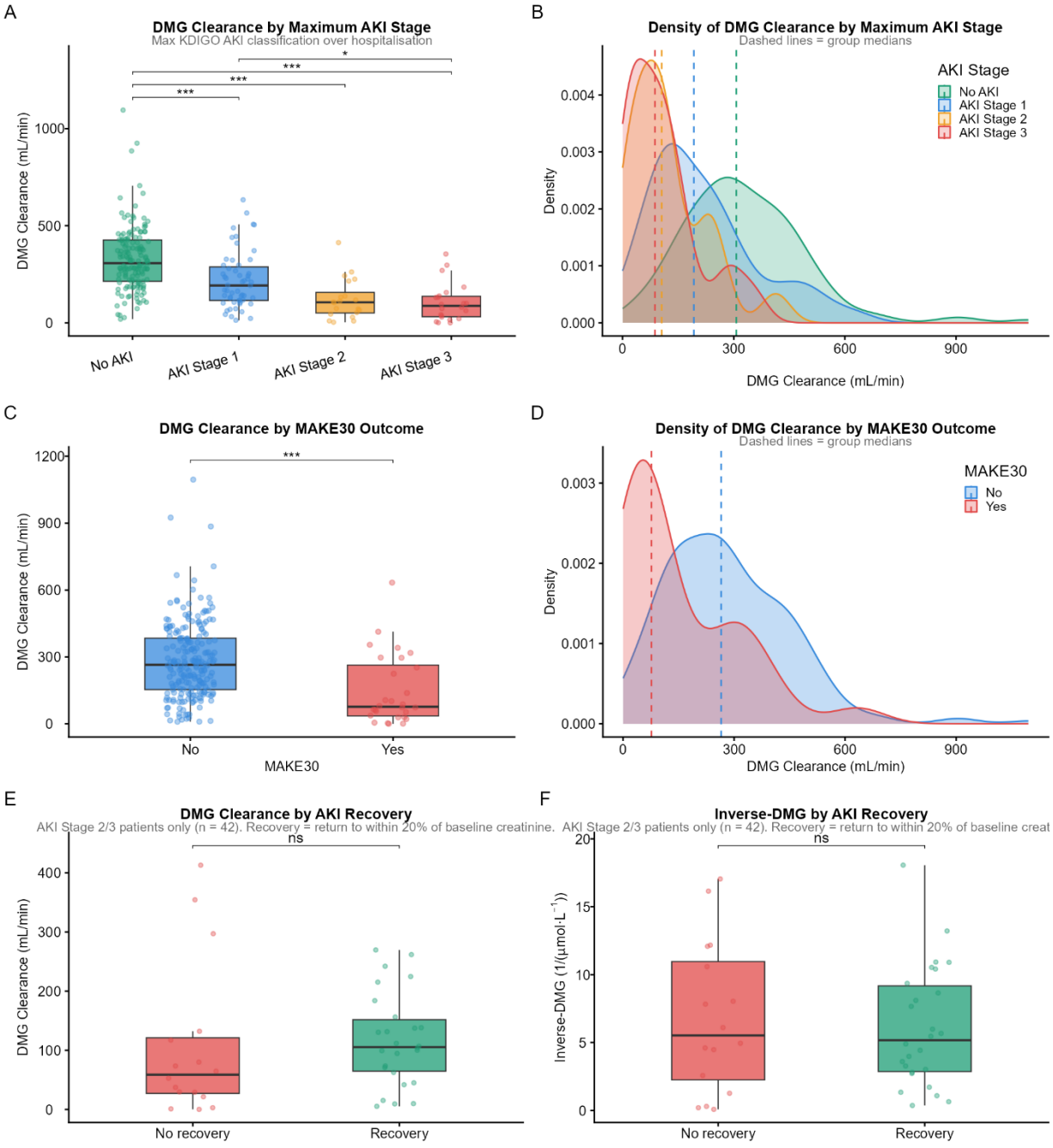

Significance: * p<0.05 ** p<0.01 *** p<0.001
AKI stage panels: Kruskal-Wallis + Dunn post-hoc (Bonferroni) | MAKE30 & recovery panels: Wilcoxon rank-sum | Baseline = Visit 1
Panels E-F: AKI Stage 2/3 patients only.

Figure C.2. Baseline DMG clearance stratified by maximum AKI severity, 30-day kidney outcome, and AKI recovery status. Box plots with individual data points showing baseline DMG clearance (mL/min) stratified by (A) maximum AKI stage over the course of hospitalization (KDIGO criteria) and (C) MAKE30 outcome (No vs. Yes). Density plots illustrating the distribution of DMG clearance by (B) maximum AKI stage and (D) MAKE30 outcome; dashed vertical lines indicate group medians. Box plots showing DMG clearance (E) and inverse plasma DMG concentration (F) stratified by AKI recovery status, defined as return of serum creatinine to within 20% of baseline. In panel A, groups were compared using the Kruskal-Wallis test with Dunn post-hoc correction (Bonferroni). In panels C, E, and F, groups were compared using the Wilcoxon rank-sum test. Box plots display median with IQR. * $p<0.05$, ** $p<0.01$, *** $p<0.001$.

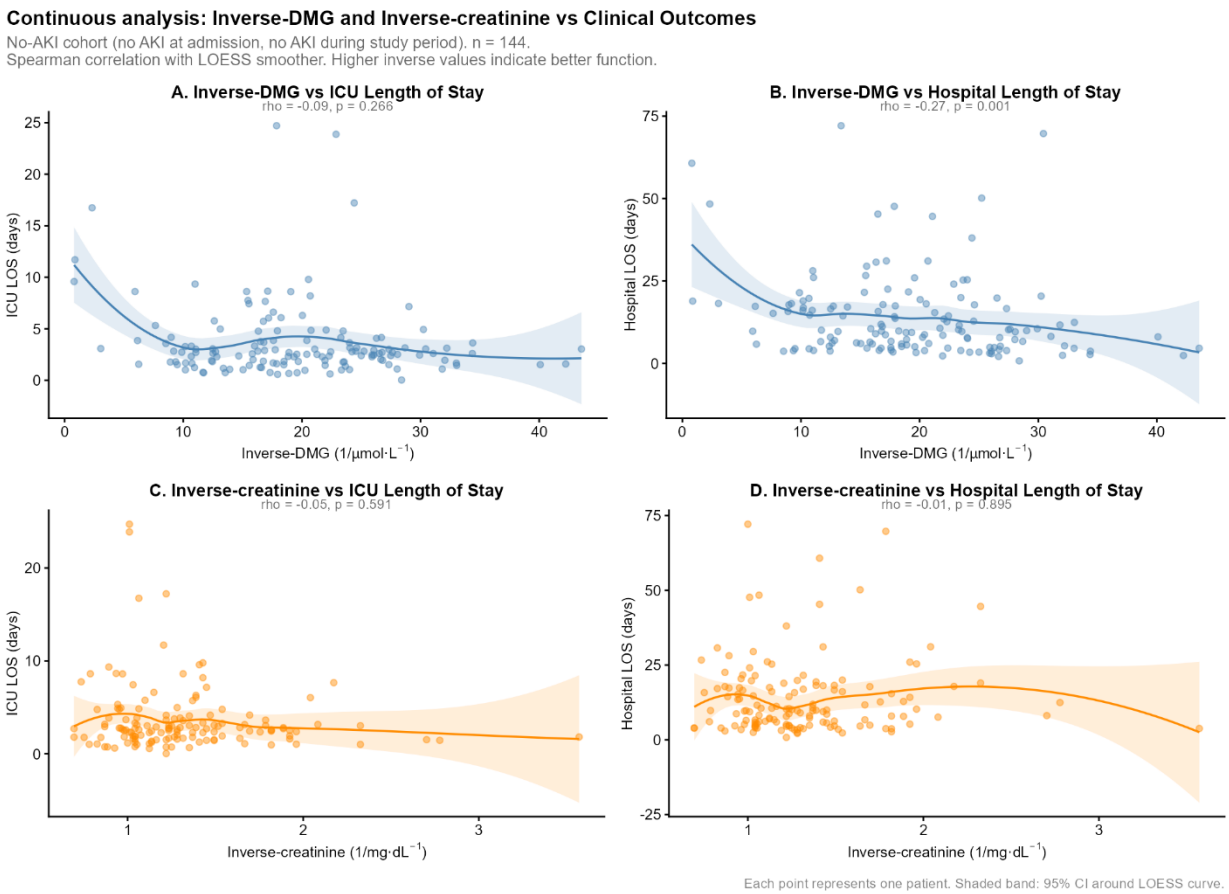

Figure C.3. Continuous association between baseline inverse plasma concentration reference ranges for DMG and creatinine in patients without AKI. Scatter plots with LOESS smoothers showing the relationship between baseline inverse-DMG (panels A–B, blue) and inverse-creatinine (panels C–D, orange) and length of stay outcomes in patients with no AKI at admission and no AKI during the study period (n = 144). Panels A and C show ICU length of stay; panels B and D show hospital length of stay. Spearman rank correlation coefficients (rho) and associated p-values are shown above each panel. Shaded bands represent 95% confidence intervals around the LOESS curve. Higher inverse concentration values indicate better secretory function.

REFERENCES

1. Kaufman DP, Basit H, Knohl SJ. Physiology, Glomerular Filtration Rate. In: *StatPearls*. StatPearls Publishing; 2025. Accessed January 26, 2025. http://www.ncbi.nlm.nih.gov/books/NBK500032/

2. Acharya V, Olivero J. The Kidney as an Endocrine Organ. *Methodist Debakey Cardiovasc J*. 2018;14(4):305-307. doi:10.14797/mdcj-14-4-305

3. DeLuca HF. Overview of general physiologic features and functions of vitamin D23. *The American Journal of Clinical Nutrition*. 2004;80(6):1689S-1696S. doi:10.1093/ajcn/80.6.1689S

4. Mahadevan V. Anatomy of the kidney and ureter. *Surgery (Oxford)*. 2019;37(7):359-364. doi:10.1016/j.mpsur.2019.04.005

5. Epstein M. Alcohol's Impact on Kidney Function. *Alcohol Health Res World*. 1997;21(1):84-92.

6. Bello-Reuss E, Reuss L. Homeostatic and Excretory Functions of the Kidney. In: Klahr S, ed. *The Kidney and Body Fluids in Health and Disease*. Springer US; 1983:35-63. doi:10.1007/978-1-4613-3524-5_2

7. Traynor J, Mactier R, Geddes CC, Fox JG. How to measure renal function in clinical practice. *BMJ*. 2006;333(7571):733-737. doi:10.1136/bmj.38975.390370.7C

8. Iatridi F, Carrero JJ, Cornec-Le Gall E, et al. KDIGO 2024 Clinical Practice Guideline for the Evaluation and Management of Chronic Kidney Disease in Children and Adults: a commentary from the European Renal Best Practice (ERBP). *Nephrol Dial Transplant*. 2024;40(2):273-282. doi:10.1093/ndt/gfae209

9. Mehta RL, Cerdá J, Burdmann EA, et al. International Society of Nephrology's 0by25 initiative for acute kidney injury (zero preventable deaths by 2025): a human rights case for nephrology. *The Lancet*. 2015;385(9987):2616-2643. doi:10.1016/S0140-6736(15)60126-X

10. Clarkson MD, Platt KM. Kidney anatomy: A Survey of Historical Illustrations and Methods of Depiction. *J Biocommun*. 2025;49(2):e5. doi:10.5210/jbc.v49i2.14482

11. Theodorou C, Leatherby R, Dhanda R. Function of the nephron and the formation of urine. *Anaesthesia & Intensive Care Medicine*. 2021;22(7):434-438. doi:10.1016/j.mpaic.2021.05.004

12. Wang K, Kestenbaum B. Proximal Tubular Secretory Clearance. *Clin J Am Soc Nephrol*. 2018;13(8):1291-1296. doi:10.2215/CJN.12001017

13. Menon MC, Chuang PY, He CJ. The Glomerular Filtration Barrier: Components and Crosstalk. *Int J Nephrol*. 2012;2012:749010. doi:10.1155/2012/749010

14. Pavenstädt H, Kriz W, Kretzler M. Cell Biology of the Glomerular Podocyte. *Physiological Reviews*. 2003;83(1):253-307. doi:10.1152/physrev.00020.2002

15. Fenton A, Montgomery E, Nightingale P, et al. Glomerular filtration rate: new age- and gender- specific reference ranges and thresholds for living kidney donation. *BMC Nephrol*. 2018;19:336. doi:10.1186/s12882-018-1126-8

16. Robertson EE, Rankin GO. Human renal organic anion transporters: Characteristics and contributions to drug and drug metabolite excretion. *Pharmacology & Therapeutics*. 2006;109(3):399-412. doi:10.1016/j.pharmthera.2005.07.005

17. Ohtsuki S, Asaba H, Takanaga H, et al. Role of blood–brain barrier organic anion transporter 3 (OAT3) in the efflux of indoxyl sulfate, a uremic toxin: its involvement in neurotransmitter metabolite clearance from the brain. *Journal of Neurochemistry*. 2002;83(1):57-66. doi:10.1046/j.1471-4159.2002.01108.x

18. Chawla LS, Amdur RL, Shaw AD, Faselis C, Palant CE, Kimmel PL. Association between AKI and Long-Term Renal and Cardiovascular Outcomes in United States Veterans. *Clin J Am Soc Nephrol*. 2014;9(3):448-456. doi:10.2215/CJN.02440213

19. Hotait ZS, Lo Cascio JN, Choos END, Shepard BD. The sugar daddy: the role of the renal proximal tubule in glucose homeostasis. *Am J Physiol Cell Physiol*. 2022;323(3):C791-C803. doi:10.1152/ajpcell.00225.2022

20. Hoenig MP, Brooks CR, Hoorn EJ, Hall AM. Biology of the proximal tubule in body homeostasis and kidney disease. *Nephrol Dial Transplant*. 2024;40(2):234-243. doi:10.1093/ndt/gfae177

21. Nigam SK. What do drug transporters really do? *Nat Rev Drug Discov*. 2015;14(1):29-44. doi:10.1038/nrd4461

22. Nigam SK, Wu W, Bush KT, Hoenig MP, Blantz RC, Bhatnagar V. Handling of Drugs, Metabolites, and Uremic Toxins by Kidney Proximal Tubule Drug Transporters. *Clin J Am Soc Nephrol*. 2015;10(11):2039-2049. doi:10.2215/CJN.02440314

23. Chevalier RL. The proximal tubule is the primary target of injury and progression of kidney disease: role of the glomerulotubular junction. *Am J Physiol Renal Physiol*. 2016;311(1):F145-F161. doi:10.1152/ajprenal.00164.2016

24. Schneider R, Sauvant C, Betz B, et al. Downregulation of organic anion transporters OAT1 and OAT3 correlates with impaired secretion of para-aminohippurate after ischemic acute renal failure in rats. *American Journal of Physiology-Renal Physiology*. 2007;292(5):F1599-F1605. doi:10.1152/ajprenal.00473.2006

25. Wagner CA. Beyond SGLT2: proximal tubule transporters as potential drug targets for chronic kidney disease. *Nephrol Dial Transplant*. 2025;40(Suppl 1):i18-i28. doi:10.1093/ndt/gfae211

26. Mark PB, Stafford LK, Grams ME, et al. Global, regional, and national burden of chronic kidney disease in adults, 1990–2023, and its attributable risk factors: a systematic analysis for the Global Burden of Disease Study 2023. *The Lancet*. 2025;406(10518):2461-2482. doi:10.1016/S0140-6736(25)01853-7

27. Chen DC, Potok OA, Rifkin D, Estrella MM. Advantages, Limitations, and Clinical Considerations in Using Cystatin C to Estimate GFR. *Kidney360*. 2022;3(10):1807-1814. doi:10.34067/KID.0003202022

28. Tan HT, Liu Q, Teo TL. Advancing Accuracy in Chronic Kidney Disease Diagnosis and Management: Reference Materials and Reference Measurement Procedures for Clinical Markers. *Ann Lab Med*. 2025;45(4):367-380. doi:10.3343/alm.2024.0583

29. Cockcroft DW, Gault MH. Prediction of creatinine clearance from serum creatinine. *Nephron*. 1976;16(1):31-41. doi:10.1159/000180580

30. Inker LA, Eneanya ND, Coresh J, et al. New Creatinine- and Cystatin C–Based Equations to Estimate GFR without Race. *N Engl J Med*. 2021;385(19):1737-1749. doi:10.1056/NEJMoa2102953

31. Delgado C, Baweja M, Crews DC, et al. A Unifying Approach for GFR Estimation: Recommendations of the NKF-ASN Task Force on Reassessing the Inclusion of Race in Diagnosing Kidney Disease. *American Journal of Kidney Diseases*. 2022;79(2):268-288.e1. doi:10.1053/j.ajkd.2021.08.003

32. Delanaye P, Guerber F, Scheen A, et al. Discrepancies between the Cockcroft–Gault and Chronic Kidney Disease Epidemiology (CKD-EPI) Equations: Implications for Refining Drug Dosage Adjustment Strategies. *Clin Pharmacokinet*. 2017;56(2):193-205. doi:10.1007/s40262-016-0434-z

33. Niemantsverdriet MSA, Pieters TT, Hoefer IE, et al. GFR estimation is complicated by a high incidence of non-steady-state serum creatinine concentrations at the emergency department. *PLoS One*. 2021;16(12):e0261977. doi:10.1371/journal.pone.0261977

34. Seki M, Nakayama M, Sakoh T, et al. Blood urea nitrogen is independently associated with renal outcomes in Japanese patients with stage 3–5 chronic kidney disease: a prospective observational study. *BMC Nephrol*. 2019;20:115. doi:10.1186/s12882-019-1306-1

35. Soveri I, Berg UB, Björk J, et al. Measuring GFR: A Systematic Review. *American Journal of Kidney Diseases*. 2014;64(3):411-424. doi:10.1053/j.ajkd.2014.04.010

36. Taubert M, Schaeffner E, Martus P, et al. Advancement of pharmacokinetic models of iohexol in patients aged 70 years or older with impaired kidney function. *Sci Rep*. 2021;11:22656. doi:10.1038/s41598-021-01892-1

37. Bjornstad P, Karger AB, Maahs DM. Measured GFR in Routine Clinical Practice – The Promise of Dried Blood Spots. *Adv Chronic Kidney Dis*. 2018;25(1):76-83. doi:10.1053/j.ackd.2017.09.003

38. Okusa MD, Davenport A. Reading between the (guide)lines—the KDIGO practice guideline on acute kidney injury in the individual patient. *Kidney Int*. 2014;85(1):10.1038/ki.2013.378. doi:10.1038/ki.2013.378

39. Levin A, Stevens PE, Bilous RW, et al. Kidney disease: Improving global outcomes (KDIGO) CKD work group. KDIGO 2012 clinical practice guideline for the evaluation and management of chronic kidney disease. *Kidney International Supplements*. 2013;3(1):1-150. doi:10.1038/kisup.2012.73

40. Suchy-Dicey AM, Laha T, Hoofnagle A, et al. Tubular Secretion in CKD. *J Am Soc Nephrol*. 2016;27(7):2148-2155. doi:10.1681/ASN.2014121193

41. Sirich TL, Aronov PA, Plummer NS, Hostetter TH, Meyer TW. Numerous protein-bound solutes are cleared by the kidney with high efficiency. *Kidney Int*. 2013;84(3):585-590. doi:10.1038/ki.2013.154

42. Wang K, Zelnick LR, Chen Y, et al. Alterations of Proximal Tubular Secretion in Autosomal Dominant Polycystic Kidney Disease. *Clin J Am Soc Nephrol*. 2020;15(1):80-88. doi:10.2215/CJN.05610519

43. Wang K, Zelnick LR, Hoofnagle AN, et al. Differences in proximal tubular solute clearance across common etiologies of chronic kidney disease. *Nephrol Dial Transplant*. 2020;35(11):1916-1923. doi:10.1093/ndt/gfz144

44. Chen Y, Zelnick LR, Wang K, et al. Kidney Clearance of Secretory Solutes Is Associated with Progression of CKD: The CRIC Study. *J Am Soc Nephrol*. 2020;31(4):817-827. doi:10.1681/ASN.2019080811

45. Chen Y, Zelnick LR, Huber MP, et al. Association Between Kidney Clearance of Secretory Solutes and Cardiovascular Events: The Chronic Renal Insufficiency Cohort (CRIC) Study. *Am J Kidney Dis*. 2021;78(2):226-235.e1. doi:10.1053/j.ajkd.2020.12.005

46. Lidgard B, Bansal N, Zelnick LR, et al. Association of Proximal Tubular Secretory Clearance with Long-Term Decline in Cognitive Function. *J Am Soc Nephrol*. 2022;33(7):1391-1401. doi:10.1681/ASN.2021111435

47. Chen Y, Zelnick LR, Hoofnagle AN, et al. Prediction of Kidney Drug Clearance: A Comparison of Tubular Secretory Clearance and Glomerular Filtration Rate. *J Am Soc Nephrol*. 2021;32(2):459-468. doi:10.1681/ASN.2020060833

48. Bhatraju PK, Chai XY, Sathe NA, et al. Assessment of kidney proximal tubular secretion in critical illness. *JCI Insight*. 6(10):e145514. doi:10.1172/jci.insight.145514

49. Granda ML, Prince DK, Fiehn O, et al. Metabolomic Profiling Identifies New Endogenous Markers of Tubular Secretory Clearance. *Kidney360*. 2022;4(1):23-31. doi:10.34067/KID.0004172022

50. Lian S, Yin J, Lv X, Li X. Mechanistic Insights into Label-Free SERS Discrimination of Structurally Similar Small-Molecule Biomarkers: A DFT Study of 4-HBA and 4-HPAA on Au Clusters. *Langmuir*. 2026;42(17):11966-11978. doi:10.1021/acs.langmuir.6c00447

51. Du M, Wang X, Hang D, et al. Metabolomic pattern of ultra-processed food intake and its association with colorectal cancer risk. *Gut*. Published online December 24, 2025:gutjnl-2025-335618. doi:10.1136/gutjnl-2025-335618

52. Seki M. Biological significance and development of practical synthesis of biotin. *Medicinal Research Reviews*. 2006;26(4):434-482. doi:10.1002/med.20058

53. Cozzolino C, Villani GR, Frisso G, et al. Biochemical and molecular characterization of 3-Methylcrotonylglycinuria in an Italian asymptomatic girl. *Genetics and Molecular Biology*. 2018;41(2):379. doi:10.1590/1678-4685-GMB-2017-0093

54. Kanda T, Azuma K, Sakai F, Tazaki Y. Increase in cerebrospinal fluid and plasma levels of 3-methoxy-4-hydroxyphenylglycol in acute stroke. *Stroke*. 1991;22(12):1525-1529. doi:10.1161/01.STR.22.12.1525

55. Ladwig PM, Bergert JH, Larson TS. Capillary Electrophoresis Method to Measure p-Aminohippuric Acid in Urine and Plasma for the Assessment of Renal Plasma Flow. *Clin Chem*. 2003;49(4):664-666. doi:10.1373/49.4.664

56. Lis-Kuberka J, Orczyk-Pawiłowicz M. Sialylated Oligosaccharides and Glycoconjugates of Human Milk. The Impact on Infant and Newborn Protection, Development and Well-Being. *Nutrients*. 2019;11(2):306. doi:10.3390/nu11020306

57. SCBT. 2-Hydroxyphenylacetic Acid | CAS 614-75-5 | SCBT - Santa Cruz Biotechnology. Accessed May 17, 2026. https://www.scbt.com/p/2-hydroxyphenylacetic-acid-614-75-5

58. PubChem. 1,4-Cyclohexanedicarboxylic acid. Accessed May 17, 2026. https://pubchem.ncbi.nlm.nih.gov/compound/14106

59. Birdsall TC. 5-Hydroxytryptophan: a clinically-effective serotonin precursor. *Altern Med Rev*. 1998;3(4):271-280.

60. PubChem. 4-Acetamidobutyric acid. Accessed May 17, 2026. https://pubchem.ncbi.nlm.nih.gov/compound/18189

61. SCBT. L-Homocitrulline | CAS 1190-49-4 | SCBT - Santa Cruz Biotechnology. Accessed May 17, 2026. https://www.scbt.com/p/l-homocitrulline-1190-49-4

62. Behavioural Pharmacology. Accessed May 17, 2026. https://journals.lww.com/behaviouralpharm/abstract/2019/12000/acetylsalicylic_acid_and_its_metabolite_gentisic.3.aspx

63. Lenchner JR, Santos C. Biochemistry, 5 Hydroxyindoleacetic Acid. In: *StatPearls*. StatPearls Publishing; 2026. Accessed May 17, 2026. http://www.ncbi.nlm.nih.gov/books/NBK551684/

64. Frontiers | Kynurenic Acid: The Janus-Faced Role of an Immunomodulatory Tryptophan Metabolite and Its Link to Pathological Conditions. Accessed May 17, 2026. https://www.frontiersin.org/journals/immunology/articles/10.3389/fimmu.2017.01957/full

65. Vitamin B6 (Pyridoxine). Medicine LibreTexts. September 2, 2018. Accessed May 17, 2026. https://med.libretexts.org/Courses/Dominican_University/DU_Bio_1550%3A_Nutrition_(LoPresto)/7%3A_Vitamins/7.3%3A_Water_Soluble_Vitamins/Vitamin_B6_(Pyridoxine)

66. Shigematsu Y, Hata I, Tanaka Y. Stable-isotope dilution measurement of isovalerylglycine by tandem mass spectrometry in newborn screening for isovaleric acidemia. *Clinica Chimica Acta*. 2007;386(1):82-86. doi:10.1016/j.cca.2007.08.003

67. Bolati D, Shimizu H, Yisireyili M, Nishijima F, Niwa T. Indoxyl sulfate, a uremic toxin, downregulates renal expression of Nrf2 through activation of NF-κB. *BMC Nephrol*. 2013;14:56. doi:10.1186/1471-2369-14-56

68. Gryp T, Vanholder R, Vaneechoutte M, Glorieux G. p-Cresyl Sulfate. *Toxins (Basel)*. 2017;9(2):52. doi:10.3390/toxins9020052

69. Defects in purine nucleotide metabolism lead to substantial incorporation of xanthine and hypoxanthine into DNA and RNA | PNAS. Accessed May 17, 2026. https://www.pnas.org/doi/10.1073/pnas.1118455109

70. Bennett MJ, Powell S, Swartling DJ, Gibson KM. Tiglylglycine excreted in urine in disorders of isoleucine metabolism and the respiratory chain measured by stable isotope dilution GC-MS. *Clin Chem*. 1994;40(10):1879-1883.

71. Li H, Yu W, Pan M, et al. Multi-Degree-of-Freedom Stretchable Metasurface Terahertz Sensor for Trace Cinnamoylglycine Detection. *Biosensors (Basel)*. 2024;14(12):602. doi:10.3390/bios14120602

72. Ticinesi A, Guerra A, Nouvenne A, Meschi T, Maggi S. Disentangling the Complexity of Nutrition, Frailty and Gut Microbial Pathways during Aging: A Focus on Hippuric Acid. *Nutrients*. 2023;15(5):1138. doi:10.3390/nu15051138

73. Plummer C. Solid-Phase Extraction: From Sample Prep Fundamentals to Best Practices. Waters Blog. October 6, 2025. Accessed March 29, 2026. https://www.waters.com/blog/solid-phase-extraction-from-sample-prep-fundamentals-to-best-practices/

74. Karabacak M, Cinar Z, Cinar M. A structural and spectroscopic study on *para*-aminohippuric acid with experimental and theoretical approaches. *Spectrochimica Acta Part A: Molecular and Biomolecular Spectroscopy*. 2012;85(1):241-250. doi:10.1016/j.saa.2011.10.001

75. Theodoridis G, Fiehn O, Holčapek M, et al. What's in a name? Metabolite identification: challenges and pitfalls in untargeted metabolomics. *Metabolomics*. 2026;22(2):22. doi:10.1007/s11306-025-02387-0

76. R Core Team. _R: A Language and Environment for Statistical Computing_. Published online March 11, 2026. https://www.R-project.org/

77. Hoste EAJ, Bagshaw SM, Bellomo R, et al. Epidemiology of acute kidney injury in critically ill patients: the multinational AKI-EPI study. *Intensive Care Med*. 2015;41(8):1411-1423. doi:10.1007/s00134-015-3934-7

78. Moledina DG, Parikh CR. Phenotyping of Acute Kidney Injury: Beyond Serum Creatinine. *Semin Nephrol*. 2018;38(1):3-11. doi:10.1016/j.semnephrol.2017.09.002

79. Molitoris BA. Therapeutic translation in acute kidney injury: the epithelial/endothelial axis. *J Clin Invest*. 2014;124(6):2355-2363. doi:10.1172/JCI72269

80. Kellum JA, Romagnani P, Ashuntantang G, Ronco C, Zarbock A, Anders HJ. Acute kidney injury. *Nat Rev Dis Primers*. 2021;7(1):52. doi:10.1038/s41572-021-00284-z

81. Junge W, Wilke B, Halabi A, Klein G. Determination of reference intervals for serum creatinine, creatinine excretion and creatinine clearance with an enzymatic and a modified Jaffé method. *Clinica Chimica Acta*. 2004;344(1):137-148. doi:10.1016/j.cccn.2004.02.007

82. Melsom T, Norvik JV, Enoksen IT, et al. Sex Differences in Age-Related Loss of Kidney Function. *Journal of the American Society of Nephrology*. 2022;33(10):1891. doi:10.1681/ASN.2022030323

83. Demirjian S, Huml A, Bakaeen F, et al. Sex Bias in Prediction and Diagnosis of Cardiac Surgery Associated Acute Kidney Injury. *Res Sq*. Published online March 14, 2024:rs.3.rs-3660617. doi:10.21203/rs.3.rs-3660617/v1

84. Soranno DE, Awdishu L, Bagshaw SM, et al. The role of sex and gender in acute kidney injury—consensus statements from the 33rd Acute Disease Quality Initiative. *Kidney International*. 2025;107(4):606-616. doi:10.1016/j.kint.2025.01.008

85. Denic A, Glassock RJ, Rule AD. Structural and functional changes with the aging kidney. *Adv Chronic Kidney Dis*. 2016;23(1):19-28. doi:10.1053/j.ackd.2015.08.004